The gas quality in a hydrogen distribution grid

Computation of the influences of distribution through the existing grid on the hydrogen quality

by

T.M. Hillen

to obtain the degree of Master of Science

at the Delft University of Technology,

to be defended on Thursday November 7, 2019 at 09:00 AM.

Student number:	4303792	
Project duration:	February 26, 2019 – November 7, 2019	
Thesis committee:	Prof. dr. A. J. M. Van Wijk,	TU Delft, supervisor
	Dr. A. Purushothaman Vellayani,	TU Delft
	Dr. ir. M. J. B.M. Pourquie,	TU Delft
	Ing. F. H. M. Van Alphen,	Stedin, supervisor

This thesis is confidential and cannot be made public until November 7, 2024.

TU Delft STEDIN.NET

Preface

This report was written to fulfill the requirements for graduation from the Masters degree Sustainable Energy Technology at Delft University of Technology. Six years of knowledge, skills and experience gained at this university are embodied within this thesis. From the end of February until the beginning of November I have been engaged in conducting this research, and it is with the greatest pleasure that I now finally present this report.

This project was brought to me in January by my supervisor Frank van Alphen, employed at Stedin. On the third day of my internship at Stedin, I was invited to attend a meeting with other distribution network operators to discuss the establishment of a *Hydrogen grid research group*, a platform for network operators to share research concerning hydrogen in the gas grid. To this day I am honoured to have taken part in and to have experienced the establishment of this organisation. Furthermore, I am happy to know that this thesis will contribute to solving a large amount of unsolved questions about hydrogen distribution through the grid and that there is much interest in my work.

I am fortunate to have received supportive guidance throughout the course of this project. For that I would like to express my gratitude to my two supervisors Frank van Alphen and Prof. Ad van Wijk. Not only has their feedback and supervision been very helpful, but is has also been a pleasure collaborating with them. I have benefited from all the constructive criticism that I have received during this project. Frank has made me feel trusted from the start of my internship at Stedin and his suggestions and reminders to step out of my tunnel vision to look for a broader perspective have been very helpful.

Finally, I would like to thank Mathieu Pourquie, thesis committee member, for all the insights he gave me whenever I was stuck in my Matlab model. During all our conversations he expressed his enthusiasm for his field of expertise, which has reflected into my work. I would also like to thank Aravind Purushothaman Vellayani for the time and effort he took into reading this report and joining the thesis committee.

I hope you enjoy reading this report.

T.M. Hillen
Rotterdam,
November 2, 2019

Abstract

Although the Dutch energy supply is gradually progressing from fossil fuels to renewable energy sources, the consequences for the grid are becoming increasingly evident. Meanwhile, the gas extraction from the Groningen natural gas reserve is declining as the induced earthquakes in the northern Netherlands persist. Hydrogen, as a flexible carbon-free molecule, offers a potential solution to the overcapacity of the electricity grid and thus has the potential to fulfill an important role in the future energy supply. It has recently been proved that by making few adjustments in the grid assets, the existing gas grid can be made compatible with hydrogen. A relating issue to hydrogen distribution through the gas grid is the resulting hydrogen quality. Similarly to natural gas, the roll-out of a national hydrogen grid needs a national quality standard. There will be a variety of end-use applications, such as hydrogen boilers and fuel cell technologies that have different quality requirements.

This report researches the influences of the distribution of hydrogen through the existing gas grid. There are five sources of contamination: odorant, inward permeation of air through polymer pipelines, particles circulating in the grid, leaks causing an entrance for contaminants and byproducts from hydrogen production technologies. All five sources are considered, but the focus of this report is on inward permeation of air through low pressure polymer pipelines. There are three significant risks which are linked to the permeation of air: feed dilution, explosion risk and damage to fuel cells. Fick's laws for diffusion were used to create a computation model, from which relationships were found between seven variables and the amount of contamination. Correlations were found between the amount of permeated air and the pipeline material, pressure, inner diameter, wall thickness, flow velocity, temperature and soil type. Pure hydrogen was modelled to be distributed through the low pressure grid at different conditions. After traveling 100 meters through an MDPE pipeline with 26 mm inner diameter and wall thickness of 3 mm at a flow velocity of 1 m/s, 1.4 mg oxygen and 1.9 mg of nitrogen per m^3 hydrogen will have diffused into the pipeline. The results have been implemented in a case study in Stad aan 't Haringvliet in Goeree-Overvlakkee, and the contamination for the farthest distance in the grid was found to be 0.057 ppm oxygen and 0.085 ppm nitrogen at a flow velocity of 1 m/s.

Following the research set out above, no issues were found in connecting hydrogen boilers to the existing grid. Low temperature PEM fuel cells are more sensitive to impurities than boilers and some concerns were found under certain specific conditions with exceeding the current hydrogen fuel contamination limit for oxygen stated in ISO 14687-2. After traveling 529 m through MDPE and 5.8 km through HDPE the oxygen limit was exceeded. This is not considered as a constraint for the development of a future hydrogen grid, as this upper limit was set for the fuel requirement of metal hydride storage, and existing hydrogen road vehicles have another means of storage. A positive side effect of the presence of oxygen in the hydrogen feed is that it reacts with carbon monoxide, thereby decreasing fuel cell poisoning effects. Nitrogen contamination of the hydrogen feed can dilute the fuel and only at high concentrations increase fuel cell cathode poisoning caused by carbon monoxide. These high concentrations are not expected to be achieved as a result of inward permeation of nitrogen. Consequently, through the obtained results in this research it is believed that a sufficiently high purity hydrogen can be achieved in the existing distribution grid.

List of Figures

List of Tables

Nomenclature

List of Abbreviations

AE	Alkaline Electrolysis
AFC	Alkaline Fuel Cell
ATR	Autothermal Reforming
CCS	Carbon Capture and Storage
CHP(-FC)	Combined Heat and Power (Fuel Cell)
CHP	Combined Heat and Power Plant
CPE	Chlorinated Polyethylene
G-gas	Groningen Gas
GHG	Greenhouse Gas(ses)
GTS	Gasunie Transport Services
H-gas	High Calorific Natural Gas
HDPE	High Density Polyethylene
HHV	Higher Heating Value
LDPE	Low Density Polyethylene
LHV	Lower Heating Value
LNG	Liquefied Natural Gas
MCFC	Molten Carbonate Fuel Cell
MDPE	Medium Density Polyethylene
NAP	Amsterdam Ordnance Datum
PAFC	Phosphoric Acid Fuel Cell
PEM(FC)	Proton Electrolyte Membrane (Fuel Cell)
ppm	parts per million (mole)
PSA	Pressure Swing Adsorption
PVC	Polyvinylchloride
SatH	Stad aan 't Haringvliet
SMR	Steam Methane Reforming
THT	Tetrahydrothiophene

List of Constants

R	gas constant	Joule K^{-1} $mole^{-1}$

List of Symbols

α	air fraction	-
μ	dynamic viscosity	Ns mm^{-2}
ν	kinematic viscosity	mm^2 s^{-1}
ρ	density	kg m^{-3}
τ	dimensionless time	-
C	Concentration	mg m^{-3}
D	Diffusion constant	mm^2 s^{-1}
d	diameter	mm
D_0	Diffusion constant at 0°C	mm^2 s^{-1}
d_{in}	inner diameter	mm
d_{out}	outer diameter	mm
D_T	Turbulent diffusivity	mm^2 s^{-1}
E_D	Activation energy for diffusion	Joule $mole^{-1}$
G	Gibbs free energy	Joule
G_f°	Standard Gibbs free energy of formation	Joule/-mole
H	Enthalpy	Joule
H_S	Enthalpy of solution	Joule $mole^{-1}$
J	Flux	mg mm^{-2} s^{-1}
L	pipeline length	mm
M	Molair mass	g m^{-1}
m	mass	mg
P	Permeability constant	cm^3 cm^{-1} s^{-1} atm^{-1}
p	pressure	Pa
p_p	partial pressure	Pa
Q	Volumetric flow rate	m^3 s^{-1}
R	dimensionless radial distance	-
r	radial distance	mm
r_m	average radius	mm
r_{in}	inner radius	mm
r_{out}	outer radius	mm
S	Solubility constant	cm^3 cm^{-3} atm^{-1}
s	Entropy	Joule/K
S_0	Solubility constant at 0°C	cm^3 cm^{-3} atm^{-1}
T	Temperature	° C, K
t	time	s
u_τ	friction velocity	mm s^{-1}
V	volume	m^3
v	flow velocity	mm s^{-1}
v_{mean}	average flow velocity	mm s^{-1}
v_T	turbulent flow velocity	mm s^{-1}
w	wall thickness	mm
x	axial distance	m
Re	Reynolds Number	-

Contents

1

Introduction

In 1959 the largest European natural gas reserve was discovered in Groningen, the Netherlands. Natural gas was seen as a cleaner gas than the traditional town gas, which was produced from coal and contains carbon monoxide. A national operation started to provide households with a natural gas connection and to convert every stove. Within 4.5 years the changeover from town gas to natural gas in every Dutch household had been completed. The Netherlands became the largest natural gas producers and has a leading position in the European gas market.

After the successful gas transition in the 60s, the Netherlands is about to face the same fate again because of two important motivations. Starting from 2014, the inhabitants in the vicinity of the gas fields areas protested against gas extraction as a consequence of increased induced earthquakes. The Rutte government decided to cut down on gas extraction until completely shutting it down in 2030. The second motive is that alternative energy sources are needed to succeed in cutting greenhouse gas emissions. This means that carbon containing natural gas, which has a contribution of almost 40% of the total Dutch energy use, needs to be replaced [1]. Over the last few years, hydrogen has gained popularity as an energy carrier and plays an important role in the climate agreement [2]. Multiple reports predict a prominent role for the Netherlands in a hydrogen economy [3–5]. In accordance with Figure 1.1, the climate agreement states that hydrogen will play the following 5 prominent roles:

- As GHG emission free feedstock in processes. The current hydrogen demand in industry will grow as a consequence of the rise of new chemical processes.
- As a source of high temperature heat for industry. Hydrogen generates heat more energy efficiently than electricity predominately at temperatures from 250 °C.
- To compensate for the difference between renewably generated electricity supply and demand. At moments of electricity oversupply, electricity can be transformed to hydrogen by electrolysis, and converted back to electricity when needed. Hydrogen has proven to have a better performance on long term energy storage compared to batteries.
- As fuel in energy-intensive mobility and transport. The advantage of hydrogen fuel cell vehicles is that large amounts of energy can be stored in tanks enabling large driving ranges. Electric vehicles can replace the passenger vehicles covering average distances.
- As energy carrier in households in areas where all-electric, a heating network, isolation and geothermal are impracticable options for heat supply [2].

Currently there are two existing methods to transport hydrogen: via tube trailers or liquid hydrogen tankers. To transport hydrogen through tube trailers, hydrogen first needs to be compressed to approximately 500 bar. Using tube trailers is feasible for low demand and short distances, but further scale-up is limited. Liquid hydrogen tankers have more capacity than tube trailers and could be interesting for overseas transport. However, neither of these solutions offer the possibility of a gas infrastructure on big scale, while this is needed in order for hydrogen to fulfill the five roles above.

The most profound advantage of hydrogen as energy carrier is the ability to be distributed via the existing gas grid. In fact, according to Terlouw et al., making use of the existing gas grid for the distribution of renewable and low-carbon gases can save the EU €217 billion annually compared to a completely electrified energy supply in households [7]. Recently a study by Hermkens et al. has been published in which it is found that the materials and components of the existing Dutch gas grid are suitable for the distribution of hydrogen [8]. This requires for a few adjustments in the grid, as a result of hydrogen's smaller molecule size, lower energy density, broader flammability range and flame speed compared to natural gas. In addition, similar to natural gas, hydrogen flames are invisible and scentless. Also on the side of the end-user there will be changes required, as with a different gas comes different end-use appliances. Especially hydrogen fuel cells are gaining popularity, as they offer a clean alternative for gasoline vehicles. The same fuel cells are known to have a degraded performance as a result of impurities in hydrogen fuel and thus demand high purity fuel, while hydrogen burners, for example, are not that selective. The fact that polymers are dominant materials in the distribution grid and that the pipelines have been distributing natural gas for several decades leads to the suspicion that high hydrogen purity might not be achieved without the addition of a purification system. It is assumed that air could permeate into polymer pipelines and dilute the hydrogen fuel. Furthermore, it is known that the plastic walls of the pipelines are absorbed with elements of natural gas after several decades of distribution. This is

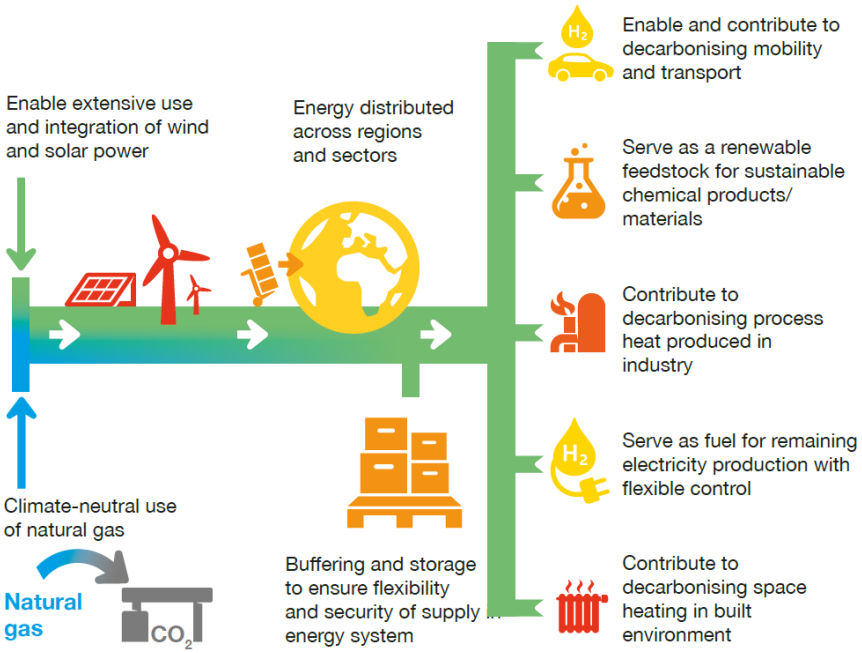

Figure 1.1: The five functions and roles of hydrogen for the future [5, 6]

also expected to cause a decreased purity of hydrogen fuel upon supply to the end-user. Distribution network operators currently ensure that natural gas is distributed according to gas quality regulation. Similar regulations are expected in a future hydrogen grid. While high purity hydrogen fuel comes at a high cost, so do fuel cells that are tolerant to low purity hydrogen. What follows is a chicken or egg question of what hydrogen purity will become the standard in a future hydrogen grid.

The objective of this research is to analyse the hydrogen quality through the existing gas grid. This includes the entire hydrogen supply chain from production to end-use, but the main focus of this study is to find the influences of distribution through the existing gas grid on the hydrogen quality. Quantifying the contamination caused by pipeline distribution is relevant for the future establishment of a hydrogen grid, as impurities in hydrogen fuel have consequences for the end-user. The coming sections will provide background information and will elaborate on the scope, research questions and methodology.

1.1. Background

The current day gas grid has proven its reliability and safety after decades of being in operation. Compared to the electricity grid, the gas grid delivers ten times the amount of energy and has a four times larger storage capacity, also called *linepack*. Distribution network operator (DNO) Stedin is the owner of the distribution grid in the most dense urban areas in the Netherlands. As DNO, Stedin is expected to anticipate on developments in the future energy supply. This is a challenge, because sustainable heat supply is a complex issue.

This chapter will provide useful background information for this thesis. Firstly, the scale of the problem will become clear as the natural gas dependency in the energy supply is elaborated upon. Then the lay-out of the Dutch gas grid will be explained, including how it is operated and by whom. Afterwards alternatives for hydrogen as low-carbon heat suppliers are given. Then the differences between hydrogen and natural gas are listed.

1.1.1. Gas dependency in the Dutch energy supply

The Dutch energy supply is heavily reliant on natural gas. In fact, natural gas has the largest share in the annual energy consumption, that is 40% in 2018 equal to 1,243 PJ [9]. Of this 1,243 PJ, 60% is for direct use and 40% is used for the conversion to electricity.

Figure 1.2 shows the energy consumption curve throughout one year. Whereas the electricity consumption is more or less constant throughout the year, except for small fluctuations, the gas demand has both daily and seasonal fluctuations. Similar consumption curves can be found in countries with similar climates. In countries with hotter climates the electricity

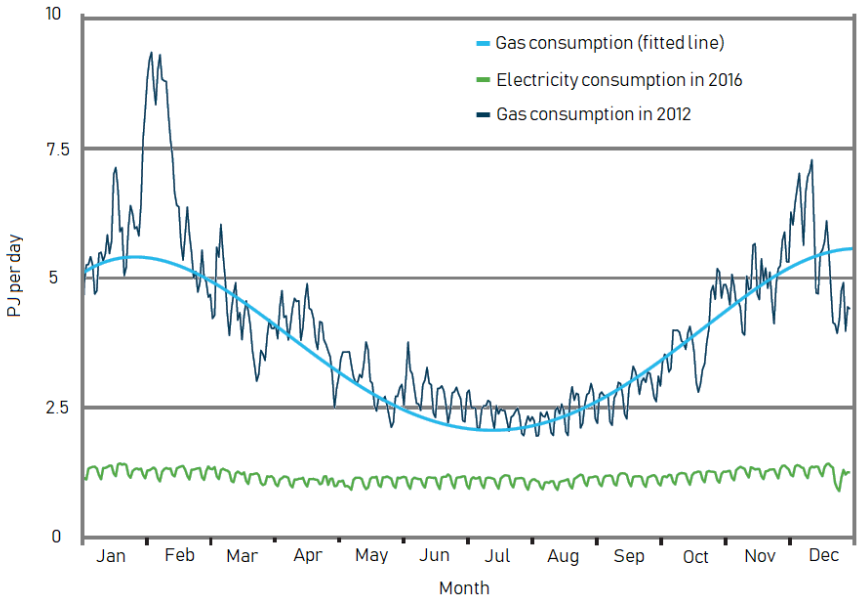

Figure 1.2: The total electricity and natural gas consumption profile in PJ per day. The green line represents the electricity demand. The dark blue line represents the gas consumption in 2012, which included a cold winter. The light blue line represents a fitted line showing the trend of gas consumption throughout a year. Edited from EBN.

demand is dominating due to extensive use of air conditioning and less use of space heating. It is also expected that due to climate change, the gas demand curve will slightly flatten. In Dutch households 82% of the energy consumption is heat, of which 87% is powered by natural gas [9]. Gas is used for space heating by CVs (78 %), for heating water heating by boilers (20%), or to cook with (2%), on hobs and gas powered ovens [10]. Partly because of this, the share of natural gas in energy consumption for heat and cooling is the largest in the Netherlands when compared to other European countries.

The total natural gas demand can be supplied by the Slochteren gas refinery. However, as a consequence of the induced earthquakes in Groningen, the production has already been halved in reference to 2013 (1,160 PJ in 2018 compared to 2,600 PJ in 2013). Instead gas is imported and as a result, the gas consumption has been stable around 1,300 PJ for a couple of decades, while the goal is to eventually reduce gas production to zero to zero [1].

1.1.2. Options for sustainable heat

While renewable electricity is gaining momentum, the transition to sustainable heat is more complex. Due to the fact that the heat demand is larger than the electricity demand in countries with a cold climate, sustainable heat asks for a large-scale solution. Most presumably in the future sustainable heat will be provided by a mix of solutions. Hydrogen promises to fulfill an important role in the future energy supply, as there are many benefits:

- The ability to recycle grid assets which comes with cost-effectiveness
- The increase in flexibility of renewable energy sources
- The familiar benefits of gas, among others: big storage capacity, robustness, low transmission costs.
- Its scalability offers an effective route to achieve climate goals
- It offers the Netherlands to take the leading role in the hydrogen economy
- Job creation

Beside hydrogen there are other options for sustainable heat:

Biogas

Biogas is produced from organic material such as agricultural waste and can be turned into biomethane when upgraded with a booster. It can be used for similar purposes as natural gas. Biogas is an advantageous option for sustainable heat because similar to hydrogen, it can be transported and distributed through the existing gas grid. A disadvantage of biogas compared to hydrogen is that it emits CO_2, as biogas contains carbon. Biogas as waste product from agricultural waste

contributed to 0.4% of the gas supply in 2018 [1]. The biggest issue around biogas lies in its limited availability and the debate surrounding its questionable sustainability. As the Netherlands is densely populated, and Stedin area even more so, from the current prospect biogas will not succeed in becoming a large scale option.

Electrification

All-electric heat pumps, electric vehicles and induction cooking are alternatives for the use of natural gas in households. All-electric heat pumps are, however, a big investment and depending on the situation can not easily be placed in townhouses because of the required outside area for the installation. In areas with predominately detached houses electrification is therefore a plausible solution. An advantage of electric vehicles over hydrogen vehicles is smaller required storage space. Electric vehicles have a head start on hydrogen cars and are therefore momentarily a preferred alternative for gasoline passenger cars. A problem of electrification is the increased strain on the electricity grid. The current grid is reaching its maximum capacity and upgrading the electricity grid is expensive. In addition, transporting electricity via cables is ten to twenty times more expensive compared to transporting molecules via pipelines.

District heating network

District heating networks are estimated to be able to provide heat for half of the grid connections by 2050. The heat comes from surrounding (gas fired) power plants and industry. This heat can be waste heat from industry or can be produced according to the local heat demand. A district heating network is a feasible option for sustainable heat in populous areas with older buildings adjacent to industrial areas providing excess heat.

1.1.3. The Dutch Gas Grid

When the Groningen gas field was discovered it was then the largest natural gas reserve in the world. As a result, the Netherlands have been a natural gas exporter over the decades that followed, exporting 1,500 PJ per year on average [1]. 2018 was the first year where the amount of gas import exceeded the amount of export [11]. Gas can be imported either by pipeline from Russia or Norway or in the form of LNG from Qatar. There is a difference in composition of the gas when comparing Groningen gas (G-gas or L-Gas) to gas from Russia or Norway (H-gas). As a result of this difference, the Wobbe-index, stating the amount of stored energy, is lower for G-gas than for H-gas. G-gas is thus low calorific gas, whereas H-gas has a higher calorific value.

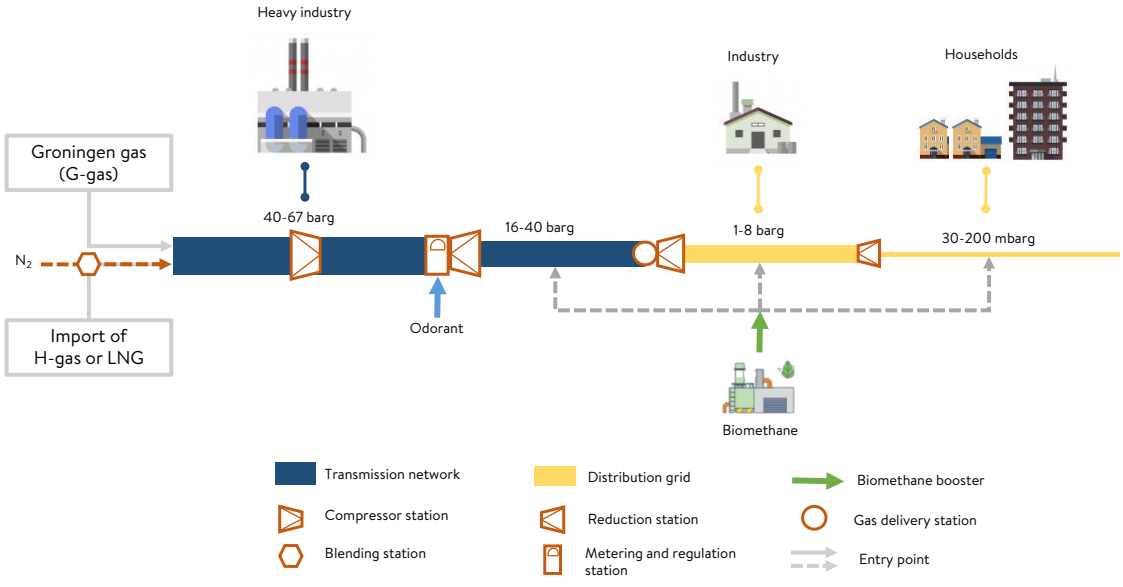

Figure 1.3: Lay-out of the Dutch natural gas grid.

H-gas is only consumed by industry, but can also be admixed with nitrogen in blending stations to be added with and be used as G-gas. The imported gas reaches the Netherlands either through the pipeline, or transported in the form of LNG.

The Dutch government has appointed Gasunie Transport Services (GTS) owner of the national transmission network, which exists of a high pressure grid (40-67 bar atm) and a medium pressure grid (16-40 bar atm). GTS is responsible for maintaining the national transmission network and balancing demand and supply. GTS delivers H-gas and G-gas via the high pressure grid directly to industrial consumers. In the high pressure grid compressor stations compress natural gas to allow for further transport. H-gas can also be blended with nitrogen, so that it can be fed into the G-gas grid. GTS reduces the pressure from high pressure to medium pressure at 93 metering and regulation stations in the country. At most of these stations odorant is added to natural gas, as natural gas is an odorless gas otherwise. GTS delivers G-gas via the high pressure grid and the medium pressure grid to regional transport network at 8 bar, which is owned and operated by regional network operators, such as Stedin. This happens at *gas delivery stations*. At *district stations* the pressure from 8 barg pipelines is reduced to a lower pressure. Within the distribution network the pressure varies between 30 mbarg and 8 barg. Larger consumers (such as farms and green houses) are directly connected to the regional distribution network through a *house connection station*, whereas households are connected to lower pressured gas (<1 bar atm). Components within the distribution network assure safe and secure supply. Rubber and polyoxymethylene seals are used to interconnect grid components. The 8 barg pipelines are predominantly made from steel, but polyethylene is increasingly replacing these. Pipelines are interconnected by a weld connection whereas PVC/CPE pipelines and pipelines with smaller diameter can also be connected through a sleeve. As PVC/CPE cannot be welded, this material is not used for higher pressure pipelines. Once every five years each pipeline undergoes above-ground leak detection. The main causes of leaks are subsidence and excavation damage [12].

The distribution grid is a robust network, as it is designed to withstand the yearly peak demand which takes place at -12 °C ambient temperature. As -12 °C occurs only 13 hours per year on average [13], in all the remaining hours in the year the grid is overdesigned, which indicates the large capacity of the network. The electricity grid on the other hand, is increasingly being strained by new renewable energy plants while the gas grid is capable of expanding.

The upcoming changes in the Dutch energy system calls for distribution network operators to deliberately anticipate developments at an early stage. Some relevant developments are the susceptibility of the electricity grid to decentralised renewable energy feed-in, disconnecting current clients from the gas grid, the feed-in of green gases and hydrogen. Stedin operates in provinces South Holland, Utrecht and also in a couple of figurative islands in the provinces North Holland and Friesland. The responsibilities of a distribution network operator are:

- Connecting customers with the gas and electricity distribution network and operating these networks.
- Ensuring safety surrounding the gas and electricity network and security of supply.
- Being able to do investments on network extensions cost-efficiently and timely.

As Stedin is an initiator of this research, the focus of this research will be on the distribution network.

1.1.4. Differences between hydrogen and natural gas

While it has been proven by Hermkens et al. that the gas distribution grid is capable of distributing hydrogen, there are many differences between the two gases. Alternatively to natural gas, hydrogen is a clean, carbon-free gas. Relevant differences in properties of the two gases are listed in Table 1.1.

In addition to Table 1.1, hydrogen is the smallest existing molecule in nature. The lower and higher heating values (LHV and HHV, respectively) are given in weight and volume, in Table 1.1 and stand for the amount of heat released at combustion. The heating values per volume for hydrogen are approximately three times smaller than the heating values for G-gas. As a result, to achieve the same amount of energy to flow through the grid there are three times higher flow velocities needed. Currently the maximum allowable flow velocity is set to 30 m/s, because of limitations regarding noise hindrance. Normally the gas consumption of consumers is measured with net metering devices measuring the volumetric flow. With three times higher flow velocities it is uncertain whether the existing net metering devices will measure the flow rates with similar accuracy. Whether three times higher flow velocities will be achieved is dependent on the future gas demand. For example, hydrogen appliances might have a higher efficiency compared to natural gas, thus lowering the gas demand.

G-gas and hydrogen are both odourless, but hydrogen flames are nearly invisible. Combining this with the wider flammability range and lower ignition energy raises the issue of safety. But hydrogen has a small molecular diameter and large volatility and therefore travels through air with 6 times the speed of natural gas [15]. However, the ignition energy of hydrogen is dependent on the concentration of hydrogen in air. The ignition energies stated in Table 1.1 are the minimum ignition energies, and at low concentrations of hydrogen in air the amount of energy to initiate combustion is similar to natural gas [15]. Hydrogen rather disperses than accumulate, thus lowering the chance of ignition. Nevertheless, extra precaution with hydrogen distribution is advisory and more information is needed about the risk of excavation damage or construction work. Also, the twenty times lower dynamic viscosity of hydrogen will result in a twenty times higher volumetric leak

Table 1.1: Differences between hydrogen and natural gas [6, 8, 14]

Property	Hydrogen	G-gas	Unit
Molecular formula	H_2	CH_4 (81.3%), N_2 (14.3%), C_2H_4 (2.9%), C_3H_8, C_4H_{10}, C_5H_{12}, C_6H_14, O_2 and CO_2 (<1%) [a]	-
Molar mass	2.02	18.64	g/mole
Lower heating value (LHV)	33.3 3.0	10.6 8.8	kWh/kg kWh/Nm^3
Higher heating value (HHV)	39.4 3.5	11.7 9.8	kWh/kg kWh/Nm^3
Flammability range	4.1 - 74	4.7 - 16.6	vol% in air
Ignition energy	0.02	0.2	mJ
Dynamic viscosity	0.88×10^{-6}	1.1×10^{-6}	Pa s

[a] An indication of a possible composition, the exact composition can vary.

through cracks compared to natural gas [8]. A specific hydrogen BowTie risk analysis method is expected to be the subject of one of the coming projects by the hydrogen project group of Dutch DNOs and can elaborate on this. All in all, there is no indication that the distribution of hydrogen will be insufficiently safe. Differences in properties also have implications for the design of hydrogen appliances, but more about this can be read in Chapter 2.

1.1.5. The pathway to 100% hydrogen

The roll-out of a hydrogen grid will require a step-by-step approach. A study by Oprinsen describes a plan for the conversion to a hydrogen grid for the Dutch village Stad aan 't Haringvliet. For such a conversion, all the pipelines need to be rinsed to assure the absence of natural gas in the pipelines, and the gas appliances in the households need to be replaced for hydrogen appliances. The area needs to be sectioned into smaller isolated areas to avoid that the entire area is cut off from gas during the entire period of construction.

An important role in this operation can be fulfilled by blending hydrogen in the gas grid. Blending can provide a short to medium term solution to increase integration of renewables in the grid, while increasing the flexibility of renewables and avoiding straining the electricity grid. Melaina et al. indicate the feasbility of blending low concentrations of hydrogen (5 - 15 vol%) produced with renewables into the grid without increasing safety risks [17]. Blending can pave the way for hydrogen by creating more demand on the hydrogen market. The possibilities and advantages of blending is a current research topic. An advantage of blending is the gradual changeover to a different gas, as it could be rolled out in phases, step by step increasing the injection of hydrogen and reducing the natural gas consumption. However, at a certain critical hydrogen - natural gas ratio end-use appliances do no longer function. The reason behind this is elaborated upon in Chapter 2. Stedin has gained experience with blending during a 4-year project on Ameland, one of the Wadden islands [18]. Concentrations of up to 20% hydrogen were blended in the grid, and in a laboratory natural gas cookers and burners were tested with a concentration of 30%. The grid materials and components were tested and had not shown irregularities. There have also been no relevant complaints from the inhabitants in Ameland. Overall, the results of the experiment in Ameland indicate that blending can be a stepping stone for a 100% hydrogen grid.

1.1.6. Relevant ongoing pilot projects

Not only in the Netherlands much research is being done, but also neighbouring countries are gaining knowledge and experience on residential use of hydrogen. At the moment there are a number of ongoing pilot projects that are, or will be relevant to this research:

- The Power2Gas project in Rozenburg, South-Holland where an electrolyser was placed to heat one apartment complex. First the electrolyser produced synthetic natural gas but starting from 2019 it produced hydrogen. Hydrogen is led to a hydrogen boiler room, from which heat is distributed to the apartments.
- H21 North of England in Leeds, where 3.7 million households will be converted to hydrogen [19].

- HyNet in the North West of England, a recently kicked-off project planning on realising an entire hydrogen economy involving 2 million households [20].
- A hydrogen street in the Green Village on the campus of TU Delft, hosted by a collaboration of DNOs, under which Stedin.
- Entrance in Groningen is similar to the hydrogen street in the Green Village, also hosted by a collaboration of gas companies.
- HYPOS H2-netz, a project by Mitnetz in Germany to gain experience with hydrogen through the existing distribution network.

1.2. Methodology

Every link in the chain has its contribution to the hydrogen quality upon arrival by the end user. The chain can be divided into four parts: production, transport, distribution and end use, as can be seen in Figure 1.4. Each stage has its implication

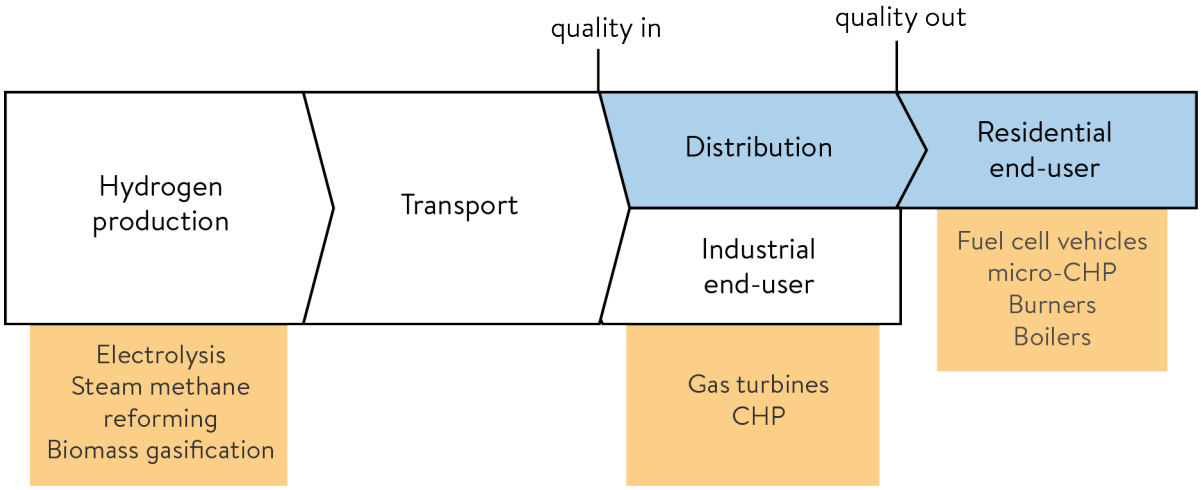

Figure 1.4: Flowchart of the research's methodology.

on the overall hydrogen quality that needs to be considered. The chain starts at the production of hydrogen, which is relevant because of the byproducts that are produced. Each production technology has different byproducts that are always, to a certain extent, present in the product. After production the hydrogen enters the national transport network. No significant impacts are expected on the hydrogen quality during this stage, as the existing industrial hydrogen pipeline, which is similar to natural gas transport pipelines, has not shown any issues. Hydrogen then enters the distribution network. In this stage lies the focus of this research. The distribution infrastructure connects end-users to the hydrogen network. Beside the conversion box in Figure 1.4 are a number of conversion technologies mentioned: fuel cells, burners, boilers and CHP. The tolerance towards impurities in the hydrogen fuel of each appliance differs, and for that reason each needs to be considered. Inconsistently, the sequence in Figure 1.4 does not correspond with the order in which they are treated. Firstly, research has been done on existing and future hydrogen end use applications to find their tolerance to impurities. Especially fuel cells have specific intolerance to impurities which is the root of this hydrogen quality issue.

A study by Hermkens et al. invites other researchers to do further research on the suitability of the distribution grid for high purity hydrogen. It raises concern about four causes of contamination in particular:

1. Elements in natural gas that are absorbed in the pipe wall. Especially the odourant used in natural gas, tetrahydrothiophene, but also higher alkanes are a threat to the performance of fuel cells.
2. Air surrounding the pipelines has the ability to permeate into the pipe as a result of a concentration difference.
3. Dust and dirt particles inevitably exist in the current day gas grid as a result of maintenance work but also steel corrosion.
4. Leaks in the pipeline serving as an entrance to contaminants.

These sources of contamination were adopted in this research and the contamination as a result of hydrogen production was added as a fifth source. The five sources of contamination has been confirmed by representatives from other Dutch network operators during a monthly meeting about the development of a national hydrogen grid.

To gain more understanding of these five topics, open literature was collected as well as literature from consulting companies, such as *Kiwa* and *DNV GL*, and others. Also other DNOs have contributed to this research by sharing information. However, because of the novelty of the subject, only theoretical studies are available rather than experimental studies. Figure 1.5 visualises the framework persisted in this research.

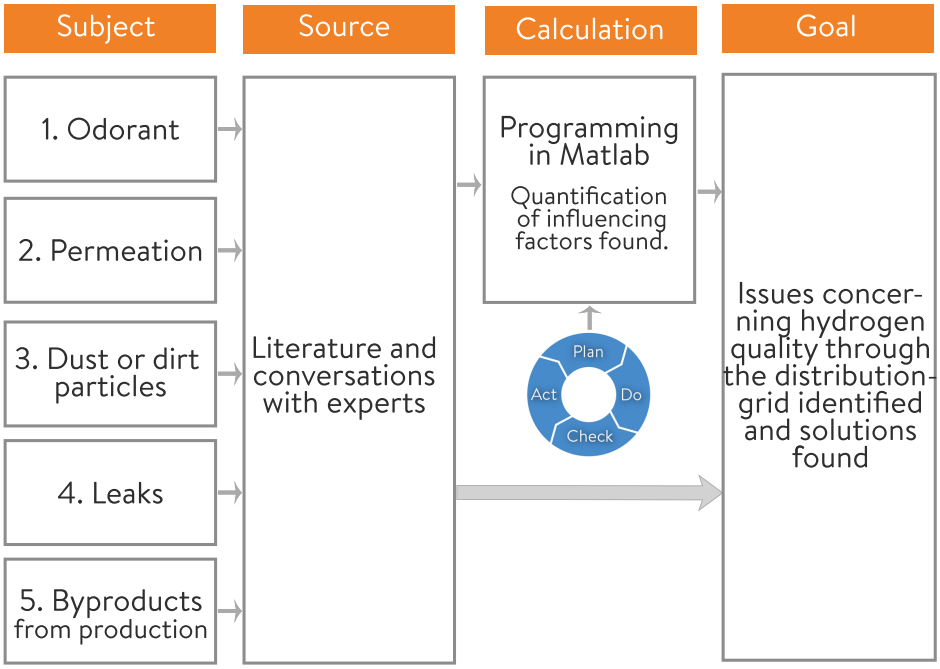

Figure 1.5: Thesis' framework.

Out of the five subjects in Figure 1.5, the subject of byproducts from hydrogen production technologies is found substantially in literature. The remaining four subjects are influences that also currently exist in the gas grid. Knowledge gaps were found upon doing literture review on the current state of the gas grid and the influences of distribution on the natural gas quality. As residential consumers predominantly utilise gas in combustion appliances, such as boilers and central heating, the gas quality is of less importance now, while it will become very relevant in a hydrogen grid. In absence of experimental research about the four subjects in Figure 1.5, odorant, permeation, particles and leaks a theoretical approach was chosen when possible. Permeation of gases through solids is a phenomenon that has been a subject of interest in the last decades, and based on these mature theories found in literature a computation model was constructed using MATLAB. As a result of the abundance of theoretical framework concerning this phenomenon, contamination caused by permeation has become the focus of this research. As permeation can be solved for a wide range of variables, the model was used to relate certain situations in the grid with the amount of permeation. For example, the amount of contamination caused by permeation of air into a pipeline is dependent on the material of that pipeline, but also on the length of the pipeline. The results from the computation model are used to find the significance of contamination under different situations. These results are then compared with literature to get insight on whether or not problems will occur with connecting hydrogen appliances to the distribution grid, and if so, to identify what these problems are and how they can be solved.

1.3. Research questions

The above leads to the following main research question:

What influences will distribution through the existing gas grid have on the quality of hydrogen?

To answer the main research questions the following sub-questions need to be addressed:

1. Which impurities can be found in hydrogen fuel caused by known production technologies?
2. What are the relevant parameters which determine the hydrogen quality in the distribution grid?
3. How tolerant are different fuel cell technologies to impurities in the hydrogen fuel?

4. How tolerant are other hydrogen fueled appliances to impurities?
5. What options are there to guarantee high purity hydrogen?

1.4. Scope

In this study calculations have been performed on a fragment of the actual grid. The grid in the town Stad aan 't Haringvliet in Stedin area has been taken as case study, as it will be the first town in the Netherlands to have a hydrogen grid. Stad aan 't Haringvliet (SatH) is a village on the island Goeree-Overvlakkee. and has over 1,300 residents in almost 600 households. There are about 100 businesses in the area, but there is no industry located. Nearly all buildings are from before the year 2000, and as a result most buildings are poorly insulated.

(a) Goeree-Overvlakkee's location within the Netherlands.

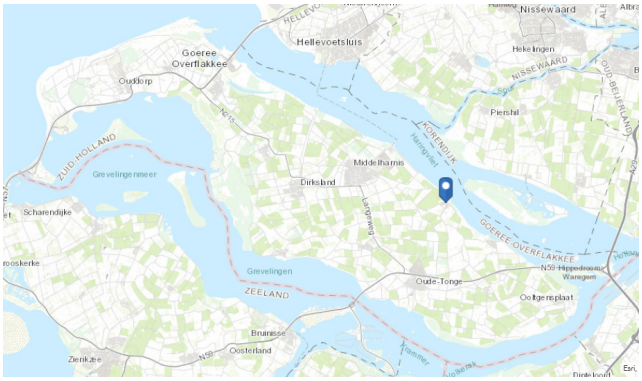

(b) A closer view of Goeree-Overvlakkee. The pin point represents the location of the village Stad aan 't Haringvliet.

Figure 1.6: The geographical location of Goeree-Overvlakkee and Stad aan 't Haringvliet.

In 2017 a covenant was signed between the government and multiple companies, under which Stedin, called *Programme green hydrogen economy*. As part of the programme Goeree-Overvlakkee will transform into an *energy island*, starting with establishing a hydrogen grid in Stad aan 't Haringvliet. Goeree-Overvlakkee was selected for this programme because of its advantageous location near an existing industrial hydrogen pipeline and potential for solar and wind energy. The properties of the grid in this area used in the calculations are similar to any other location in the Netherlands. Similar calculations for a different grid in another country, for example, might result in different results. Any effects of pipeline transport through the transmission network are neglected in this study. This study rather focuses on the low pressure distribution grid. While blending has the potential to play an important role in the roll-out of a hydrogen grid, this report focuses on the long term by considering a 100% hydrogen grid. Furthermore, despite impurities from hydrogen production being treated in this study, the calculations are based on the simplification that hydrogen enters the distribution grid without any contamination. As especially a challenge lies in delivering high quality hydrogen at the end of a long and branched network, the focus of this report is on residential users. As a result, hydrogen appliances for residential users, such as boilers, cookers or stationary systems for buildings, are the most relevant for this study.

1.5. Structure

This report starts with an overview of hydrogen technologies; how hydrogen can be produced and consumed, and what the ongoing and future pilot projects involving hydrogen are. Chapter 3 is dedicated to the significance of impurities, where they come from and what impact they have on hydrogen appliances mentioned in Chapter 2. Numbers are gathered from literature on the limits of these applications on the tolerance to impurities. Chapter 3 also gives solutions for how hydrogen can be purified. Chapter 4 explains the theoretical framework behind the computational model surrounding the inward permeation, from which the results are presented in Chapter 5. The results are discussed in Chapter 6, which leads to the final conclusions that can be drawn from this research in Chapter 7. Finally, in the same chapter the limitations of this report and suggestions for further research are given.

2

Hydrogen production, transport and consumption

Despite hydrogen usually being associated with novel energy carriers, the Netherlands has in fact already been a big European hydrogen producer for years. The current hydrogen production in the Netherlands is estimated to be 9.2 billion m^3 per year, which is mostly used in industry [21].

This chapter provides an overview of a future hydrogen economy in the Netherlands, including production technologies and end-use applications. Firstly, an overview is given of future plans for hydrogen producers. Secondly, plans for a national hydrogen transport network are explained. Thirdly, hydrogen end-use applications are listed.

2.1. Production Technologies

Out of the total current hydrogen production, 80% is produced by reforming natural gas and 20% is a byproduct from industry [22]. In both cases the product is considered as *grey hydrogen*, which means that it is produced from fossil fuels, often natural gas, and includes CO_2 as byproduct. In combination with carbon capture, utilisation and storage (CCUS), grey hydrogen can be turned into blue hydrogen. The addition of CCUS leads to an increase in CAPEX of approximately 50% [23]. At this moment the most inexpensive technology to produce hydrogen is by reforming natural gas. The coming years small-scale hydrogen producers will arise, until large-scale production technologies become competitive with grey hydrogen production technologies. Another scenario is that hydrogen will be produced with grey technologies in countries where natural gas will continue to be abundant and exported, as fuel costs account for 45% to 75% of total costs [23]. According to the most recent future prospect of hydrogen by IEA, hydrogen produced from natural gas in the Middle-East is more than 1.5 times as cheap as hydrogen produced in Europe including CCUS, and almost twice as cheap excluding CCUS [23]. In Figure 2.1 the levelised costs (production costs) of green hydrogen production technologies are compared.

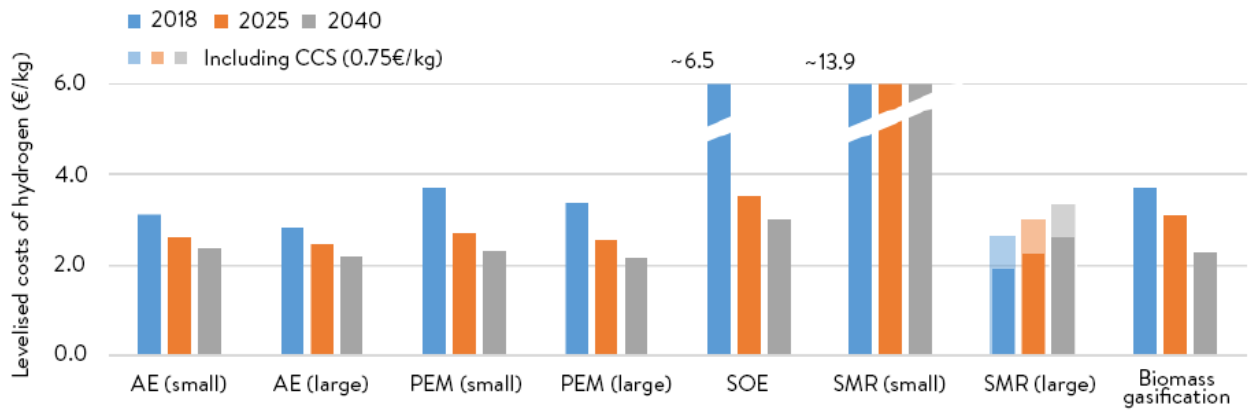

Figure 2.1: The expected development in levelised costs of green hydrogen for alkaline electrolysis (small and large scale), PEM electrolysis (small and large scale), Solid Oxide electrolysis, steam methane reforming with biomethane (small and large scale) and biomass gasification [24].

It is expected that in 2040 the production costs of all green hydrogen production technologies will be similar. However, these costs are still above the costs for hydrogen production from natural gas: $1.7/kg, or $2.3/kg with CCUS in 2018 (is approximately equal to €1.5/kg and €2.3/kg) [23]. Compared to the still be To summarise, based on current development it can be expected that the trend for hydrogen producers will be as follows:

- Hydrogen will be produced decentralised and will come from varying technologies.
- It is possible that at a certain point the demand for hydrogen will exceed the Dutch capacity for hydrogen production. In this case hydrogen might be imported from countries that have an abundance in either natural gas resources or on longer term renewable energy.

- While first hydrogen supply will come from reforming natural gas (grey), the number of hydrogen produced by blue or green hydrogen will increase as wind and PV production increase, and blue and green hydrogen production become cost-competitive.

Alternatively, hydrogen can be produced from coal. Hydrogen production through coal gasification is a well advanced technology, especially in China where 80% of the coal gasification plants are located [23]. Hydrogen production from coal emits two times as much CO_2 as hydrogen production from natural gas. Therefore coal gasification is not expected to play a role in the future supply of hydrogen and is out of the scope of this research. The coming sections elaborates on four hydrogen production technologies. The first three technologies are grey technologies, but can be turned into blue production technologies by the addition of CCUS. Electrolysis is the subject of Subsection 2.1.4, and is a green technology.

2.1.1. Steam methane reforming

Steam methane reforming (SMR) is a process to strip the carbon from methane in natural gas and form hydrogen. Reforming is worldwide the most common technology for producing hydrogen today. Figure 2.2 illustrates a simplified overview of the SMR process.

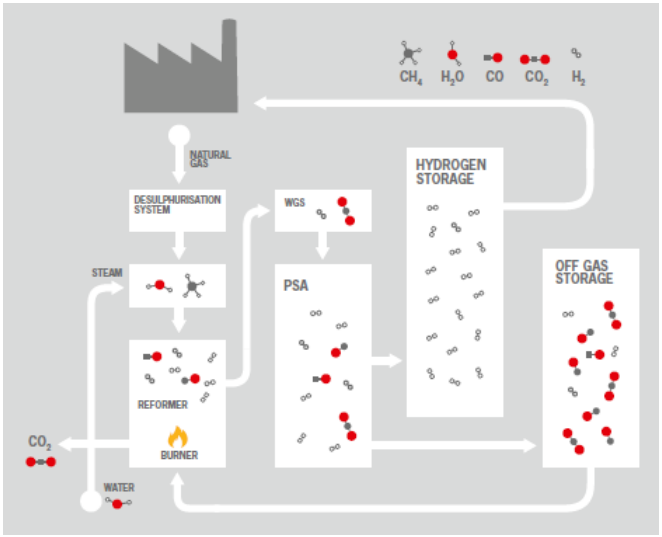

Figure 2.2: A typical steam methane reforming process taken from the brochure of Hygear [25]. After desulphurisation of natural gas in the first step natural gas is simply noted as methane.

First the sulphur in natural gas is removed in the desulphurisation system to avoid interaction with steam, which is a reactant in reforming methane. Desulphurisation happens in two steps; first all sulphur compounds are converted into H_2S compounds and afterwards natural gas and H_2S is separated by adsorption [26]. Also the water used to make steam is purified prior to entry. The pure water steam is introduced to sulphur-free methane in metal catalyst filled tubes at a temperature of 700°C - 1,100°C [27]. Then the natural gas and steam mixture is heated to be reformed catalytically through the following reaction:

$$CH_4 + H_2O(\text{steam}) \rightarrow CO + 3H_2. \tag{2.1}$$

The product carbon monoxide is internally reformed as a result of the high temperatures through the water gas shift (WGS) reaction:

$$CO + H_2O \rightarrow CO_2 + H_2. \tag{2.2}$$

A result of this reaction is a higher hydrogen yield. The product from the water gas shift reaction is led into the pressure swing adsorber (PSA), that filters out impurities (off gas) in the mixture. In Subsection 3.3.1 the technology of pressure swing adsorption is elaborated. In PSA hydrogen is separated from the off gases, which can be reused as fuel for the burner delivering the required heat for the process. SMR systems often operate at pressures in the range of 20 bar to meet the demand from the market, and also to meet the inlet requirements of PSA. The energy conversion efficiency of SMR is approximately 75% [27]. The Hygear SMR unit from Figure 2.2 has a start-up time of 0.5 - 3 hours depending on the operation temperature; 0.5 hours for high temperatures and 3 hours for low temperatures. CO_2 produced by SMR can be captured, thereby decreasing up to 90% of carbon emissions.

2.1.2. Autothermal Reforming

Similar to SMR, autothermal Reforming, or ATR, is a process in which a hydrocarbon is converted into syngas (H_2 and CO). Syngas can be separated into hydrogen and CO as a final step in the process to obtain a pure hydrogen stream. ATR is a combination of SMR and partial oxidation. Whereas in SMR water is used as an oxidant, in partial oxidation oxygen functions as oxidant. Natural gas, refinery offgas or another hydrocarbon is first desulphurised, then pre-heated, optionally pre-reformed and then partially oxidised with oxygen and steam. The resulting reaction becomes:

$$4CH_4 + O_2 + 2H_2O(\text{steam}) \rightarrow 4CO + 10H_2. \tag{2.3}$$

Partial oxidation is an exothermic process and as a result, ATR requires less thermal energy to be applied compared to SMR and the carbon monoxide reforms within the reformer. As a consequence a larger amount of CO_2 can be captured for lower costs compared to SMR [23]. Nevertheless, as oxygen is required for ATR there is additional electricity required resulting in carbon emissions. Dependent on the separation technology, ATR generally produces low quality hydrogen of 90% [21]. The remaining 10% consists of byproducts H_2O and CO. ATR produces a lower quality fuel than SMR because of the complexity of separating CO from hydrogen. The pilot project in Leeds, UK uses ATR combined with CCS, because of the beneficial CAPEX and OPEX and its proven technology, among other things [19].

2.1.3. Biomass Gasification

The gasification of biomass is an endothermic thermochemical process where organic material is converted to syngas, which is a flammable gas mixture of hydrocarbons, H_2, H_2O, CO and CO_2. Upon entry to the reactor biomass is first dried, as the biomass needs to be below a certain moisture content. Four common biomass gasification reactor types are fixed bed, fluidised bed, circulating fluidised bed and entrained flow gasifier. Depending on the reactor type, biomass potentially needs to be pre-treated through pyrolysis or torrefaction for the improvement of the processes in the reactor. The production of syngas takes place in a gasifier with the presence of an added oxidant (O_2, H_2O or air). The produced syngas is then cooled to correspond to the favourable low temperature condition for the water gas shift reaction that follows afterwards. CO is shifted to CO_2, while simultaneously H_2 is produced. A general reaction formula for biomass gasification is [28]:

$$\alpha C_l H_m O_n + \beta H_2O + \text{heat} \rightarrow aH_2 + bCO + cO_2 + dCH_4 + eC + f\,\text{tar}, \tag{2.4}$$

in which $C_lH_mO_n$ represents biomass the general formula of biomass. Hydrogen production through biomass gasification is currently in the demonstration phase and is expected to become commercially available for industrial purposes in 5 to 15 years [24]. The green hydrogen road map for the Northern Netherlands by van Wijk includes a 1,000 MW biomass gasification plant by 2026 developed in stages [3]. An advantage of biomass gasification is that a wide range of biomass can be used as input. The prospect of hydrogen produced by biomass gasification is uncertain due to the insufficient availability of biomass. Biomass gasification can rather be seen as a short to medium term solution than as a long term solution. Other more direct applications of biomass, such as biofuels or feedstock are potentially more promising, as the demand for climate friendly carbon will be increasingly high.

2.1.4. Electrolysis

While grey and blue hydrogen production is important for the hydrogen economy, especially in the early stages, the ultimate goal is to have clean power generation by means of green hydrogen. From the current global hydrogen production less than 0.1% is produced from electrolysis [23]. Hydrogen production from electrolysis is most commonly used for consumers that require high purity hydrogen. The concept of electrolysis, splitting H_2O into H_2 and O_2, dates from the 18th century. It goes through the following reaction:

$$2H_2O \rightarrow O_2 + 2H_2. \tag{2.5}$$

This total reaction can be splitted into two half-reactions, which are based on the characteristics of the electrolyser. In all cases, an electric current provided by a power source runs through a circuit, causing electrons to react with H_2O at the cathode. The electrons cause water to reduce through which ions are created. The electrolyte, which is a substance positioned between the anode and the cathode, is permeable only for these ions. The ions travel through the electrolyte towards the anode, where they initiate an oxidation reaction which forms water. Depending on the configuration of the electrolyser, hydrogen is created at the anode and oxygen at the cathode or vice versa.

Approximately 9 litres of water is needed for the production of 1 kg hydrogen [23]. Seawater can be used as a source for H_2O, but desalination is necessary, which increases the costs of electrolysis by approximately €0.01/kg [23]. Electrolysers have the exact opposite working of fuel cells. Because the focus of this research is more on hydrogen consumption, this section only briefly lists the different technologies. A more elaborate explanation about these technologies can be read

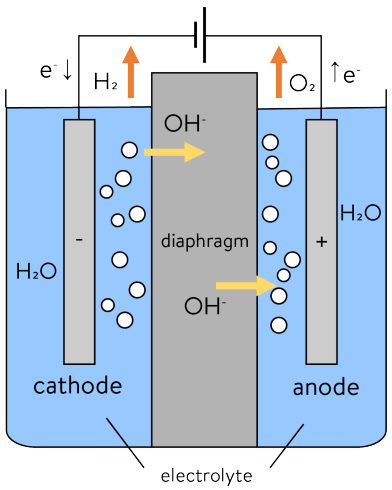

Figure 2.3: Schematic overview of an alkaline electrolyser.

in Section 2.3. Similar to fuel cells, various electrolysis configurations exist, but the most common technologies are Solid Oxide, Alkaline and Proton Exchange Membrane electrolysis. The comparison of hydrogen costs for these technologies can be found from Figure 2.1. Depending on the full load hours of the electrolyser, the costs of electricity can be a large fraction of the total levelised costs of hydrogen, as can be seen from Figure 2.4.

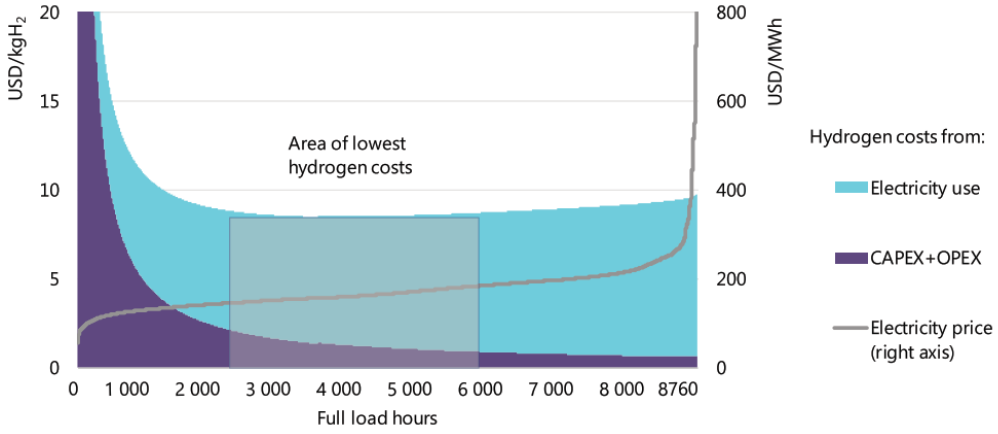

Figure 2.4: Costs of hydrogen production by electrolysis using electricity from the grid from the hydrogen prospect report by IEA. A CAPEX of $800/kW electricity, efficiency of the electrolyser of 64% and discount rate of 8% [23].

At a high number full load hours, the CAPEX account for an increasingly low fraction of the levelised costs of hydrogen. While running electrolysis on cheap surplus renewable energy would seem cost efficient, Figure 2.4 indicates that extracting electricity from the grid for hydrogen production can result in lower levelised costs of hydrogen as a result of a higher number of full load hours. A dedicated renewable energy source for electrolysis could decrease the hydrogen production costs significantly, as costs can be saved on transmission costs.

Alkaline

At this moment Alkaline Electrolysis (AE) is the most advanced technology. An alkaline electrolyer consists of two metal electrodes with a liquid electrolyte, namely a solution of potassium hydroxide and and sodium hydroxide. The two half-reactions of AE are as follows:

$$4OH^- \rightarrow O_2 + 2H_2O + 4e^- \tag{2.6}$$

$$2H_2O + 2e^- \rightarrow H_2 + 2OH^- \tag{2.7}$$

at the anode and cathode, respectively. As shown in Figure 2.3, a diaphragm situated between the anode and the cathode functions as a separation medium for the product gases and as a transport medium for OH^- ions. Due to the highly acidic

environment there are better reaction kinetics and thereby avoiding the need for an expensive catalyst. The efficiency range of an AE is 60 - 80%, depending on the operating temperature and current density. Multiple alkaline electrolysers have been built since the 1920s, up to an electric capacity of 165 MW, but some have also been decommissioned after the introduction of SMR technology [23]. Examples of AE manufacturers and their achieved hydrogen purities are Indian company Airox Nigen Equipments Pvt. Ltd with 99.8 - 99.9998%, market leading Norwegian company Nel Hydrogen Electrolyser with 99.9% and Canadian Hydrogenic Corporation with 99.9% [29]. These purities can be reached after drying to separate water from hydrogen.

Proton Exchange Membrane

The first PEM (proton exchange membrane or polymer exchange membrane) electrolysers were developed for space applications in the USA by General Electric in the 1970s [29]. The PEM electrolyser has a thin solid polymer membrane, that is only permeable to H^+ ions. The two half-reactions in PEM electrolysis are

$$2H_2O \rightarrow 4H^+ + O_2 + 4e^- \tag{2.8}$$

$$2H^+ + 2e^- \rightarrow H_2 \tag{2.9}$$

at the anode and cathode, respectively. It is a relatively expensive technology as a result of high costs for this sophisticated membrane and for precious metals used for the electrodes and catalysts. It is the most effective electrolysis technology, but it is also the technology with the highest degradation. Another advantage of the PEM electrolyser is the high flexibility due to high dynamics, which is beneficial for integration with renewables. PEM electrolysers achieve a higher hydrogen purity over 99.99% than alkaline electrolysers as a result of the presence of alkali in water [24, 29].

Solid Oxide

Solid Oxide electrolysers (SOE) have a solid electrolyte made of a ceramic material. The half-reactions of the SOE are:

$$2O^{2-} \rightarrow O_2 + 4e^- \tag{2.10}$$

$$H_2O + 2e^- \rightarrow H_2 + O^{2-} \tag{2.11}$$

at the anode and cathode, respectively. The material costs are low and the operation temperatures are high. SOEs operate at temperatures above 800°C, thereby increasing the reaction rate. Advantages of this technology are the high efficiency (excluding the energy required for heat), affordable materials and broad range of applications. In addition, in contrast to the alkaline and PEM electrolyer, a SO electrolyser can operate in reverse direction to function as a fuel cell. Due to the high operating temperatures, however, switching on and off is a difficulty as a result of thermal expansions. Cost reductions are expected (Figure 2.1), but the future success of SOEs can not be confirmed yet.

2.1.5. Planned projects

Until now, few definite plans exist for the construction of large-scale hydrogen producers. As a result, the forecast of future hydrogen producers can only be estimated. Before green hydrogen production on large scale can kick-start, renewable energy needs to become more accessible and electrolysis more cost-efficient. There are a couple of pilot projects running, which mostly still are in the feasibility phase. All projects together amount to 588 MW. The projects are:

- Project Duwaal: A Lagerwey and Hygro 4.8 MW turbine integrated with a 2 MW electrolyser in Wieringermeer. Trucks will deliver hydrogen from the storage at 500 bar to five gas stations. It is not sure when the project is expected to be completed.
- ISPT Hydrohub: The Hydrohub in Groningen will facilitate a test centre for a 1 MW electrolyser. It is expected to be completed in 2020.
- A 20 MW electrolyser by Nouryon and Gasunie is planned to be built before 2022 in Delfzijl. The produced hydrogen is meant to fuel 300 buses.
- Tata Steel, Port of Amsterdam and Nouryon are exploring the feasibility of a 100 MW electrolyser in IJmuiden. In 2021 it will be determined if they can start the construction, which will take until 2023.
- The first battolyser of 15 kW/60 kWh was planned to be built in Eemshaven in the beginning of 2019, but has delayed until further notice.
- Engie and Gasunie are planning to start the construction of a 100 MW electrolyser from 2020 in Groningen.
- A collaboration of Gasunie, TenneT and Thyssengas are working on a 100 MW electrolyser in North Germany, planned in 2022.

- BP, Nouryon and Port of Rotterdam have signed a letter of intent to explore the feasibility of a 250 MW electrolyser. The produced hydrogen will be used in the BP refinery in the Port of Rotterdam, which currently consumes grey hydrogen.
- RWE is currently doing a feasbility study on a 100 MW electrolyser in Eemshaven in Groningen.

In addition there is the possibility that the North Sea Wind Power Hub, which is a utility-scale offshore wind farm, with a current capacity of 13 GW and a future capacity of 50 GW in 2030, will be combined with an onsite electrolyser in the future [23].

2.2. Large scale storage and transport

As molecules can be stored more easily than electricity, hydrogen could offer a solution to the inflexibility of renewables. Similar to natural gas, hydrogen can be stored underground. Hydrogen can be stored in man-made salt caverns, or porous rocks such as aquifers, depleted natural gas or oil reservoirs. Compared to salt caverns, aquifers and depleted natural gas or oil reservoirs have a much larger scale of several billion m^3. Underground storage involves low investment costs, a small footprint and allows for high pressures. The pilot project in Leeds plans on implementing both intra-day and inter-seasonal storage by using nearby salt-caverns [19]. In the northern Netherlands hydrogen storage in salt caverns could be realised in a capacity range of 2,000 to 7,200 tonnes [21]. Also in the eastern Netherlands there are suitable salt caverns for hydrogen storage. The locations of these salt caverns are beneficial as they are in the vicinity of the transport network.

Not only the distribution network is suitable for hydrogen, but also the GTS transport network can be retrofitted to transport hydrogen. While the gas consumption decreases in the coming years, an increasing number of transport pipelines can be made out of order to make place for hydrogen. GTS plans to implement this 10-15 GW hydrogen *backbone* before 2030 [4]. Figure 2.5 depicts a possible hydrogen infrastructure in Stedin region.

Van Wijk et al. suggests a regional connection to the hydrogen backbone through two pipelines: a high quality and a low quality hydrogen pipeline. The reason behind the two separate pipelines is to establish a dedicated pipeline for fuel cells with hydrogen produced by electrolysis and another dedicated pipeline for other purposes with hydrogen produced by SMR.

2.3. Fuel cells

The principle behind fuel cells is the opposite of electrolysis. But while for electrolysis electricity is needed, a fuel cell is a *galvanic cell*, meaning that the reaction occurs spontaneously. The ions created at the anode must travel to the cathode to keep the reaction running. Meanwhile, the electrons must travel through the circuit, resulting in an electric current. Hereby the electrolyte serves as a permeable membrane for ions, while not letting electrons pass. At the cathode, the ions react with oxygen and the electrons to form water. Despite the fact that a fuel cell is a galvanic cell, the reactions do not take place endlessly, as for the half-reactions at the anode and cathode to continue to take place an activation energy is needed, in the form of heat or electricity, for example. There are three ways to increase the possibility of a molecule having enough energy: increasing the cell temperature, increasing the area of the electrodes and using catalysts. Because the performance of a fuel cell is determined by the the electrode area, the current is often represented as the current density: the current per unit area. The current density can be increased by making use of a porous surface.

Another important term in understanding the working of fuel cells is the *Gibbs free energy*. The Gibbs free energy (G) is the maximum amount of reversible energy that is released at constant temperature and pressure, given by the following equation:

$$G = H - T \cdot s, \tag{2.12}$$

where H stands for the enthalpy and s for the enthropy. In fuel cells the change in Gibbs free energy is used to express the amount of electrical energy that is released in the cell. The Gibbs energy can also be expressed in another form, called the standard free energy of formation, G_f°, the change in Gibbs free energy as a result of the formation of a compound under standard temperature and pressure. The difference in Gibbs free energy of formation between the products and the reactants, ΔG_f°, is equal to the amount of electrical energy created in the cell, given by:

$$\Delta G_f^\circ = (G_f^\circ)_{H_2O} - (G_f^\circ)_{O_2} - (G_f^\circ)_{H_2}, \tag{2.13}$$

often also represented per mole, described by lower case letter g, Δg_f°. A negative difference in Gibbs free energy of formation ($\Delta g_f^\circ < 0$) indicates a spontaneous reaction. In the case of no losses, ΔG_f° describes the electrical work done by the cell.

Figure 2.5: An example of a possible hydrogen infrastructure in the province South Holland, part of Stedin area. The original image was edited for translation [4].

The difference in Gibbs free energy is directly related to the *open-circuit voltage* of the fuel cell, which is the voltage that spontaneously runs through the circuit if no external loads are applied and determines the cell efficiency. However, if the current density of a fuel cell is plotted against voltage, the actual operating voltage will not achieve the high theoretical value of the 'no loss' voltage, shown in Figure 2.6. The decreasing slope in Figure 2.6 is due to irreversibilities in the cell, namely:

- Activation losses, which are a result of slow reaction kinetics.
- Fuel cross-over, which can be defined as a voltage leakage from the anode to the cathode.
- Ohmic or resistive losses.
- Mass transport losses as a result of a decreasing concentration of reactants as the reactions progress, lowering the reaction kinetics.

A fuel cell always contains a stack of cells in series to increase the current density. The fuel cell stack must be designed to minimise resistance. Stacks allow for a modular design of fuel cells so that fuel cells can be used for a wide range of

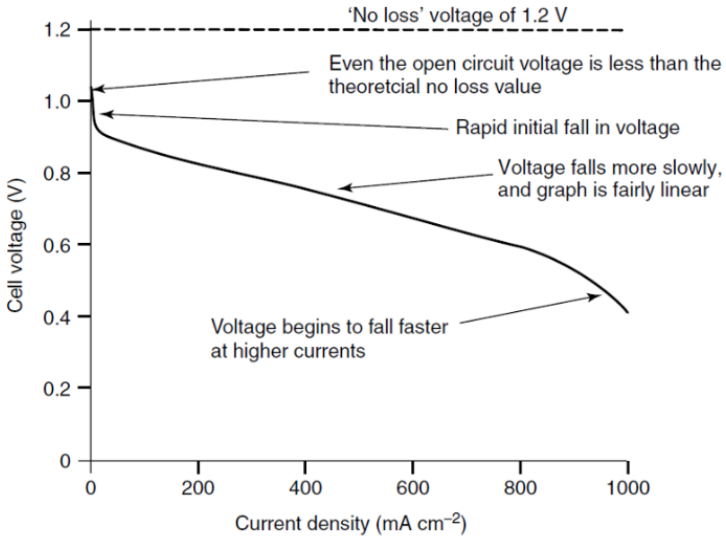

Figure 2.6: Current density versus the cell voltage in a fuel cell [30]

applications, from home systems (1-5 kW) to central power plants (1-200 MW or more) [31]. This section proceeds with elaborating on five different fuel cell technologies: proton exchange membrane, solid oxide, alkaline, molten carbonate and phosphoric acid fuel cells. Because most fuel cells operate at high temperatures, fuel cells are often combined with heat systems. These are called combined heat and power fuel cell systems.

2.3.1. PEM fuel cells

The PEM fuel cell (PEMFC) is the simplest fuel cell; it has a solid membrane as electrolyte, often made from the Nafion, in which protons are mobile [27]. Figure 2.7 illustrates the working principle of a PEMFC. The two half-reactions at either side are

$$2H_2 \rightarrow 4H^+ + 4e^- \tag{2.14}$$

$$2O_2 + 4H^+ + 4e^- \rightarrow 2H_2O. \tag{2.15}$$

at the anode and the cathode, respectively.

PEMFCs are low temperature fuel cells and have an operating temperature of 30 - 100 °C, which results in low reaction kinetics [32]. As compensation for the low reaction kinetics advanced catalysts are included in the PEMFC design or alternatively there are specific electrodes required. The low temperature of the PEMFC also results in a short start-up time. The anode, solid electrolyte and cathode can be made in thin layers so that high current densities are reached. Furthermore, the PEMFC can operate in any orientation. Out of all fuel cell technologies the PEMFC achieves the highest power density and specific power [32]. Everything combined makes the PEMFC the most suitable technology for mobile fuel cells. It is also the most cost-efficient technology at the moment, the two hydrogen cars on the Dutch market: the Hyundai ix35 Fuel Cell and Toyota Mirai both contain PEM fuel cells. Challenges for the PEM fuel cell are cost reduction of expensive catalysts and increasing its tolerance to fuel impurities.

2.3.2. SO fuel cells

Similar to PEMFCs, solid oxide fuel cells (SOFC) contain a solid electrolyte. The two half-reactions are the exact opposite of the SOE:

$$O_2 + 4e^- \rightarrow 2O^{2-} \tag{2.16}$$

$$H_2 + O^{2-} \rightarrow H_2O + 2e^- \tag{2.17}$$

at the anode and cathode, respectively. The solid oxide fuel cell must be seen as an integral system instead of just a fuel cell, because it operates at high temperatures (600-1000 °C) and is thus a system generating both electricity and heat. In SO fuel cells O^{2-} is the mobile ion and the electrolyte is made of ceramics. Due to the high operating temperature, high reaction

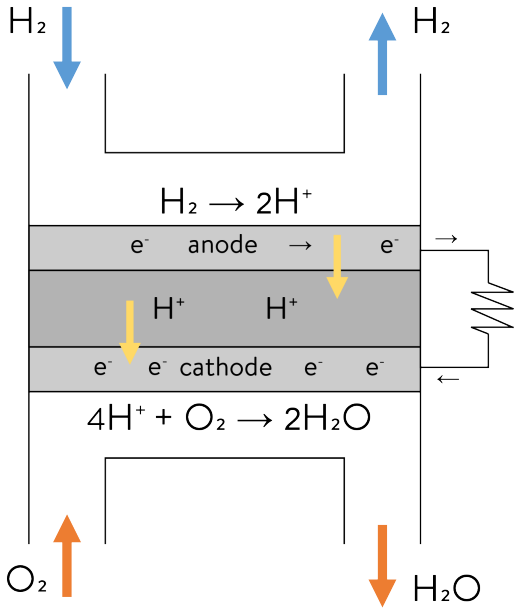

Figure 2.7: The working principle of a PEM fuel cell including its half-reactions at the anode and cathode.

rates are achieved, thereby avoiding the need for expensive catalysts. Furthermore, in the SOFC also methane can be used as fuel, as it will internally reform as a result of the high operating temperature. However, it also results in long start-up and shut-down in the scale of 12 hours [33]. SOFCs achieve a conversion efficiency of 60% [34]. The high operating temperature range of the SOFC results in a trade-off between increasing conversion efficiency by increasing operating temperature and decreasing the required start-up time.

2.3.3. Alkaline fuel cells

In alkaline fuel cells, OH^- is the mobile ion. The half-reactions at the anode and cathode are:

$$H_2 + 2OH^- \rightarrow 2H_2O + 2e^- \tag{2.18}$$

$$O_2 + 2H_2O + 4e^- \rightarrow 4OH^- \tag{2.19}$$

Before the PEM fuel cells became popular, the alkaline technology was more commonly used. The Apollo space ship, for example, was equipped with an alkaline fuel cell. Alongside with the early development of the alkaline fuel cell from the 1950s, other applications were demonstrated in tractors, trucks, power cars, boats, etc. [30]. The rise of PEM fuel cells and the high material costs of the alkaline fuel cell subsequently have hindered the further development of alkaline fuel cells. Another problem of this type of fuel cells is the sensitivity to CO_2 and H_2O. If CO_2 and H_2O are not removed from the incoming air, the fuel cell has a reduced reaction rate and several losses are increased [30]. The removal of CO_2 and H_2O contribute to the high manufacturing costs of the alkaline fuel cell. If these costs can be reduced, the alkaline fuel cell is a fair option for stationary applications of fuel cells.

2.3.4. Molten carbonate fuel cells

The electrolyte of a MCFC is made from molten carbonated alkali metal, such as lithium and sodium carbonates. The MCFC operates at temperatures ranging from 700-900° C. The carbonate (CO_3^{2-}) provides ionic conduction. Unlike other fuel cells, MCFC has not only oxygen as a reactant, but also carbon dioxide. CO_2 forms into CO_3^{2-} at the cathode, and back into CO_2 at the anode. The half-reactions at the anode and the cathode are respectively:

$$H_2 + CO_3^{2-} \rightarrow H_2O + CO_2 2e^- \tag{2.20}$$

$$O_2 + 2CO_2 + 4e^- \rightarrow 2CO_3^{2-} \tag{2.21}$$

CO_2 can easily be circled through the cell to be reused. Because of the high operating temperature, CO can be converted and hydrocarbons can be internally reformed in contrast to PAFC and PEMFC. MCFCs achieve a conversion efficiency of approximately 60% [35]. Worldwide there currently are over 50 MCFC systems producing 300 MW of power, but further maturity is limited by the sensitivity to impurities and high investment costs [34].

2.3.5. Phosphoric acid fuel cells

Phosphoric acid fuel cells are another type of high temperature fuel cells. Besides that, this type of fuel cell is similar to the PEMFC: a proton conducting electrolyte, same catalyst material (platinum), and the same reactions that take place at the anode and cathode. PAFCs get their name from their electolyte material, phosphoric acid. PAFCs have been commercially available for several years and large plants of several MWs exist in Japan and the USA, for example. The conversion efficiency of PAFCs is relatively low: 40 - 50% [34]. PAFCs operate at medium temperatures of approximately 200°C. While the technology is mature, the PAFC is not yet economically competitive compared to alternative power sources.

2.3.6. Combined heat and power fuel cell systems

When the generated heat in fuel cells is put to use, the system is called a combined heat and power fuel cell system (CHP-FC). CHP-FCs have an energy efficiency of 60-90% compared to 30-50% efficiency for fuel cells alone and 28-30% for internal combustion engines [36]. In Japan 300,000 of these residential fuel cell systems have been rolled out in a subsidised program, developed by *Panasonic*. More than 90% of these CHP-FCs are based on the PEMFC technology. These are available for a price of $21,000 - $ 27,000 per kW, although the costs have decreased with 85% in the last ten years [37]. Because of the low operating temperature of PEMFC, the quick start-up and low costs, these CHP-FCs are more suitable for residential use. Besides PEM CHP-FCs, also other fuel cell technologies can be used for CHP-FCs and they are listed in Table 2.1.

Table 2.1: CHP-FC systems and their capacity and technology readiness [38].

Technology	**Capacity**	**Technology readiness**
PEMFC	1-3 kW	Over 150,000 systems in Japan and Korea.
SOFC	1-1,000 kW	10% of global market share.
PAFC	100-450 kW	First system commercially available in the 1970s.
MCFC	3-60 MW	Market leader for large industrial systems

SOFCs are more suitable for bigger residential systems, due to the high operating temperature, high efficiency, greater fuel flexibility and higher electrical efficiency. *Kyocera Corporation* and *Mitsubishi Hitachi Power Systems* are two companies that have been developing micro CHPs based on SOFCs for years, and are designed to operate on natural gas [32]. MCFCs are the largest industrial systems with high operating temperatures. MCFCs have low capital costs in the range of £3,000 per kW but have the highest yearly degradation [38]. PAFCs fail to become a commercially available product because of high costs and material corrosion [37]. According to Staffell et al., CHP-FCs have a higher total efficiency (combined thermal and electrical efficiency) compared to conventional technology. Also the product lifetime and reliability have improved to the point that CHP-FCs are now similar to conventional gas fired boilers [33]. Several European boiler manufacturers such as *Bosch* and *Viessmann* have partnered with Japenese manufacturers like Panasonic or are developing residential CHP-FC products [39]. Figure 2.8 shows a micro CHP system on the German market by Viessmann called the *Vitovalor PT2*, containing a PEM fuel cell of 0.75 kW for central and water heating [40]. It is able to cover the majority of the average annual heat demand of a detached house and generates up to 18 kWh electricity per day. The PEM fuel cell stack generates the electrical energy, while heat is provided by the reformed natural gas, the burner exhaust and heat is recovered from the fuel cell stack [41]. This thermal energy is applied to the inlet water stream to generate hot water. Natural gas first enters a reformer, is then shifted and purified before it enters as hydrogen into the fuel cell stack. The required heat for this reaction is provided by the combustion of natural gas. Also the waste stream from the fuel cell stack can be reused for combustion which decreases the required amount of natural gas.

2.3.7. Fueling stations

There are four existing hydrogen fueling stations in the Netherlands, in Rhoon, Arnhem, Delfzijl and Helmond, but there will be more built in the near future. In an average scenario 300,000 hydrogen passenger cars are expected by 2030, which would require 125 filling points [4]. Due to the large storage volume that is required, hydrogen fuel cell vehicles are a promising technology for heavy vehicles, such as buses. Seven cities in the province South-Holland are expected to have a hydrogen bus infrastructure including a refilling point [4]. There are two hydrogen cars today on the Dutch market, the Toyota Mirai model and Hyundai Nexo, which both have a carbon fiber storage tank [42, 43]. Existing fueling stations compress hydrogen to either 350 or 700 bar and also a pre-cooler is added to cool hydrogen at -40 ° C to avoid overheating during refueling [44]. An average hydrogen tank can be refilled in 5 minutes, similar to conventional gasoline cars. The most common compressors in hydrogen refueling stations are reciprocating compressors (rotary piston and cylinder movements and diaphragm pumps) and in refueling stations under demonstration also ionic and centrifugal compressors

Figure 2.8: Viessmann's micro CHP unit. The tank on the left is a 220 litre hot water storage tank, the lower right part of the unit is the PEM fuel cell stack, made by Panasonic. Above the fuel cell cell stack is a gas condensing boiler for peak heat demand coverage.

are used [44]. Reciprocating compressors are a commonly used technology for moderate flows, as they achieve high outlet pressures and they are oil-free. As compression is an adiabatic process, compression to high pressures is done in stages to increase the energy efficiency and avoid excessively high temperatures [45]. An alternative for mechanical compression is electrochemical compression. *HyET* is developing an electrochemical compressor based on a membrane technology. HyET's membrane does not consist of moving parts and is therefore a more reliable technology compared to mechanical compressors. According to HyET, it has a lower energy use and lower OPEX and CAPEX. It has the capacity to compress 5 kg hydrogen per day at a range of inlet pressure of 1.05 and 100 bar with an energy consumption of less than 5 kWh per kg hydrogen. HyET's product only currently exists on lab scale, but is near commercialisation [21].

2.4. Other end-use applications

Besides fuel cells, there are other possibilities for hydrogen fuel. Considering that hydrogen needs to replace natural gas in the future, there are many other applications imaginable, such as cooking on hydrogen, hydrogen boilers, gas turbines and for feedstock in industry. Also a section dedicated to storage is added because hydrogen vehicles, for example, include a storage compartment and it is relevant to understand the mechanisms behind this. It is important to note that with the scope on residential users, residential hydrogen applications are the most relevant to this study.

Current-day gas hobs and boilers include burners for the supply of thermal energy. Existing hobs and boilers are not suitable for pure hydrogen fuel; the burners must be adjusted because of the higher flame speed of hydrogen compared to natural gas (2.7 m/s instead of 0.37 m/s [46]) and a bigger flammability range. Existing Dutch boilers have successfully been tested on hydrogen/natural gas mixtures up to 30% during the pilot project in Ameland [18]. Above the mixing limit of 30% hydrogen with natural gas it is able to cause a flashback in existing burners, which means that flames propagate back through the burner. This effect is illustrated in Figure 2.9, in which on the left hydrogen and oxygen mix such that flames form inside the burner. In a hydrogen burner on the right in Figure 2.9 the oxygen and hydrogen outlets are separated so that the fuels mix outside of the burner.

A second concern of adapting conventional boilers to hydrogen fuel is the higher NO_x emissions. At high combustion temperatures, nitrogen in the air oxidises and forms NO_x. NO_x is an air polluter and a toxic gas. Because of the higher flame temperature of hydrogen compared to natural gas, there is a higher chance of NO_x formation. This challenge will be one of the key design requirements of hydrogen burners. The threat of NO_x can also be diminished by dilution of the hydrogen feed or flame temperature control [19]. Another concern with hydrogen combustion is the invisibility of hydrogen flames. This is

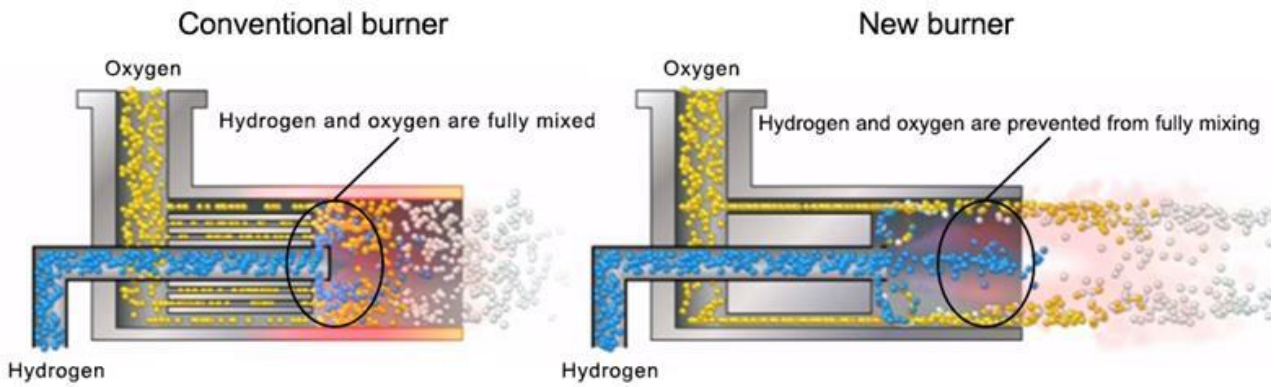

Figure 2.9: A simplified illustration of hydrogen in a conventional burner (left) compared to a hydrogen burner made by Toyota (right) [47].

not only a problem for gas stoves, but also for boilers as current boilers often have flame detection devices inside. Potentially a flame colourant will be added in the combustion part of the burner itself [46]. To avoid issues with hydrogen flames, a new design could potentially be a catalytic burner. Catalytic burners give a flameless combustion at lower temperatures with similar exhaust heat. With these different design parameters there are two possible options for future burner products; either new products will be designed to be adaptable to a different fuel or new products will be designated for hydrogen fuel. This uncertainty might cause induction cooking technology to be the favourable tool for cooking. Induction cooking is also beneficial in terms of safety when compared to hydrogen hobs, which require hydrogen pipelines within homes.

2.4.1. Boilers

Remeha and *Bekaert* currently have a hydrogen demonstration boiler in the pilot project in Rozenburg. The hydrogen boiler has the same design as conventional natural gas boilers, but the interior is different. Also *Giacomini* (UK), *Worcester Bosch* (UK) have developed a demonstration boiler. The demonstration boiler from Worcester Bosch is also able to be fueled on natural gas. Figure 2.10 shows the hydrogen fueled boiler made by Remeha.

Figure 2.10: A hydrogen boiler by Remeha.

Hydrogen boilers have a similar working to conventional gas fired boilers. As explained previously, the combustion part of the hydrogen boiler requires a different design from a conventional boiler. Due to different gas properties, the design of a hydrogen boiler should consider safety aspects, such as the avoidance of gas leakage and the concentration of hydrogen in cavities within the boiler.

2.4.2. Small scale storage

Especially small fuel cell systems of up to 50 kWs include a storage compartment, as over 50 kWs it is more cost effective to directly fuel the fuel cell [32]. Larger vehicles (buses, aircrafts or spacecrafts) that allow for larger storage space make use of compressed or liquid hydrogen storage in tanks. Two other ways to store hydrogen are compression and liquefaction. Alternatively hydrogen can be stored in materials by two means: chemical and physical storage. Chemical storage is based on metal-hydrides and hydrocarbons, whereas physical storage involves porous and nanostructured materials [27]. Metal hydrides have a high volumetric density but low gravimetric density. Furthermore, the operating conditions for the release of hydrogen require high temperatures, resulting in poor thermodynamic and kinetic properties. For these reasons metal hydrides are inadequate materials for storage in vehicles [48]. Physical storage relies on materials with a high specific surface density in which hydrogen can be absorbed and released. Suitable physical storage materials include carbon based materials, such as carbon nanotubes and nanofibres, or non-carbon based materials such as metal organic frameworks or zeolites.

2.4.3. Gas turbines

Hydrogen gas turbines are able to increase the flexibility of renewable energy sources. One of the three Magnum Combined Cycle Power plants in Groningen are planned to be transformed to run on hydrogen in 2025. They will use blue hydrogen imported from Norway, where also the carbon will be captured. Before 2030 the other two Combined Cycle turbines will follow, so that the Magnum plant will be CO_2 neutral in 2030 [49]. The plant is expected to provide electricity for almost 3 million households. These turbines were designed to be compatible with a range of gases, including hydrogen. A similar conversion of older natural gas turbines will be more complex or impossible [4].

2.4.4. Industry

In industry hydrogen is traded between manufacturers. Industrial gas companies producing hydrogen as a byproduct sell it to petroleum, ammonia and methanol manufacturers for the production electronics, chemicals, petrochemicals, food and metal refineries and more [50]. The use of oil and coal as feedstock in industrial processes can in some cases be replaced by hydrogen without many adaptions in the process. Besides feedstock hydrogen can offer carbon-free heat. This is especially interesting for industry, as in industry the heat demand is the largest and producing heat or electricity onsite can save energy costs.

3
Contamination

Present day the gas in our gas grid is being contaminated by external influences. *Regulation gas quality* determines the lower or upper limit of certain parameters influencing the quality of our gas [51]. When hydrogen replaces natural gas in the gas grid, a similar regulation is expected concerning hydrogen quality, but what standard for hydrogen fuel purity should be adopted has until now not been determined. One norm has been established for the specification of hydrogen fuel purity, named ISO 14687, which specifies the upper limit of a list of contaminants.

In this research five factors are included affecting the hydrogen quality in the distribution network. This chapter first introduces four sources of contamination. Afterwards the significance of impurities in hydrogen fuel on end-use applications is elaborated upon, with an emphasis on fuel cells. While there is a considerable amount of contaminants in ISO 14687, only the contaminants that are relevant for these five factors are mentioned in this chapter. The last section in this chapter provides insight on hydrogen purification technologies.

3.1. Sources of impurities

This section elaborates on four of the five sources of contamination identified in this research: byproducts from production technologies and storage, odorant, particles and leaks. The fifth source of contamination, inward permeation of air, is the main focus of the remaining chapters of this research.

3.1.1. Byproducts from production technologies and storage

Table 3.1 lists five hydrogen production technologies and their potential impurities. The production technologies under the column *Technology* were earlier elaborated upon in Chapter 2. Note that the product of SMR and biomass gasification is shifted syngas, and not pure hydrogen. There is always a separation step required to gain hydrogen, and in the case of Table 3.1 the hydrogen purity for these two technologies are considered after purification by PSA.

Another source of contamination before hydrogen enters the grid is impurities in from underground storage. In depleted natural gas reserves residue of natural gas can be present in the pores. Because of this, traces of natural gas can be expected to be found in the first cycles of hydrogen storage. It is uncertain, however, how natural gas and hydrogen will interact and thus what fraction of natural gas in hydrogen can be expected [53]. Hydrogen is not expected to react with rock salt in salt cavern storage, but the presence of other impurities in the salt cavern might contaminate hydrogen.

3.1.2. Odorant and safety

Natural gas is an odorless and combustible fluid. To ensure safety, an odorant is added so that leakages can be detected before the leak can cause an explosion. Similar to many other countries in Europe, in the Netherlands Tetrahydrothiophene or THT, is added to natural gas in the distribution grid [54]. The average concentration of THT is 18 mg per m^3 gas, which is the equivalent of 18×10^{-3} ppm, as stated by *Regulation gas quality*. At this concentration the majority of people is able to detect a concentration of 1% natural gas in air, which is one sixth of the lower flammability level [14, 55]. THT has the molecular formula $(CH_2)_4S$ and is added because of its alarming scent.

Hydrogen is also a scentless fluid and leakages can cause hazardous situations. It is possible that hydrogen will be odorised as a safety measure for residential use. Currently odourant is essential not only for indoor leak detection, but also for leak detection on outdoor locations. In the existing hydrogen infrastructure in the industrial area no odorant is added, mainly because of the need for pure hydrogen. Because the hydrogen does not contain an odorant, industries monitor incoming mass flows securely to ensure the absence of gas leakage. The intolerance of fuel cells towards hydrogen sulphide is inconvenient as sulphur compounds are a widely used odorant. At this moment, Gasunie is doing research on possible odorants that can be added to hydrogen, preferably without being harmful for fuel cells. 5-Ethylidene-2-norbornene is a suitable candidate, as no additional damage to fuel cells have yet been discovered [56]. Also ethyl isobutyrate and 2,3-butanedione are promising candidates as they have shown no fuel cell degradation on the short term [57]. It is debatable, however, whether adding another odorant than THT is preferable as people have been recognising the scent of THT as gas for decades. Furthermore, it has not yet been proven that adding an odorant has the same performance as with natural gas, as hydrogen is much more volatile than natural gas. Especially in underground leakages hydrogen has the ability to diffuse

Table 3.1: Production technologies and their impurities.

Technology	**Purity (%)** [24, 52]	**Byproducts**	**Cause**
PEM	99.99 - 99.999	H_2O	Unconverted fuel
		O_2	Unconverted fuel
		N_2	Air intake
		CO_2	Air intake
SO	99.999	H_2O	Unreacted fuel
		O_2	Unreacted fuel
		N_2	Air intake
		CO_2	Air intake
Alkaline	99.9	N_2	Insufficient purging after shutdown
		H_2O	Unreacted fuel
		O_2	Unreacted fuel
		Ar	Impurity of N_2 used for purging
SMR	98 - 99.9999[a]	CO	Product from reversible water-gas shift reaction
		CO_2	Product from reversible water-gas shift reaction
		N_2	Present in natural gas
		CH_4	Present in natural gas
		H_2O	Product of reversible water-gas shift reaction
Biomass gasification	98 - 99.9999[a]	Hydrocarbons	Unreacted fuel
		CO	Product from reaction
		CO_2	Product from reversible water-gas shift reaction
		H_2O	Unreacted steam
		Tar	Product from reaction

[a]Purity achieved after PSA.

faster through soil than odorant. This questions the effectiveness of adding an odorant. Similar issues can occur concerning hydrogen storage technologies based on adsorption, where odourant could separate from hydrogen. Another disadvantage of odourant as safety measure, is that an individual needs to be in the vicinity of the leak to be able to detect it. If odorant is decided to be added to hydrogen, fuel cell and other hydrogen appliance manufacturers ought to take the addition of an odorant to hydrogen into account in their design. An odorant entering a fuel cell needs to be disposed of.

A possibility for safety insurance concerning hydrogen leaks in residential areas is placing the hydrogen fueled equipment on the exterior of the building, so that leaking hydrogen can immediately escape to the environment rather than accumulate indoors. An alternative for hydrogen detection is using sensors. Hydrogen sensors could possibly fulfill a similar function as carbon monoxide sensors, for example. Hydrogen sensors exist having a lower detection limit in a range of hundred ppb, which is 400,000 times the lower flammability limit of hydrogen [58]. Chauhan and Bhattacharya refer to a considerable amount of hydrogen sensing methods with a sufficiently low detectability. But the use of hydrogen sensors raises other questions, such as where such a sensor needs to be placed in order to be effective and whether it is sufficiently safe. Assuming that in the case of a leakage hydrogen accumulates in a roof, one could also think of ventilation so that hydrogen can be released to the environment [59].

3.1.3. Particles

The presence of particles in the gas grid can be a cause of dirt entering the pipeline during installation or corroded steel, for example. Because of this, gas passes three filters upon arrival at the customer. The filters remove particles above 5 µmol diameter and they are replaced every 6 to 9 months [60]. The exact amount of particles in the pipelines has never been measured, and no research has been found on this topic. The upper limit in ISO 14687 has been set to 1 mg/kg to reduce the risk of gas leaks and for conservation of fragile components within fuel cells. There has been no evidence for direct harm to the performance or endurance of fuel cells [61]. In ISO 14687 no maximum allowable size of particulate matter has been included, but the diameter of the particles ought to be kept as small as possible. To automotive fuel cells a bigger

threat than particles in the pipeline is particulate matter in the direct surrounding of fuelling nozzles [61].

3.1.4. Leaks

Through leaks in the the grid contaminants can potentially enter the interior of the pipeline. The majority of leaks are caused by subsidence and excavation damage [12]. Pipelines laying in bog or clay subsurface soils are prone to endure higher stresses as a result of subsidence. One of the biggest concerns for distribution network operators are the pipelines connecting the street to the interior of homes. Distribution network operators have limited insight in the state of the connections behind the facade, especially since some homeowners prefer to have self-made constructions. In addition, excavation damage is one of the prominent causes for leaks, responsible for half of the leakage incidents per year. The expected contaminants as a result of a leak are water, dirt or soil and potentially also air.

3.1.5. Water permeation

A recent study about the influence of permeation of water through polyethylene pipes was done on the water dew point of natural gas by *Kiwa Technology* [62]. In the current-day *Regulation gas quality* for natural gas there is an upper limit defined for the moisture content in gas to avoid that large amounts of water are needed to be removed at compressor stations [51]. At CNG (compressed natural gas) stations natural gas is compressed to 250 bar, which is the required pressure for CNG vehicles. Similar pressure differences can be expected in low pressure storage tanks at hydrogen fuelling stations. The experimental results of the study by [62] show a permeation rate of 81 mg mm m^{-2} per day for pipelines under water. The permeation rate of water into polymer pipes was found to be independent of depth and ground level. At the maximum amount of 30 mg per m^3 natural gas a CNG station is required to have a gas dryer [63].

3.2. The impact of impurities on appliances

ISO 14687 specifies the upper limit of contaminants in hydrogen fuel for different purity grades. Three grades are shown in Table 3.2, which are the most relevant for this research. The lowest purity in Table 3.2 is grade A and is specified for internal combustion engines for transportation and commercial hydrogen combustion appliances, like hydrogen boilers. Grade E is specified for PEM fuel cells for stationary applications and is divided into three categories for different requirements of the fuel cell manufacturer. Category I and II of grade E are both specified for a hydrogen content of 50%, diluted with nitrogen. The norm for the highest purity hydrogen fuel (grade D) is intended for PEM fuel cells in road vehicle applications.

3.2.1. Combustion appliances

The minimum hydrogen quality for internal combustion engines for transportation and residential or commercial combustion appliances is set to 98%. Inert contaminants do not pose a threat to combustion components. On the contrary, diluted hydrogen fuel reduces NO_x formation as mentioned in Chapter 2. With today's internal combustion engine technology the flame temperature of hydrogen will need to be decreased by the addition of large amounts of nitrogen or steam. However, the amount of allowable inert gases is limited by potential corrosion in turbine blades [65]. For boilers apart from the design considerations mentioned in Section 2.4, there were not found any differences in fuel purity requirements compared to natural gas boilers in literature. The most convincing reason for this the current commercial unavailability of hydrogen boilers. For existing and future boiler manufacturers especially the eventual calorific value of hydrogen from the grid will become relevant for design considerations.

3.2.2. Road vehicles based on PEMFCs

The highest purity specification for hydrogen fuel is based on the tolerance of PEM fuel cells used for road vehicles. This standard is summarised in Table 3.2. As a result of the low operating temperature, PEM fuel cells are the limiting factor for the standardisation of hydrogen quality, but also other fuel cell technologies have an intolerance towards impurities, shown in Table 3.3. It is recognised that the specifications of grade D hydrogen in ISO 14687 might be too stringent and as fuel cells are developing rapidly a working group was appointed by ISO studying potential adaptions to the norm, or establishment of a new norm.

The tolerance of fuel cells towards impurities is proportional to the operating temperature of the fuel cell. While the working of PEMFCs and PAFCs is similar, because of the higher operating temperature PAFCs are less limited to contaminants. The following sections elaborate on the contaminants relevant for this research from Table 3.2.

Table 3.2: The upper limit of allowed concentration of impurities in hydrogen gas based as stated in ISO 14687 [64].

Characteristics	Type I, Type II Grade D	Type I Grade E Category 3	Type I Grade A	Unit
Hydrogen fuel index (minimum mole fraction)	99.97	99.9	98.0	%
Total non-hydrogen gases	300	1,000	20,000	µmol/mol
Maximum concentration of individual contaminants				
Water (H_2O)	5	*a*	*a*	µmol/mol
Total hydrocarbons (methane basis)	2	2	100	µmol/mol
Oxygen (O_2)	5	50	*b*	µmol/mol
Helium (He)	300	*c*	-	µmol/mol
Total Nitrogen (N_2) and Argon (Ar)	100	*c*	*b*	µmol/mol
Carbon dioxide (CO_2)	2	2	-	µmol/mol
Carbon monoxide (CO)	0.2	0.2	1	µmol/mol
Total sulfur compounds (H_2S basis)	0.004	0.004	2	µmol/mol
Formaldehyde (HCHO)	0.01	0.01	-	µmol/mol
Formic acid (HCOOH)	0.2	0.2	-	µmol/mol
Ammonia (NH_3)	0.1	0.1	-	µmol/mol
Total halogenated compounds (Halogenate ion basis)	0.05	0.05	-	µmol/mol
Maximum particulates concentration	1	1	*d*	mg/kg

[a]Non-condensing at all ambient conditions
[b]Combined concentration should be below 1.9 mole%
[c]Combined concentration should be below 0.1 mole%
[d]Maximum amount not specified yet, but must be below the amount sufficient to damage the fuelling station equipment

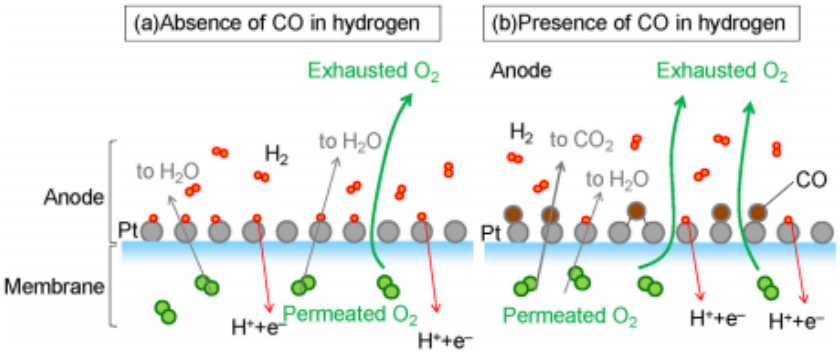

Figure 3.1: An illustration of carbon monoxide covering the platinum catalyst surface [67].

Carbon monoxide

Much experimental research has been done to get insight on the influence of CO concentration in hydrogen fuel, although each under different conditions. The principle behind CO poisoning is that CO molecules cover the surface of the Pt catalysts as CO has a stronger adsorption onto platinum than H_2, illustrated in Figure 3.1 [30]. Instead of oxygen reacting with hydrogen, it reacts with carbon monoxide at the catalyst surface to form carbon dioxide. Shabani et al. reviewed many studies scrutinising the effects of carbon monoxide poisoning and a certain important conclusions can be drawn [68]. Firstly, by increased CO concentrations, the voltage drop of the PEM fuel cell subsequently increases. In an experiment 10, 50 and 100 ppm CO were added to hydrogen fuel and caused 9%, 27% and 94% voltage loss, respectively. Another study demonstrated the effect of dilution on CO poisoning with 20 ppm CO concentration, which indicated that diluting hydrogen with 20% and 40% nitrogen resulted in a 23% and 40% reduction in hydrogen coverage on the catalyst surface, respectively, compared to 100% hydrogen. The degradation rate caused by CO poisoning depends on the current density of the cell; low degradation rates are shown when the cell operates at low current densities. Shabani et al. indicates that for a 2 ppm concentration of CO a 20 mV overpotential occurs at a current density of 0.2 A cm^{-2}, whereas an increased current density

Table 3.3: Fuel cell technologies and their intolerance to fuel impurities.

Technology	Application	Toxic Gases	Tolerance
PEM [30]	Stationary and mobile	CO	10 ppm[a]
		S	1 ppb
SO [30]	Stationary	S	0.1 ppm
AFC [66]	Mobile	CO_2	-[b]
MCFC [34]	Stationary	H_2S	0.5 ppm
		Particulate matter	10 - 100 ppm
		NH_3	1 - 3 vol%
		HCl	1 ppm
		Halogens	1 ppm
		Alkali metals	1 ppm
PAFC [30]	Stationary	CO	1×10^4 ppm[a]
		S	50 ppm[a]

[a]Temperature dependent
[b]Dependent on fuel cell size. Fuel cells of small volumes have no tolerance towards impurities, while larger systems are not that specific.

of 1.0 A cm^{-2} results in an overpotential of 250 mV. All studies reviewed by Shabani et al. were executed at constant current density or cell voltage, whereas in reality these conditions are variable. Besides the current density and carbon monoxide concentration, the amount of poisoning is also dependent on exposure time, as can be seen from Figure 3.2. Accumulation of carbon monoxide over time deteriorates the effect of poisoning. A study by Das et al. found that an increased temperature reduces the influence of CO-caused anode poisoning in a PEMFC because of the increased desorption rate of CO [69]. However, for PEMFCs the advantage of increasing the cell temperature is limited by the boiling point of water and it hinders the advantage of easy start-up [68]. While CO is toxic for PEM fuel cells, in high temperature fuel cells such as SO, CO can indirectly act as a fuel after conversion into CO_2 by the earlier mentioned water gas shift reaction.

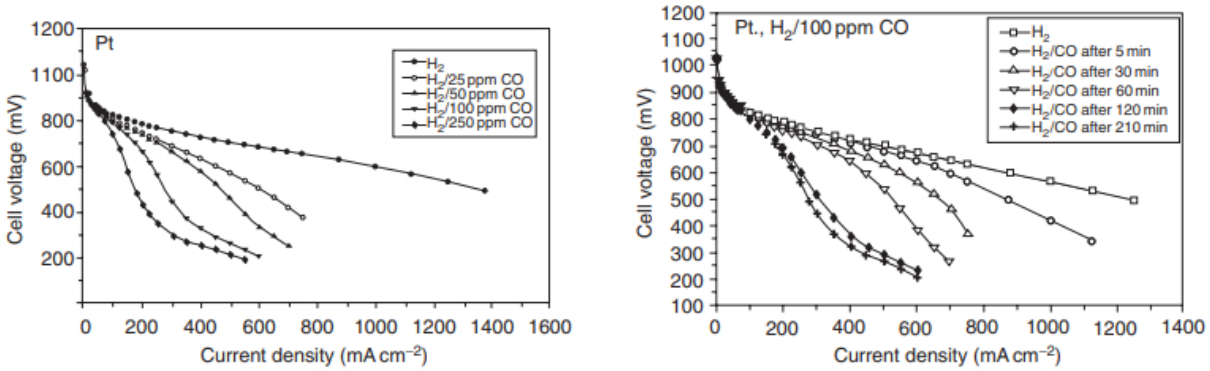

(a) Cell voltage as a function of current density for varying CO concentration. (b) Cell voltage as a function of current density after several exposure times.

Figure 3.2: The effect of carbon monoxide concentration and exposure time on the voltage drop at 80°C in PEM fuels [70].

Carbon dioxide

The only fuel cell that has a tolerance limit to CO_2 is the alkaline fuel cell. In AFCs carbon dioxide react with the electrolyte (KOH). KOH and CO_2 combined form carbonates, a poison to the cell. The small amount of CO_2 of 350 ppm in air already shows a slight detrimental effect on the current density of the electrode. In literature the severity of CO_2 depends on the volume of the electrolyte. In the case of high volumes the effect was small, but more realistically in optimised electrolyte volumes the detrimental effect of CO_2 poisoning was proven to be more significant [71]. Therefore AFCs are not often used for mobile applications, in which optimising the volume of the fuel cell is important. The effect of CO_2 was also tested in a long term experiment, in which the concentration of CO_2 was increased to 150 times the concentration of CO_2 in air. From that experiment it can be concluded that the cell could reach its average lifetime and beyond if the electrolyte would be

replaced [66]. The tolerance limit is included in Table 3.3, nevertheless [66]. Incoming air is often purged before entering the fuel cell, which leads to a higher total costs of the AFC. Less research was done on the allowed CO_2 concentration in hydrogen fuel. Due to the dependence on the cell size, the tolerance for CO_2 in Table 3.3 was set to zero.

Oxygen

The presence of oxygen in hydrogen fuel does not have a toxic effect on fuel cells. However, as a result of dilution, the fuel utilisation decreases and so does the efficiency of the fuel cell. The tolerated amount of oxygen in ISO 14687-2 is set at 5 µmol/mol because of problems for storage by means of metal hydrides. However, metal hydrides are not suitable materials for storage in vehicles, because of the low gravimetric storage capacity. In addition, a hydrogen vehicle with metal hydride storage requires refueling times of approximately one hour [32]. It is not clear from ISO 14687-2 whether fuel cells with another storage medium are allowed to have higher oxygen concentrations in the fuel. In the specification of hydrogen purity for stationary PEM fuel cells, fuel cell degradation is the cause of this limit. This statement has not been substantiated in literature, however. According to Shabani et al., adding oxygen to the fuel stream can actually mitigate carbon monoxide catalyst poisoning, as oxygen causes CO to oxidate at the platinum catalyst at which carbon monoxide is converted to carbon dioxide. Introducing 0.5% oxygen to the fuel stream (also called air bleeding) resulted in the full recovery of performance after the stack had been introduced to carbon monoxide [68]. It is important to note, however, that the presence of oxygen near the catalyst surface can also cause hydrogen to become H_2O, thereby decreasing the fuel cell efficiency. Furthermore, air bleeding can cause membrane degradation at the anode as a result of H_2O_2 formation. A study by [72] shows that the presence of 5% air bleeding causes no effects on the short term, but after 2,000 hours of operation significant degradation appears.

Nitrogen, Helium and Argon

Air contains 78.09 vol% nitrogen, 0.92 vol% argon and a small amount of helium. As air is taken as a source of oxygen, there is a possibility that these gases are present in the oxygen stream and thus included in ISO 14678-2. Each is an inert gas that therefore is not toxic for fuel cells. The exact effect of inert gases are not confirmed at the moment. Inert gases are not consumed by the fuel cell, and can increasingly accumulate in recirculating loops or internal cavities and can be difficult to remove [68]. It can The impact of inert gases in hydrogen fuel on fuel cell performance has only been studied in relation to CO poisoning. A research by Bhatia and Wang indicates that hydrogen diluted by nitrogen has significant effect on the CO poisoning in fuel cells. Pure hydrogen, except for the addition of 10 and 100 ppm CO, was compared to 40% hydrogen diluted with nitrogen. The dilution itself does not result in a voltage difference. However, the addition of 100 ppm CO to 100% hydrogen leads to the same performance drop of 40% as when adding 10 ppm CO to diluted 40% hydrogen [73]. Therefore contaminants should not only be assessed individually, but also in composites.

Water

SMR and electrolysis can both cause water to be in the hydrogen fuel stream, but water can also permeate into the pipeline or enter the pipeline through a leak. Water does not directly affect the performance of the fuel cell [74]. It might, however, attract other contaminants in Table 3.2, specifically ions that are soluble in water. In the review by Shabani et al. a study was cited that indicated that the presence of water vapour can diminish the impact of CO poisoning. There are also concerns about liquid water and ice that could negatively affect the operating conditions of the fuel cell [75].

Hydrogen sulphide

Of all impurities listed in ISO 14687-2, the lowest tolerance is shown for hydrogen sulphide. Sulphur compounds in a hydrogen stream converts to hydrogen sulphide. Metals are sensitive to H_2S, as metal ions like to form metal sulphides, as does platinum. Experimental research on hydrogen sulphide caused degradation of PEM fuel cells indicate a 47% deterioration in performance at 2 ppm H_2S after 2,5 hours of exposure [68]. Other studies have reported significant overpotential at 0.5 ppm H_2S after an hour [68]. In some cases it was also found that the performance does not recover, as opposed to CO which is a reversible contaminant. However, a study by Garzon et al. shows no significant changes in the durability at H_2S injection of 10 ppb H_2S after over 1,000 hours of exposure, but do show a significant decrease in current density at low voltages [76]. In contrast with CO, the voltage loss increases with increased temperatures, as can bee seen from Figure 3.3 [77]. Another study reviewed by Shabani et al. scrutinised not only H_2S as contaminant, but also two other sulphur compounds, SO_2 and COS, and found similar poisoning effects at 1 ppm injection. A mitigation strategy for hydrogen sulphide poisoning is *voltage pulsing*. After applying a high voltage pulse of 1.5 V and a low voltage pulse of 0.2 V afterwards for both two minutes, the power loss was almost completely reversed [68]. Currently research is being done on suitable sulphur-tolerant catalysts [30].

3.3. Purification

The previous chapters have given an indication on the significance of impurities in hydrogen fuel. Purification offers a solution to a high purity hydrogen fuel demand. Purification methods for hydrogen streams are not a new concept, but have already been deployed in industrial processes. This chapter lays out four purification methods: pressure swing adsorption

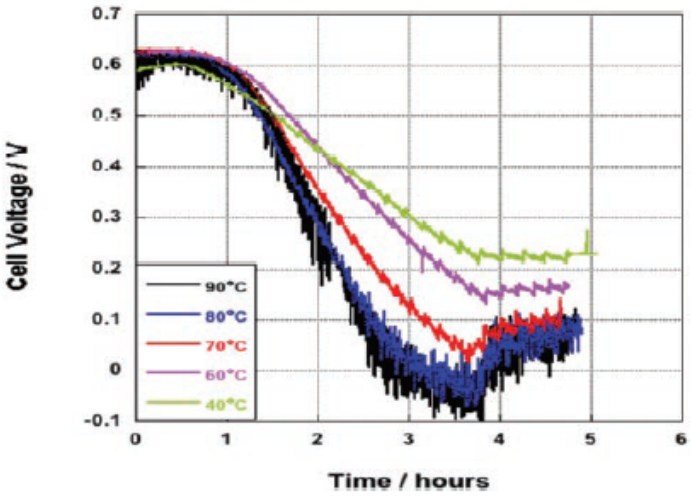

Figure 3.3: Cell voltage change due to 2 ppm hydrogen sulphide poisoning at a current density of 0.6 A/cm^2 for varying operation temperatures [77].

(PSA), cryogenic separation, membrane separation and electrochemical purification and compression. PSA and cryogenic distillation are common and widely used technologies in industry, whereas membranes and electrochemical purification and compression are less developed. The two commercial methods are also expensive methods and as a result purification is responsible for 50% of the costs of hydrogen production from SMR or gasification [78]. Table 3.4 gives an overview of the four purification methods. There are many other technologies being developed to separate hydrogen from mixed streams. Developments in hydrogen purification can potentially have a big influence on the feasibility of a hydrogen economy.

Table 3.4: Hydrogen separation technologies and their properties [52, 65, 79]

Technology	Capacity	Operating pressure	Operating temperature	Purity
PSA	10 - 400,000 Nm^3/hour	40 bar	Room temperature	<99.9999%
Cryogenic Distillation	5-75,000 Nm^3/hour	20-200 bar	-200°C	~99%
Membranes	<50,000 Nm^3/hour	20 - 200 bar	<100°C or 200 - 900°C	99 - 99.995%
Electrochemical	1 - 1,000 Nm^3/hour	up to 1,000 bar	20 - 80°C	>99.9%

3.3.1. Pressure Swing Adsorption

PSA is the most common purification technology and is widely used in existing industry; 85% of the produced hydrogen is purified by PSA. The technology of pressure swing adsorption is based on selective adsorption of impurity gases onto a porous adsorbent at high pressure. In the first step, hydrogen at ambient temperature at the inlet is compressed to a pressure of approximately 40 bar. As can be seen from Figure 3.4, the stream then enters column 1, where all the gas components are adsorbed except for hydrogen. Examples of adsorbents are a molecular sieve, activated carbon, activated alumina and silica gel [79]. For the purification of hydrogen often multiple beds are applied within one column containing different adsorbents. Then the components are desorbed from the adsorbent so the adsorbent can be reused. Desorption is done by lowering the column pressure or by purging with a small amount of hydrogen. The outlet pressure is similar to the inlet pressure except for a small pressure drop of approximately 1 bar. This entire process normally occurs in eleven stages. When multiple columns simultaneously operate within the same plant, it is called multicolumn PSA. Between each column there is a small time shift so that purification can take place almost continuously [65]. As a result, a fraction of the hydrogen product from column 1 can be used to purge column 2. Multicolumn PSA is often the last step in a SMR plant to increase the hydrogen concentration from 75% to 99.5% or higher [50]. PSA can reach a hydrogen purity of 99.9999%, making it the most suitable purification technology for reaching the high quality requirements for fuel cells [52]. The main disadvantage of this technology is the low H_2 recovery rate of 80%. In addition, a PSA installation with a large number of columns requires a large space. PSA units can also be scaled down for smaller industry. Companies Hygear, IGS and Amnis Pura offer these smaller units and are capable of reaching grade 6 hydrogen [78].

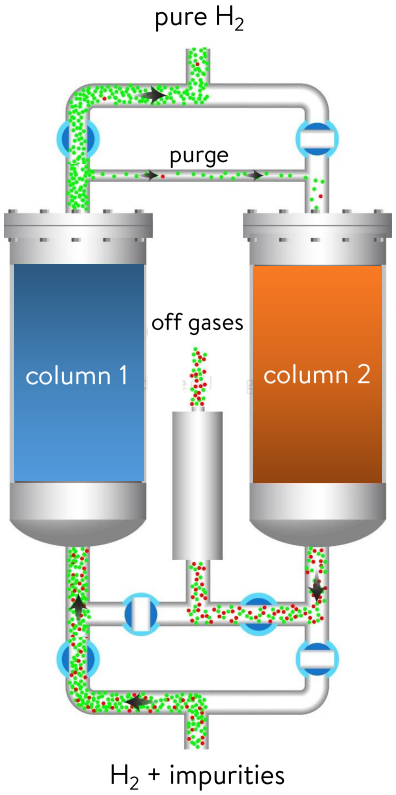

Figure 3.4: A two column pressure swing adsorber. Image edited from Holtec gas systems [80].

3.3.2. Cryogenic Distillation

The technology of cryogenic distillation builds on the separation of gas mixtures by condensing contaminants. Hydrogen has one of the lowest existing boiling points (-253°C); contaminants with a higher boiling point can be removed by condensation [79]. Cryogenic distillation typically removes hydrocarbons, and the hydrogen fuel must be pre-treated to remove CO_2 and H_2O. Compared to PSA, cryogenic distillation has a high H_2 recovery rate of 90 to 98% [52]. A cryogenic hydrogen purifier by *Airliquide* has a flow capacity range of 5 to 650 Nm^3 per hour [81]. The operating temperatures are low and pressures are low. The most dominant disadvantages of this technology are the low achieved purity (around 99%) and high costs [52]. Therefore cryogenic distillation is suitable for large industrial processes rather than smaller scale [81].

3.3.3. Membranes

Membranes separate hydrogen from a mixed stream based on difference of particle size, or more specifically the *permselectivity*. In the case of a hydrogen membrane, the membrane has a permselectivity towards hydrogen, while other gases are unable to pass the membrane. The most common types of membranes used for hydrogen separation are polymers which are able to separate hydrogen at temperatures lower than 100°C, and high temperature separation membranes such as dense metals, ion-conductive and porous membranes. Out of these membrane types, polymeric membranes are the most developed technology and are the most practical. The membranes suitable for high temperature hydrogen have a higher selectivity and are capable of separating a higher hydrogen flow, but are also expensive [65]. Metallic membranes are most frequently made from palladium, and achieve a purity of 99 to 99.995% hydrogen. The driving force for this technology is the use of a pressure gradient [79]. A higher input pressure of hydrogen results in an improved driving force. In many industrial processes waste streams are generated at such high pressure that no additional energy is needed for membrane separation. In the membrane design a thin membrane is preferred as it results in the capability of high hydrogen flux, but the thin membrane must also be able to withstand the pressure difference. A challenge for metallic membrane technology is the stability related to CO and H_2S poisoning. Membrane separation has numerous advantages, such as high flexibility, low energy use, low footprint, continuous processing and scalability [82], but it has an average recovery rate and resulting purity.

3.3.4. Electrochemical purification and compression

Electrochemical purification is similar to PEM fuel cells as it has the same components and similar working. The electrochemical compressor mentioned in Chapter 2 simultaneously purifies hydrogen. The technology, illustrated in Figure 3.5 consists of a platinum based catalyst that splits hydrogen into H^+ ions that are mobile in the permeable membrane selective to H^+ ions [45]. As a result, all other gases at the side of the anode are unable to cross the membrane. Thus in contrast to PEM fuel cells, electrochemical purification consumes electricity, which makes it similar to PEM electrolysis. As can be seen from the two half-reactions in Figure 3.5, hydrogen does not need to react with another substance. According to Schorer et al., it is possible to achieve a 100% hydrogen recovery rate [79]. The electrochemical cell is suitable for small scale systems as it has low capital and operational costs, but it can also be scaled up [79]. It follows from recent developments that HyET's purification and compression system can achieve pressures of 1,000 bar.

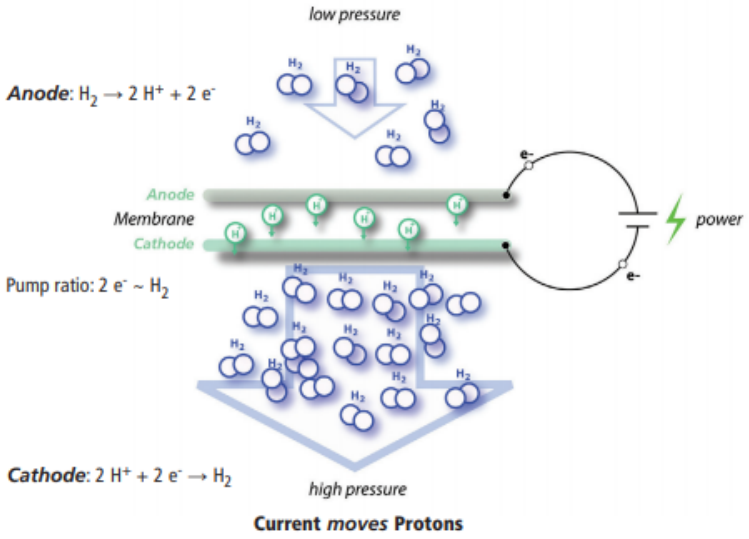

Figure 3.5: HyET's membrane technology for electrochemical purification and compression [83].

4
Permeation

The permeation of gas can be defined as the ability of a molecule to penetrate another material and diffuse through it. The permeability of polymer materials is of interest to many researchers, as it is relevant for example for plastic packaging and piping. Hydrogen being the smallest existing molecule raises concerns for the permeation of hydrogen through materials used in the gas grid. A study by the NREL is saying that admixing H_2 with natural gas up to 20% already causes a doubled gas loss in HDPE pipes [17]. But as gas loss is dominated by leakages, gas loss by permeation is often seen as insignificant. In this study permeation in the opposite direction (i.e. surrounding gases permeating into the pipe) is more relevant, and has until now not gotten much attention in literature.

This chapter describes the theoretical framework behind the calculations done on the inward permeation of air into polymer pipelines. According to literature, diffusion through polymers can be described by Fick's laws [84–88]. In this chapter the permeation of air is calculated based on the materials used in the gas grid. As the gases are insoluble in metals at room temperature, this study focuses only on permeation through polymers [89].

4.1. Fick's laws

According to permeation models, which have extensively been published in the last decades, permeation occurs in three steps:

1. Gas adsorbs on the surface of the material;
2. Gas diffuses through the material based on a partial pressure difference;
3. Gas evaporates from the surface of the interface into the low partial pressure area (desorption).

These steps correspond to Figure 4.1, where a permeant gas moves through a polymer membrane [86]. The difference in partial pressure from both sides of the membrane results in a concentration profile, as can be seen in the same figure. This concentration profile determines the permeation of gas through a medium. The phenomenon of diffusion can be described by Fick's laws. Fick's first law describes the amount of substance flowing through per unit area per unit time, flux J:

$$J = -D\frac{\partial C}{\partial x}, \tag{4.1}$$

where D is the diffusion constant of a gas in a certain medium and $\frac{\partial C}{\partial x}$ gives the concentration gradient within the medium, where x is the position in the material. Equation (4.1) thus states that the rate of permeation is determined by the derivative of the concentration profile that forms in the material. When no equilibrium profile has been formed within the material, Fick's second law for diffusion can be used to determine non steady-state diffusion:

$$\frac{\partial C}{\partial t} = D\frac{\partial^2 C}{\partial x^2}. \tag{4.2}$$

In Equation (4.2) the concentration is not only dependent on x, but also on time t, making it a partial differential equation. Rewriting Equation (4.2) in cylindrical coordinates and assuming permeation only in radial direction [90]:

$$\frac{\partial C}{\partial t} = D\left[\frac{1}{r}\frac{\partial}{\partial r}\left(r\frac{\partial C}{\partial r}\right)\right]. \tag{4.3}$$

where r is the radius of the cylinder. Fick's first and second law can often be used to approach the phenomenon of diffusion of small molecules in gas phase for diluted silutions through polymer materials. Equations (4.2) and (4.3) can be solved by defining boundary conditions.

4.1.1. Solving Fick's law

A book by Crank gives the solution to Equation (4.2) for a handful amount of shapes and a certain amount of sets of boundary conditions. The solutions for cylindrical coordinates are often complex and involve sums of multiple Bessel

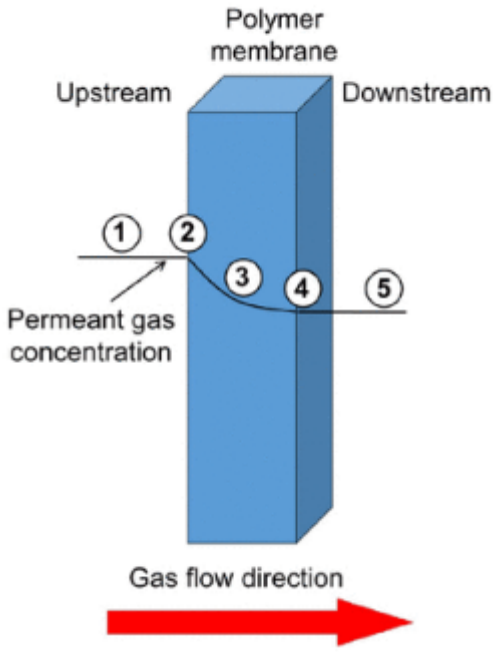

Figure 4.1: The three steps of permeation. At (2) the gas adsorbs on the polymer membrane. Afterwards diffusion drives gas through the material based on a partial pressure difference. At (4) the gas has passed the material and evaporates into the surrounding. [87]

functions. Another way to solve Equation (4.3) is by a numerical method. When executed accurately a numerical approach can reach a simplified similar solution. The numerical method used for the model in this research is the finite difference method. To apply the finite difference method to Fick's second law for cylindrical coordinates, Equation (4.2) is first rewritten so that Equation (4.3) can be treated as the equation for a slab (Equation (4.2)), as suggested by Crank. First the variables X and T are introduced:

$$\tau = Dt/r_{out}^2, \quad (4.4) \qquad R = r/r_{out}, \quad (4.5) \qquad X = \ln(R/r_{in}), \quad (4.6)$$

for time t, inner radius r_{in} and outer radius r_{out}. Then Equation (4.3) can be rewritten as

$$\frac{\partial C}{\partial \tau} = \frac{e^{-2X}}{r_{in}^2}\frac{\partial^2 C}{\partial X^2}. \quad (4.7)$$

According to the implicit finite difference method, Equation (4.7) can be discretised as follows:

$$\frac{C(i)^{t+1} - C(i)^t}{d\tau} = \frac{e^{-2X_1}}{r_{in}^2}\frac{C(i-1)^{t+1} - 2C(i)^{t+1} + C(i+1)^{t+1}{}^2}{\Delta X}, \quad (4.8)$$

where i is a step in radial direction. Note that Equation (4.8) is one dimensional. Equation (4.8) can be written in the abc form:

$$a(i)C(i-1)^{t+1} + b(i)C(i)^{t+1} + c(i)C(i+1)^{t+1} = RHS(i)^t, \quad (4.9)$$

where RHS stands for right hand side. In this case, for a, b and c we find:

$$a = -\frac{d\tau \cdot e^{-2X_1}}{r_{in}^2 \cdot \Delta X}, \quad (4.10) \qquad b = 1 + 2\frac{d\tau \cdot e^{-2X_1}}{r_{in}^2 \cdot \Delta X}, \quad (4.11) \qquad c = -\frac{d\tau \cdot e^{-2X_1}}{r_{in}^2 \cdot \Delta X}, \quad (4.12)$$

and RHS = $C(i)^t$. Note that t is a step in time by iteration. The number of time steps needed are determined by the time needed to reach steady state diffusion. Note that for the domain $r = 0$ to $r = r_{in}$ the diffusion coefficient for the diffusant

gas, in this case air, in hydrogen is taken, while in the domain $r = r_{in}$ to $r = r_{out}$ the diffusion coefficient of the diffusant gas in the polymer is taken. Now a, b, c and RHS are defined, Equation (4.8) can be rewritten in the matrix form:

$$A \times C = RHS, \tag{4.13}$$

where A is a matrix formed by a, b and c.

$$\mathrm{A} = \begin{bmatrix} b & c & 0 & 0 & 0 & ... \\ a & b & c & 0 & 0 & ... \\ 0 & a & b & c & 0 & ... \\ ... & ... & ... & ... & ... & ... \\ ... & 0 & 0 & 0 & a & b \end{bmatrix}. \tag{4.14}$$

A has the size i_{max-2} by i_{max-2}, where i_{max} stands for the maximum number of steps in radial direction. In this case, i_{max} is on the edge of the outer radius, r_{out}. Equation (4.13) can be solved for $i = 2$ to $i = i_{max-1}$, because $C(1)$ and $C(i_{max})$ are two special cases. These cases include the boundary conditions. In each case, the outer boundary condition is the same. It is assumed that air has formed an equilibrium or steady state concentration profile within the wall. The steady state concentration is given by the following equation:

$$C(r) = \frac{C_1 \ln(r_{out}/r) + C_2 \ln(r/r_{in})}{\ln(r_{out}/r_{in})}, \tag{4.15}$$

where C_1 represents the concentration at $r = r_{in}$ and C_2 at $r = r_{out}$, where the initial concentration at $r = r_{in}$ is zero. In the discrete case, C_1 is $C(r_{in}/dr+1)$, and C_2 is $C(i_{max})$. The concentration of air outside of the annulus is constant. As a result, $C(i_{max})$, remains at a constant value. This value can be calculated by assuming that the total concentration in a pipe segment is proportional to the solubility of the gas, S in the polymer. Solubility S describes the volume of gas that can be dissolved per volume of polymer, dependent on the pressure. Consider a pipe segment with length L, inner radius r_{in} and outer radius r_{out}, such that the material volume is 1 cm^3. The amount of substance dissolved in that segment is given by

$$\int_0^L \int_{r_{in}}^{r_{out}} C(r) 2\pi r dr dx = S \cdot p_p \cdot \rho \cdot \alpha, \tag{4.16}$$

where p_p is the partial pressure of the diffusing element in air, ρ is the density of the diffusing element, and α is the air fraction in the soil, thus the fraction of the pipe that is in contact with air. The boundary condition at i_{max} is then determined by rearranging Equation (4.16). When the concentration profile in the wall is known, the amount of substance per unit area per unit time, J can then be calculated from Equation (4.1).

4.1.2. Method

The amount of diffusing substance is dependent on the concentration gradient in the pipe wall, which again is determined by the flow conditions inside the pipeline. For lower flow rates the concentration gradient that forms in the pipe wall will result in more permeation. For this reason, three models are created, one for zero flow, one for laminar flow and another for turbulent flow. To determine whether the hydrogen flow is laminar or turbulent, the following relation has been used to calculate the Reynolds number:

$$\mathrm{Re} = \frac{v \cdot d_{in} \cdot \rho}{\mu} < 2{,}300; \qquad \text{laminar} \tag{4.17}$$

$$\mathrm{Re} = \frac{v \cdot d_{in} \cdot \rho}{\mu} > 3{,}500; \qquad \text{turbulent} \tag{4.18}$$

In Equations (4.17) and (4.18) μ stands for the absolute viscosity of hydrogen. It is assumed that the absolute viscosity is not affected by air after penetration into the interior of the pipe, as this problem concerns small concentrations. Note that the density is dependent on the pressure, and thus the Reynolds number varies for different pipeline pressures.

The model was made under the following assumptions:

1. The diffusion of gases through pipeline materials follows the laws of Fickian diffusion.

2. The diffusion coefficients are assumed to be concentration independent.
3. Air is the only gas that permeates into the pipe and the share of argon (0.93%) and CO_2 (0.04%) in the atmosphere can be neglected. That leaves two permeable gases: O_2 and N_2.
4. Multiple diffusing gases are not expected to have an influence on each others diffusion [85]. Thus the outward permeation of hydrogen is not considered to be relevant in this case.
5. The partial pressures of O_2 and N_2 in the soil are equal to air.
6. There is no distinction in permeation coefficients between different soils, as the partial pressures in the atmosphere and in all soils will be equal.
7. The pipeline is assumed to be robust and made of one part.
8. The flow in every pipe is a fully developed flow.
9. The age of the pipeline does not have an influence on the diffusion or solubility coefficient.

The goal of the model is to quantify the permeation of gases into the pipeline and to find the sensitivity of variables to the amount of permeation. To achieve this each variable in turn are varied in value while all other variables are set at a constant value. The dependent variables that are studied are material, soil temperature, soil type, flow velocity, diameter, wall thickness, distance and pressure.

4.2. Grid specifications

This section gives the conditions under which the calculations have been performed in this research. The calculations are location specific for Stad aan 't Haringvliet, because the materials, diameters and thicknesses in that specific grid were used. The temperature data used in the calculations are also from an area near Stad aan 't Haringvliet. However, the conditions in other parts of the Netherlands are not expected to deviate significantly.

4.2.1. Grid materials

The grid in SatH is mainly a low pressure grid, except for one steel 8 barg pipeline. 30 barg pipelines in the transmission grid are predominately made from steel. The other materials in the 100 mbarg and 2 barg network are listed in Table 4.1. PE comes in three different categories: PE 40, PE 80 and PE 100. In other low pressure grids in the Netherlands sporadically exist other types of PE, such as PE 63. Through conversations with polymer and pipeline manufacturers it was confirmed that PE 40 is medium density polyethylene, PE 100 is high density polyethylene and PE 80 can come in either medium as high density polyethylene. Low density polyethylene is less frequently used in the DNO grid, but is often used for house connection pipelines. For the sake of completeness low, medium and high density polyethylene are considered in this research. Other frequent materials are PVC and PVC/CPE. Pipeline manufacturer *Wavin* estimates the CPE content in PVC to be 10%. A study by Shur and Ranby gives diffusion constants for PVC with a range of CPE content and a range of chloride content in CPE. The chloride content in CPE could not be retrieved, and thus a mean value of 50% chloride in CPE was chosen. This makes a total of five considered materials. Other lesser frequent materials in the grid are cast iron, fibre cement, copper, and also laminates of materials.

Table 4.1 gives an overview of the materials in the grid in the section SatH, including the inner and outer diameter, wall thickness and length of the pipeline. Note that while there are very few 30 mbarg pipelines in Goeree-Overvlakkee, in other locations in the Netherlands 30 mbarg pipelines are more common. The positioning of these pipelines are visible from Figure 4.2.

4.2.2. Constants

The permeability of a gas in a polymer is a material property, given by Barrer's equation:

$$P = D \times S. \tag{4.19}$$

Equations and values for the diffusion coefficients of gas pairs were found in a book by Roberts [92]. The diffusion coefficient of gas pairs are dependent on temperature and pressure. According to Roberts, in a 100 mbarg pipeline at 12°C, the diffusion coefficients of oxygen and nitrogen in hydrogen are both approximately 1.5 cm^2/s. In literature diffusion constants for gases in polymers are extensively researched. Diffusion of gas through polymers is dependent the size and state of the diffusant gas, but also on the molecular morphology of the polymer. Polymers are partly crystalline and partly amorphous. The amorphous fraction of the polymer is the permeable part, whereas the crystalline matrix within a polymer is impermeable. The difference between low, medium and high density polyethylene (LDPE, MDPE and HDPE, respectively)

Table 4.1: Most frequent inner and outer diameters in the 100 mbar and 2 bar grid and total length in meters.

100 mbar				
Material	d_{in} (mm)	d_{out} (mm)	thickness (mm)	Length (m)
PVC	27.2	32	1.4	175
	104.6	110	2.7	120
PVC/CPE	28	32	2	3,011
	59	63	2	1,452
	104.6	110	2.7	6,524
	152.2	160	3.9	1,291
PE 80	90	110	10	613
	97.4	110	6.3	586
2 bar				
Material	d_{in} (mm)	d_{out} (mm)	thickness (mm)	Length (m)
PE 100	26	32	3	47
PE 80	26	32	3	498
	32.6	40	3.7	553
	51.4	60	4.3	3,055
	90	110	10	3,992
	97.4	110	6.3	1,546
	141.8	160	9.1	973

lies in the crystallinity fraction. Polyethlyene manufacturer *LyondellBasell* produces polyethylene in a range from 35% to 80% crystallinity (LDPE to HDPE). A study by Michaels and Bixler compares three types of polyethylene with a crystallinity fraction of 29%, 43% and 73%. These values have been considered as LDPE, MDPE and HDPE, respectively. The full list of diffusion and solubility coefficients can be found in Table 4.2.

Table 4.2: Parameters diffusion, solubility, activation energy for diffusion and enthalpy of solution used in calculations.

N_2					
Material	T ° C	D (mm^2/s)	S (cm^3/cm^3 atm)	E_D (Joule/mol)[b]	H_s (Joule/mol)[b]
PVC/CPE [91]	25	1.6×10^{-7}	30.9×10^{-3}	33.5×10^{3}	-5.0×10^{3}
PVC [91]	25	1.2×10^{-7}	32.3×10^{-3}	30.1×10^{3}	-5.0×10^{3}
LDPE [93] [94]	25	7.4×10^{-5}	41.1×10^{-3} [a]	39.3×10^{3}	7.53×10^{3}
MDPE [93] [94]	25	3.2×10^{-5}	23.1×10^{-3} [a]	41.4×10^{3}	7.95×10^{3}
HDPE [93][94]	25	9.3×10^{-6}	11.7×10^{-3} [a]	37.7×10^{3}	2.1×10^{3}
O_2					
Material	T ° C	D (mm^2/s)	S (cm^3/cm^3 atm)	E_D (Joule/mol)[b]	H_s (Joule/mol)[b]
PVC/CPE [91]	25	5.0×10^{-7}	75.0×10^{-3}	29.3×10^{3}	-8.4×10^{3}[c]
PVC [91]	25	4.0×10^{-7}	58.9×10^{-3}	24.3×10^{3}	-8.4×10^{3}[c]
LDPE [93][94]	25	1.2×10^{-4}	71.7×10^{-3} [a]	38.9×10^{3}	2.09×10^{3}
MDPE [93][94]	25	4.6×10^{-5}	47.8×10^{-3} [a]	40.2×10^{3}	2.51×10^{3}
HDPE [93][94]	25	1.7×10^{-5}	18.1×10^{-3} [a]	36.8×10^{3}	-1.67×10^{3}

[a] Calculated from $S = P/D$.

[b] Original values in (kcal/mole) have been converted (1 kcal = 4,184 Joule).

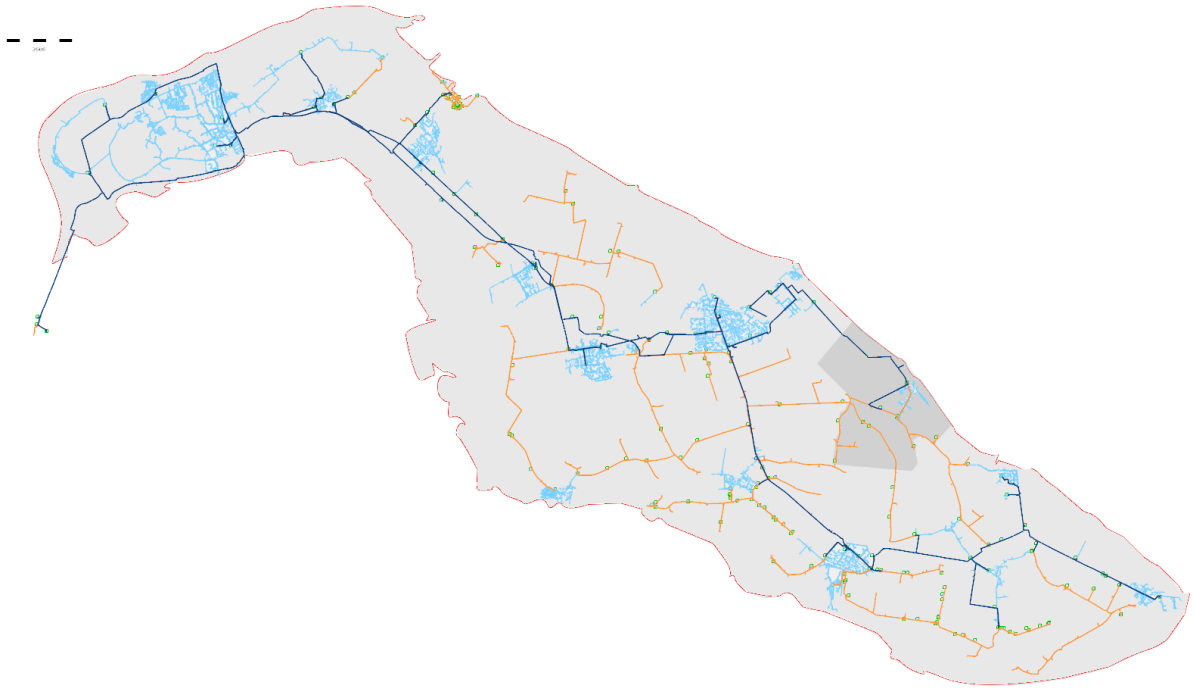

Figure 4.2: The grid in Goeree-Overvlakkee. The dark grey area represents Stad aan 't Haringvliet. The dark blue lines represent the 8 barg pipelines, the orange lines represent the 2 barg pipelines and the light blue lines are the 100 mbarg pipelines. The scale is given by the black and white striped line, which represents 2 kilometers. Data taken from software IRENE Pro.

4.2.3. Temperature data

The constants in Table 4.2 are given for $T = 25°C$, while in reality the temperature of the pipeline will have lower temperatures. The pipelines are assumed to be similar to the soil temperature at 80 cm below NAP, the same depth at which most pipelines are installed. Soil temperature data from KNMI at 50 cm and 100 cm depth were interpolated to find the soil temperature at 80 cm.

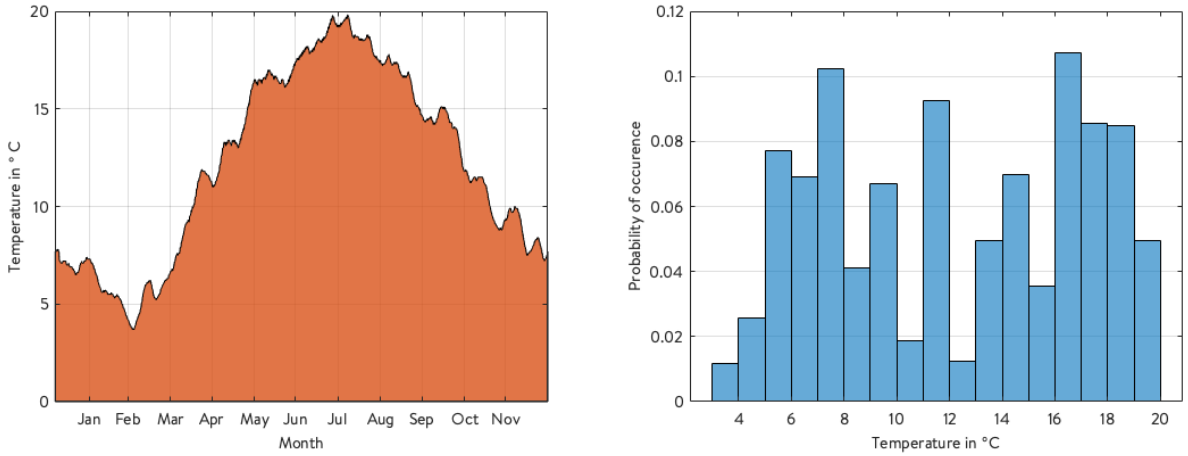

(a) Four hourly soil temperature throughout 2018.

(b) The frequency of occurrence of four hourly soil temperatures.

Figure 4.3: Soil temperatures for 2018 in Wilhelminadorp, Zeeland at 80 cm below NAP. Data interpolated from KNMI.

In Figure 4.3 a wide variety can be seen between soil temperatures throughout the year. For this reason, all calculations have been performed at average soil temperature of 12 °C, unless stated otherwise. Both the diffusion and solubility constants are temperature dependent, given by the Arrhenius relation:

$$D = D_0 \cdot e^{\frac{-E_D}{RT}} \tag{4.20}$$

and

$$S = S_0 \cdot e^{\frac{-H_S}{RT}}, \tag{4.21}$$

with E_D and H_S being the activation energy for diffusion and the enthalpy of sorption, respectively. Most coefficients found in literature are for 25°C, whereas the average soil temperature at 80 cm depth is 12 °C. With the values from Table 4.2 placed in Equations (4.20) and (4.21), Figure 4.4 was created showing the temperature dependence of the diffusion and solubility coefficients.

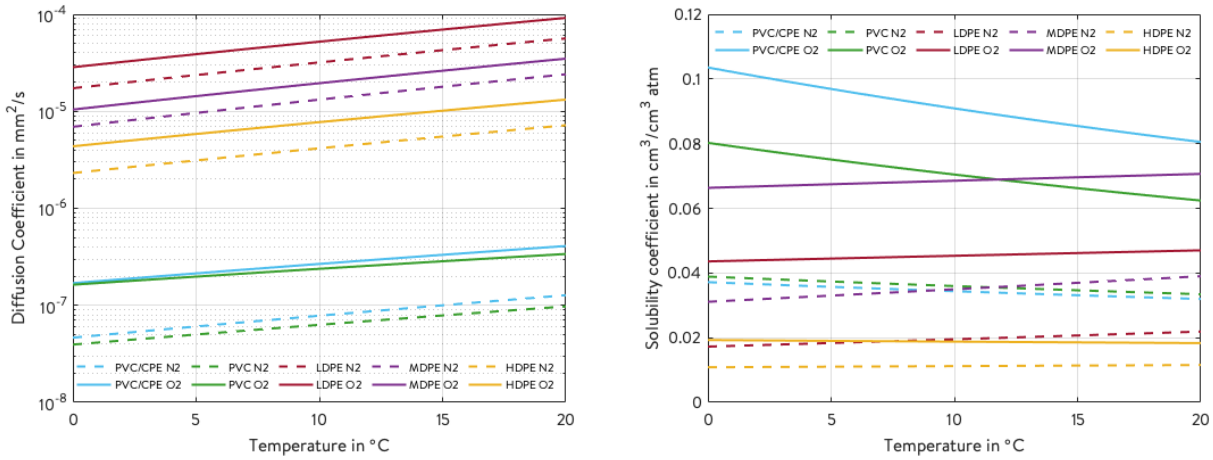

(a) Diffusion coefficients (D) on semi-log scale.

(b) Solubility coefficients (S).

Figure 4.4: Diffusion and solubility coefficients of O_2 and N_2 for pipeline materials as a function of temperature.

4.3. Zero flow

The zero flow case is illustrating the case that there are no hydrogen gas offtakers, and as a result the gas stands still. This can occur during summer when the heat demand is at its minimum. In the case without flow, C is independent of the length of the pipe, making it a one-dimensional problem, as explained in Section 4.1. As a result, the pipe reduces to an annulus. The initial condition is a steady state profile by Equation (4.15). But because there is no flow, the concentration on the inside of the annulus increases with time, until eventually a new steady state forms. After this one-dimensional numerical problem was defined in MATLAB including the boundary conditions, it was solved with a Gauss elimination solver.

To find the concentration of air in the interior of the pipe as a function of time, a pipe segment with length L is considered. The inner volume of the pipe with length L is taken to be 1 m^3. The concentration of the diffusant gas at time t is then

$$C(t) = \int_0^L \int_0^{r_{in}} C(r) 2\pi r dr dx. \tag{4.22}$$

Equation (4.22) can be used to convert the 1D result into a 3D result.

4.4. Laminar flow

Laminar flow occurs for Reynolds numbers below 2,300. As a result of laminar pipe flow, a velocity profile forms in the pipe, according to $v(r) = 2v_{\text{mean}}(1-(r/r_{in})^2)$. Because of this velocity profile, there is no radial mixing of the permeant gases with hydrogen. In the case of laminar flow, Equation (4.3) is expanded to the following equation [96]:

$$\frac{\partial C}{\partial t} = D\left[\frac{1}{r}\frac{\partial}{\partial r}\left(r\frac{\partial C}{\partial r}\right)\right] + D\frac{\partial^2 C}{\partial x^2} - 2v_{\text{mean}}\left[1-(r/r_{in})^2\right]\frac{\partial C}{\partial x}, \tag{4.23}$$

where x is the axial position. Equation (4.23) can be discretised and rewritten, similar to Equations (4.8) and (4.13). Because another term independent of D is added, t replaces τ, and after discretisation Equation (4.23) becomes a two dimensional equation.

$$\frac{C(i,j)^{t+1}-C(i,j)^{t}}{dt}=\frac{D\cdot e^{-2X_1}}{r_{in}^2\cdot r_{out}^2}\frac{C(i-1,j)^{t+1}-2C(i,j)^{t+1}+C(i+1,j)^{t+1}}{(\Delta X)^2}+D\frac{C(i-1,j)^{t+1}-2C(i,j)^{t+1}+C(i+1,j)^{t+1}}{(\Delta x)^2}-$$
$$2v_{\text{mean}}\left[1-(r/r_{in})^2\right]\frac{C(i,j)^{(t+1)}-C(i,j-1)^{(t+1)}}{\Delta x}. \quad (4.24)$$

But as a second dimension has been added in the x direction, Equation (4.9) is expanded to

$$a(i)C(i-1,j)+b(i)C(i,j)+c(i)C(i+1,j)+d(i)C(i,j-1)+e(i)C(i,j+1)=\text{RHS}(i,j). \quad (4.25)$$

In Equation (4.25) i is a step in radial direction, and j is a step in axial direction similar to Figure 4.5.

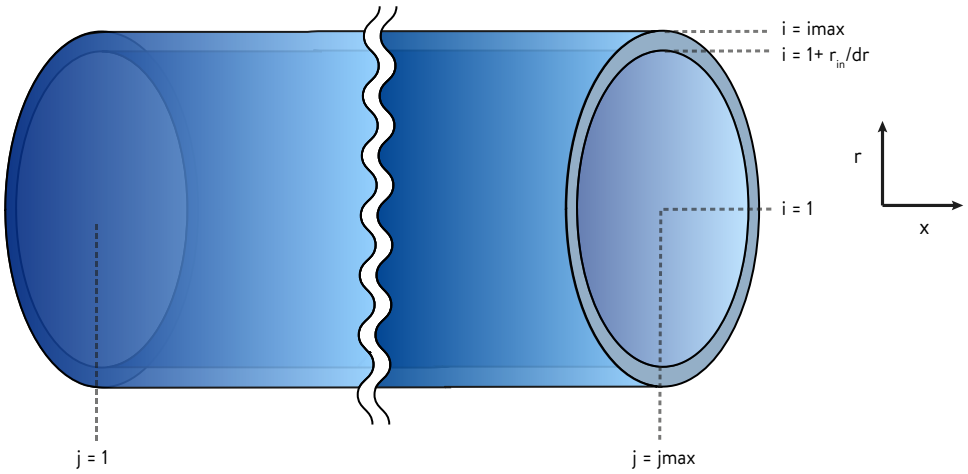

Figure 4.5: A pipe segment of undefined length, with the indicated coordinates i and j.

Similar to Equations (4.9) and (4.13), we can find coefficients a, b, c, d and e:

$$a=\frac{-D\cdot dt\cdot\exp(-2X)}{(\Delta X)^2 r_{out}^2\cdot r_{in}^2}, \quad (4.26)$$

$$c=\frac{-D\cdot dt\cdot\exp(-2X)}{(\Delta X)^2 r_{out}^2\cdot r_{in}^2}, \quad (4.27)$$

$$d=\frac{-D\cdot dt}{\Delta x^2}-\frac{2v_{\text{mean}}(1-(r/r_{in})^2)\cdot dt}{\Delta x}, \quad (4.28)$$

$$e=\frac{-D\cdot dt}{\Delta x^2}, \quad (4.29)$$

$$b=1+2\frac{D\cdot exp(-2X)}{(\Delta X)^2 r_{out}^2\cdot r_{in}^2}+2\frac{D\cdot dt}{(\Delta x)^2}-\frac{2v_{\text{mean}}(1-(r/r_{in})^2)\cdot dt}{\Delta x}. \quad (4.30)$$

After these variables were introduced in the MATLAB script, the problem was solved with a Jacobi solver. To find the amount of contamination of oxygen and nitrogen as a result of diffusion, a simple mass balance can be constructed similar to Kjeldsen.

From Figure 4.6 the following equation can be deduced:

$$QC+AJ=Q(C+\frac{\partial C}{\partial x}dx), \quad (4.31)$$

where A can be calculated by taking the mean radius, r_m between r_{in} and r_{out}, assuming a thin pipe wall :

$$A=2\pi r_m dx. \quad (4.32)$$

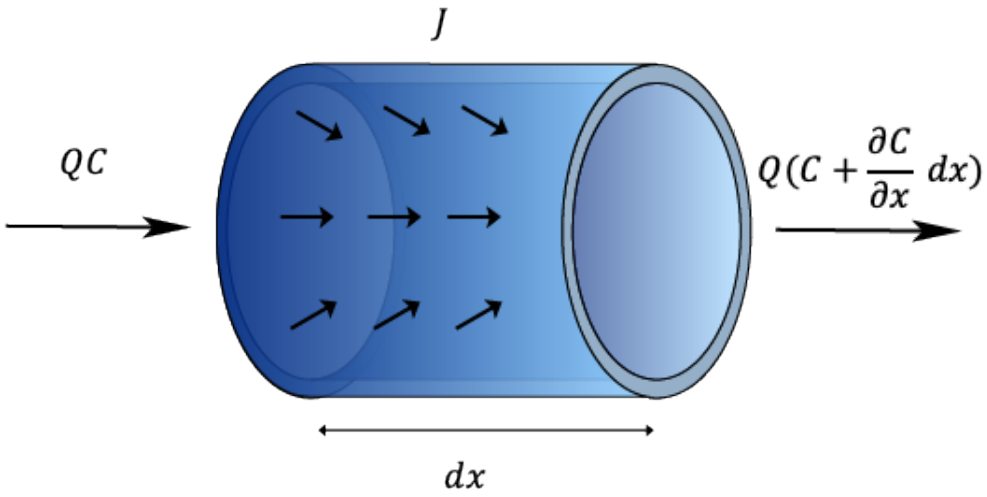

Figure 4.6: Mass balance of pipe segment dx.

If it is assumed that the concentration going into the pipe at $t=0$ is equal to zero, thus that hydrogen enters the pipeline uncontaminated, the mass balance can be reduced so that only the simple equation remains:

$$\frac{\partial C}{\partial x} = \frac{(2\pi r_m)J}{Q}. \tag{4.33}$$

Or with $Q = v \cdot \pi \cdot r_{in}^2$ in the discretised version,

$$C(j) = \frac{2r_m J dx}{r_{in}^2 \cdot v} + C(j-1). \tag{4.34}$$

Equation (4.34) is used in both the laminar and the turbulent flow models to find the contamination of oxygen and nitrogen per m^3 hydrogen.

4.5. Turbulent flow

Turbulent flow inside the pipe has a consequence for the resulting concentration gradient in the pipe wall, because of the mixing conditions within the pipe. Eddies in turbulent pipe flow result in an additional diffusion component beside molecular diffusion, called *turbulent diffusivity*, D_T, also called *eddy diffusivity* [97]. As a result of the extra diffusion term the diffusant gases mix better with hydrogen. In contrast to the diffusivity, D, the turbulent diffusivity is not a characteristic fluid property but is dependent on specific flow conditions, such as position and direction. Another difference with the laminar flow case is the velocity profile formed inside the pipe. Including turbulent velocity profile v_T and turbulent diffusivity D_T in the partial differential equation, Equation (4.23) becomes:

$$\frac{\partial C}{\partial t} = D\left[\frac{1}{r}\frac{\partial}{\partial r}\left(r\frac{\partial C}{\partial r}\right)\right] + (D+D_T)\frac{\partial^2 C}{\partial x^2} - v_T\frac{\partial C}{\partial x}. \tag{4.35}$$

Similarly to laminar flow, Equation (4.35) becomes:

$$\frac{C(i,j)^{t+1} - C(i,j)^t}{dt} = \frac{D \cdot e^{-2X_1}}{r_{in}^2 \cdot r_{out}^2}\frac{C(i-1,j)^{t+1} - 2C(i,j)^{t+1} + C(i+1,j)^{t+1}}{(\Delta X)^2} + (D+D_T)\frac{C(i-1,j)^{t+1} - 2C(i,j)^{t+1} + C(i+1,j)^{t+1}}{(\Delta x)^2} - v_T\frac{C(i,j)^{(t+1)} - C(i,j-1)^{(t+1)}}{\Delta x}. \tag{4.36}$$

with coefficients a, b, c, d and e obtained similar to laminar flow.

$$a = \frac{-D \cdot dt \cdot \exp(-2X)}{(\Delta X)^2 r_{out}^2 \cdot r_{in}^2}, \tag{4.37}$$

$$c = \frac{-D \cdot dt \cdot \exp(-2X)}{(\Delta X)^2 r_{out}^2 \cdot r_{in}^2}, \tag{4.38}$$

$$d = \frac{-(D+D_T) \cdot dt}{\Delta x^2} - \frac{v_T \cdot dt}{\Delta x}, \tag{4.39}$$

$$e = \frac{-(D+D_T) \cdot dt}{\Delta x^2}, \tag{4.40}$$

$$b = 1 + 2\frac{D \cdot \exp(-2X)}{(\Delta X)^2 r_{out}^2 \cdot r_{in}^2} + 2\frac{(D+D_T) \cdot dt}{(\Delta x)^2} - \frac{v_T \cdot dt}{\Delta x}. \tag{4.41}$$

For v_T many derivations exist in literature, especially for high Reynolds numbers. The Reynolds numbers in this research are expected to be relatively low, as the pipeline diameters are small and the flow velocities are low. v_T for low Reynolds numbers was found in Adrian et al. [98]:

$$v_T(r) = u_\tau \cdot \left[2.86 \cdot \ln\left(\frac{r \cdot u_\tau}{\nu}\right) + 4.8\right], \tag{4.42}$$

where u_τ is the friction velocity and ν is the kinematic viscosity, which is related to the dynamic viscosity by $\nu = \mu/\rho$. The value of u_τ was estimated to be $v_{\text{mean}}/14.7$ based on the study by Adrian et al. [98]. Figure 4.7 compares the resulting turbulent flow velocity profile with a laminar velocity profile.

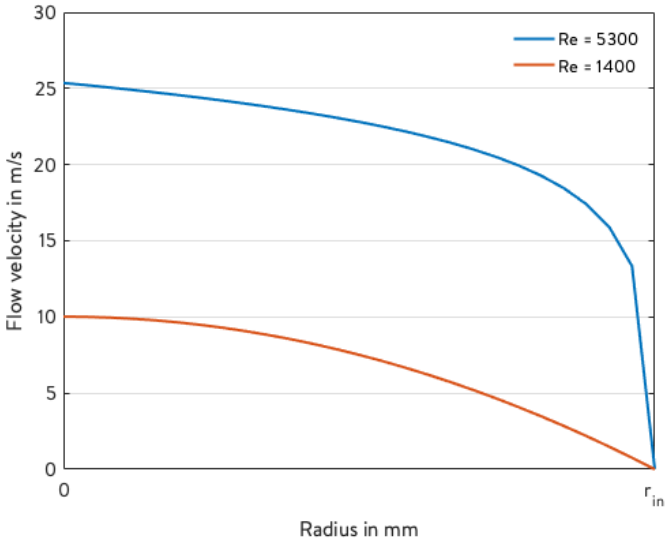

Figure 4.7: A turbulent and laminar pipe flow velocity profile with Reynolds numbers 5,300 and 1,400, respectively.

Similar to the laminar flow model, this problem was solved with a Jacobi solver. The final concentration gradient formed in the pipe wall is then used to calculate the amount of contamination in the hydrogen feed with Equation (4.34).

5
Results

This chapter gives the results of the model described in Chapter 4. The model was designed to find the relationship between the dependent variables and the amount of permeation. The following dependent variables were studied: material, soil temperature, soil type, flow velocity, diameter, wall thickness, distance and pressure. Each section is designated to one variable, which was tested in the model for fluctuating values while all other variables were not changed in the settings of the model. The standard settings of the model are given in Table 5.1.

Table 5.1: Standard settings for all calculations.

Variable	Symbol	Value
Material	-	MDPE
Temperature	T	12 ° C
Soil type	-	Sand
Flow velocity	v	1 m/s
Inner diameter	d_{in}	26 mm
Outer diameter	d_{out}	32 mm
Wall thickness	w	3 mm
Distance	x	100 m
Pressure	p	100 mbarg
Diffusion constant	$D_{O_2}^{12°C}$	2.196×10^{-5} mm^2/s
Diffusion constant	$D_{N_2}^{12°C}$	1.493×10^{-5} mm^2/s
Solubility constant	$S_{O_2}^{12°C}$	69×10^{-3} cm^3 cm^{-3} atm^{-1}
Solubility constant	$S_{N_2}^{12°C}$	35×10^{-3} cm^3 cm^{-3} atm^{-1}

Unless stated otherwise, all the results in the following sections are plotted as a function of pipe length. In other words, the distance that the gas has traveled. All calculations as a function of length have been done for a maximum distance of 100 m. All values in Table 5.1 except two were selected such that the results were considered to be conservative. For example, a low v, small d_{in}, small w and a low p result in more contamination. The material with the second highest permeability (MDPE) was chosen, as the material with the highest permeability (LDPE) is much less frequently used in the grid. Furthermore, for T the yearly average temperature was chosen, 12°C. Throughout Sections 5.1 to 5.5, two plots are shown, one for the oxygen diffusion and the other for the nitrogen diffusion.

5.1. Pressure

The rate of inward diffusion is not affected by the hydrogen pressure in the pipe. However, the relative amount of contamination is. The plots in the following sections are given in mg/m^3 to express the absolute contamination, independent of the hydrogen pressure. But the unit used in ISO-14786 is given in µmol/mol, in other words ppm mole, which expresses a relative contamination. Conversion goes by the following equation:

$$\frac{m_1\,[\text{mg}]}{V_2\,[\text{m}^3]} = \frac{M_1\rho_2}{M_2}\times10^{-6}\text{ppm}. \tag{5.1}$$

In this case substance 1 is oxygen or nitrogen and substance 2 is hydrogen. As density is dependent on the pressure, by converting the unit of the results the pressure dependence can be expressed. Taking a molar mass of hydrogen of 2.02 g/mole, density at 12°C of 85 g/m^3, molar mass of oxygen 32 g/mole and molar mass of nitrogen of 28 g/mole, the conversion units become:

$$\frac{m_{O_2}\,[\text{mg}]}{V_{H_2}\,[\text{m}^3]}\times\frac{2.02}{32\times10^3\times85\times p\,[\text{bara}]}\times10^6 = O_2 \quad \text{contamination in ppm}, \tag{5.2}$$

$$\frac{m_{N_2}[\text{mg}]}{V_{H_2}[\text{m}^3]} \times \frac{2.02}{28 \times 10^3 \times 85 \times p[\text{bara}]} \times 10^6 = N_2 \quad \text{contamination in ppm,} \tag{5.3}$$

where p stands for the absolute hydrogen pressure of the pipeline.

5.2. Material

The differences in permeability between pipeline materials have already been introduced in Table 4.2 in Chapter 4. Figures 5.1a and 5.1b plot the amount of diffused oxygen and nitrogen per unit length of the pipe for five materials used in the grid, respectively. The fixed parameters used for these plots can be found in Table 5.1.

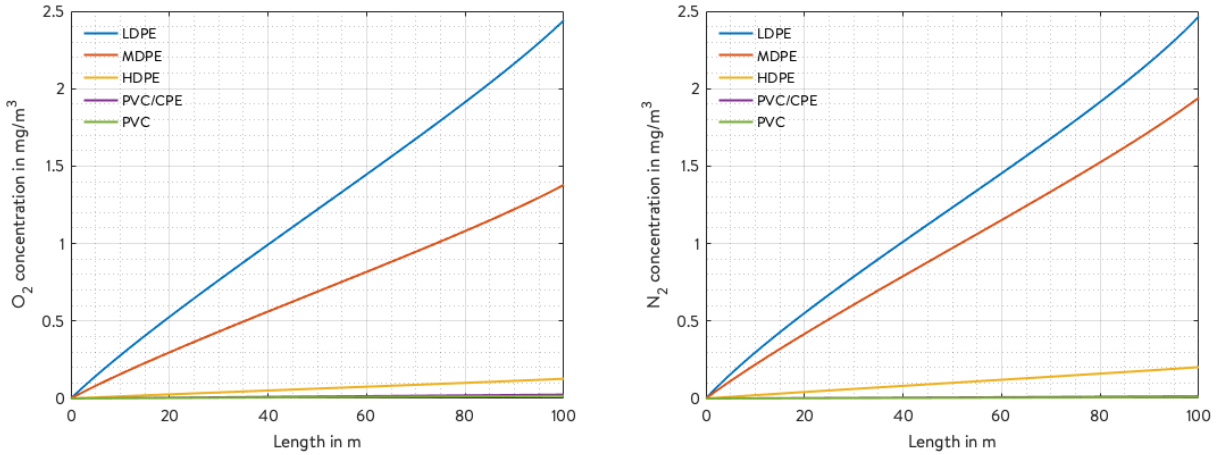

(a) Oxygen contamination.

(b) Nitrogen contamination.

Figure 5.1: The amount of O_2 and N_2 contamination with wall thickness of 3 mm for 1 m/s in 12° C for materials LDPE, MDPE, HDPE, PVC/CPE and PVC.

Figure 5.1 shows that there is a difference in order or 10^2 between the five materials used in the grid. The relation between the amount of contamination for the five materials is given by the material parameter P, earlier defined in Equation (4.19). The unit used for the contamination is converted to the relative contamination by Equations (5.2) and (5.3), and the results are given in Table 5.2. Due to the large difference in permeability P, PVC/CPE and PVC are not clearly visible in Figure 5.1, but can be found in Table 5.2 instead.

Table 5.2: O_2 and N_2 contamination in ppm per 100 meters travelled for each material.

O_2					
	LDPE	MDPE	HDPE	PVC/CPE	PVC
100 mbarg	1.7	9.5×10^{-1}	8.6×10^{-2}	1.7×10^{-2}	1.1×10^{-2}
2 barg	6.2×10^{-1}	3.5×10^{-1}	3.2×10^{-2}	6.1×10^{-3}	4.2×10^{-3}
N_2					
	LDPE	MDPE	HDPE	PVC/CPE	PVC
100 mbarg	2.0	1.5	1.5×10^{-1}	8.2×10^{-3}	6.9×10^{-3}
2 barg	7.4×10^{-1}	5.5×10^{-1}	5.4×10^{-2}	3.0×10^{-3}	2.5×10^{-3}

5.3. Flow velocity

The relationship between the flow velocity of hydrogen and permeation was studied through three different models, one for zero flow, one for laminar flow and another for turbulent flow. As initially expected, lower flow velocity results in more permeation. The model was tested for a flow velocity of up to 30 m/s, the current upper limit for the flow velocity of natural gas in the gas grid. The results for oxygen and nitrogen contamination as a function of pipe length are shown in Figures 5.2a and 5.2b, respectively.

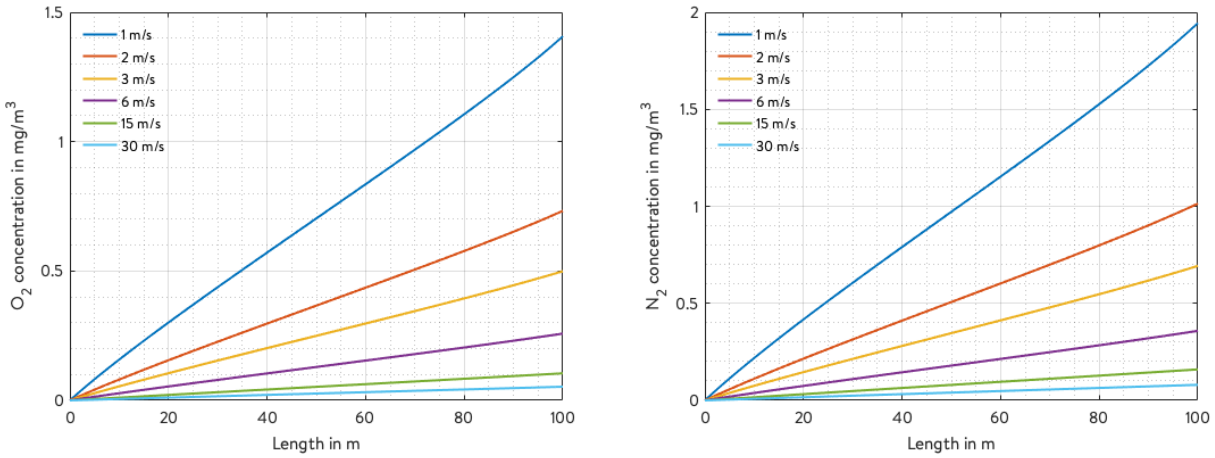

(a) Oxygen contamination as a function of pipe length.

(b) Nitrogen contamination as a function of pipe length.

Figure 5.2: The amount of O_2 and N_2 contamination with wall thickness of 3 mm for 1 m/s in 12° C for six flow velocities. The plots of 15 m/s and 30 m/s come from the turbulent hydrogen flow model.

Table 5.3: O_2 and N_2 contamination in ppm per 100 meters travelled for different flow velocities.

O_2						
	1 m/s	2 m/s	3 m/s	6 m/s	15 m/s	30 m/s
100 mbarg	9.5×10^{-1}	4.7×10^{-1}	3.4×10^{-1}	1.7×10^{-1}	7.1×10^{-2}	3.6×10^{-2}
2 barg	3.5×10^{-1}	1.7×10^{-1}	1.2×10^{-1}	6.4×10^{-2}	2.6×10^{-2}	1.3×10^{-2}
N_2						
	1 m/s	2 m/s	3 m/s	6 m/s	15 m/s	30 m/s
100 mbarg	1.5	7.8×10^{-1}	5.3×10^{-1}	2.8×10^{-1}	1.2×10^{-1}	6.6×10^{-2}
2 barg	5.5×10^{-1}	2.9×10^{-1}	2.0×10^{-1}	1.0×10^{-1}	4.2×10^{-2}	2.4×10^{-2}

The results plotted in Figure 5.2 come from both the laminar flow and the turbulent flow model. Calculating the Reynolds numbers from Equations (4.17) and (4.18) for the six plotted flow velocities, it can be found that the flow is laminar for 1 to 6 m/s, while the flow is turbulent for 15 and 30 m/s. Note that the Reynolds number is not only dependent on the flow velocity, but also on the hydrogen pressure and the inner diameter of the pipeline. Similar to the previous section, in addition to the absolute contamination also the relative contamination in ppm is given in Table 5.3.

The amount of O_2 and N_2 contamination has also been calculated under zero flow velocity condition. In contrast to the other results, the results for a flow velocity of zero were plotted as a function of time in Figure 5.3 for a time period of two days. Furthermore, instead of the standard temperature setting of 12 °C, the results were plotted for $T = 20$°C, as zero flow is most likely to occur in summer. At 20 °C, the diffusion coefficients of O_2 and N_2 in MDPE is increased by almost 60% and over 50% compared to the diffusion coefficient at 12 °C, respectively. The zero flow condition was plotted for two pipeline pressures, 100 mbarg and 2 barg. The oxygen and nitrogen contamination is highest for the zero flow condition, as in this case the hydrogen gas has the longest residence time in the pipeline.

5.4. Wall thickness

The pipe wall thickness has an influence on permeation, as a result of the distance that the diffusant gas needs to travel towards the pipe interior. A thicker pipe wall, and thus a longer distance for the gas to travel through the polymer before it reaches hydrogen inside the pipe, results in less contamination. Dimensions of the wall thickness depend on the pipe material. Pipes made of PVC and PVC/CPE have thinner walls than polyethylene pipes. Figure 5.4 shows the results for oxygen and nitrogen concentrations for wall thicknesses of 3 to 10 mm.

In addition, the relative concentration of oxygen and nitrogen in hydrogen is given in ppm in Table 5.4.

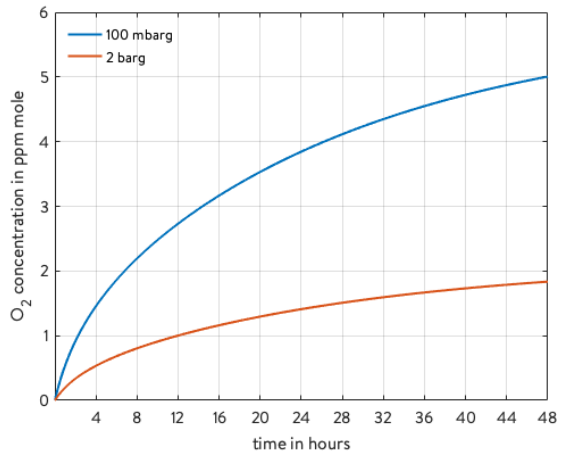

(a) The amount of oxygen contamination in ppm.

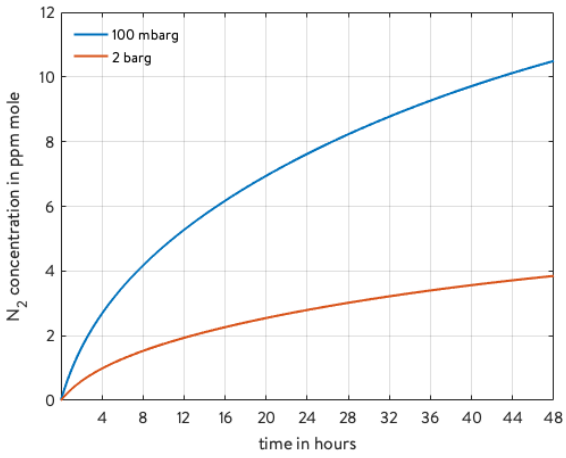

(b) The amount of nitrogen contamination in ppm.

Figure 5.3: The amount of O_2 and N_2 contamination as a function of time at 20°C plotted over two days.

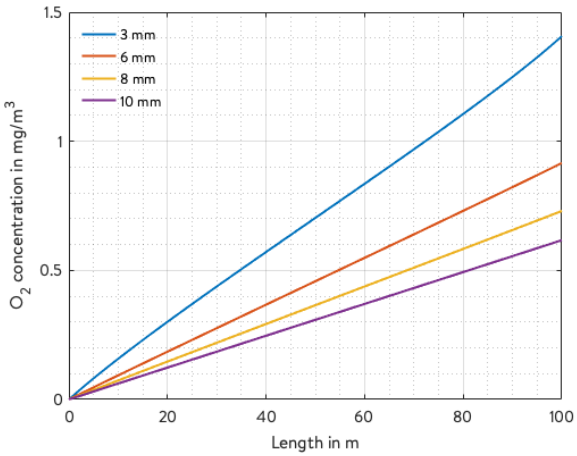

(a) The amount of oxygen contamination in a MDPE pipe with flow of 1 m/s in 12°C for five different thicknesses.

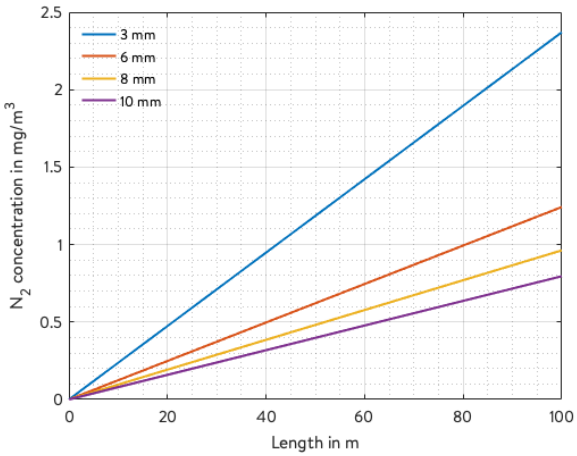

(b) N_2 contamination as a function of length.

Figure 5.4: The amount of O_2 and N_2 contamination as a function of length for four wall thicknesses.

5.5. Inner diameter

The dependence of the inner diameter on the contamination is due to the contact area of hydrogen with the pipe wall. This relationship is expressed earlier in Equation (4.34). A smaller inner diameter results in a larger contact area, and thus more contamination. This can also be seen in Figure 5.5, which plots the contamination for inner diameters of 26 mm, 32 mm, 50 mm and 90 mm.

Also the relative concentration was found by Equations (5.2) and (5.3) and the results are given in Table 5.5.

5.6. Temperature

Similar to the material dependence, the relation between temperature and permeation is given by the difference in permeability constant. The permeability is dependent on temperature by Arrhenius equations 4.20 and 4.21. Figure 5.6 plots the permeability constants of the five materials for temperatures 0°C to 20°C, the 4 hourly maximum soil temperature in 2018, on semi-log scale.

The temperature also has an influence on the diffusion constant of oxygen and nitrogen in hydrogen. In the calculations it is assumed that hydrogen takes on the same temperature as the soil. But as the diffusion coefficients of oxygen and nitrogen

Table 5.4: O_2 and N_2 contamination in ppm per 100 meters travelled for different wall thicknesses.

O_2				
	3 mm	6 mm	8 mm	10 mm
100 mbarg	9.5×10^{-1}	6.2×10^{-1}	4.9×10^{-1}	4.2×10^{-1}
2 barg	3.5×10^{-1}	2.3×10^{-1}	1.8×10^{-1}	1.5×10^{-1}
N_2				
	3 mm	6 mm	8 mm	10 mm
100 mbarg	1.5	9.4×10^{-1}	7.6×10^{-1}	6.4×10^{-1}
2 barg	5.5×10^{-1}	3.4×10^{-1}	2.8×10^{-1}	2.3×10^{-1}

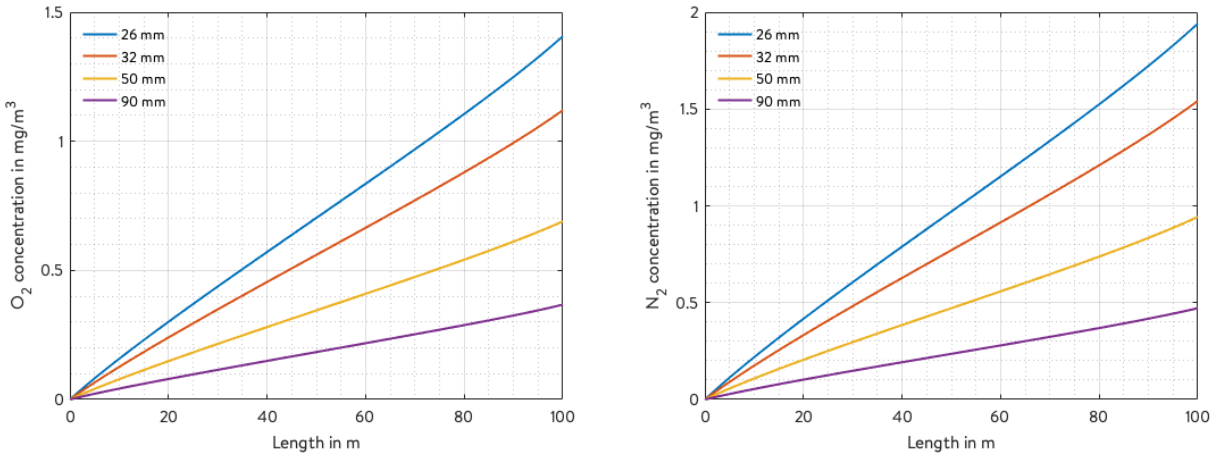

(a) O_2 contamination as a function of length.

(b) N_2 contamination as a function of length.

Figure 5.5: O_2 and N_2 contamination for four inner diameters.

Table 5.5: O_2 and N_2 contamination in ppm per 100 meters travelled for different inner diameters.

O_2				
	26 mm	32 mm	50 mm	90 mm
100 mbarg	9.5×10^{-1}	7.6×10^{-1}	4.7×10^{-1}	2.5×10^{-1}
2 barg	3.5×10^{-1}	2.8×10^{-1}	1.7×10^{-1}	9.1×10^{-2}
N_2				
	3 mm	6 mm	8 mm	10 mm
100 mbarg	1.5	1.2	6.8×10^{-1}	5.1×10^{-1}
2 barg	5.5×10^{-1}	4.4×10^{-1}	2.5×10^{-1}	1.9×10^{-1}

in hydrogen are in the range of 10^2 mm^2/s, which is 10^7 to 10^9 times the diffusion coefficient of oxygen and nitrogen in polymer, the temperature of hydrogen has a negligible influence on the permeation.

5.7. Soil

The amount of air that can reach the underground pipelines is dependent on the soil in the subsurface layer. The model is made under the assumption that the partial pressures of elements in air are equal to those in the soil. But loose soils have a higher air fraction than wet soils, as wet soils have more moisture in the pores.

The subsurface of Stad aan 't Haringvliet down to five meters depth is a mixture of fine sand, clayish sand, clay and bog. At the depth of 80 cm where the average distribution pipeline is installed, there is either clayish sand or fine sand.

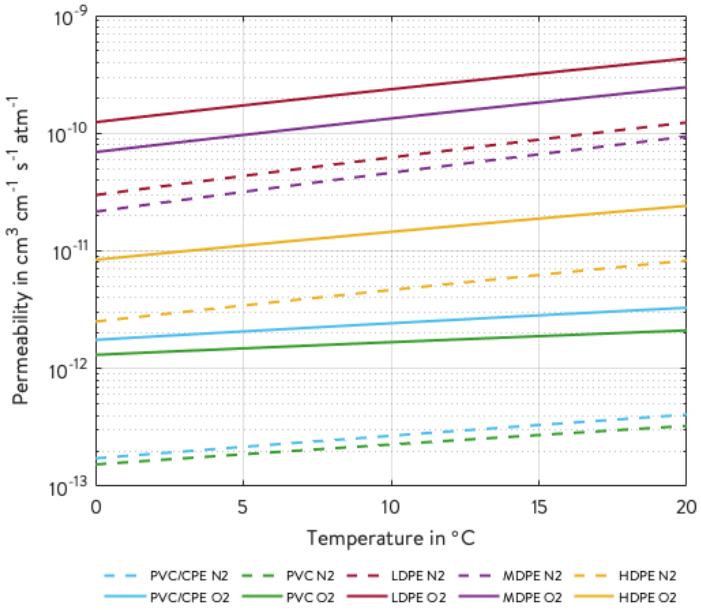

Figure 5.6: Permeability coefficients for O_2 (solid lines) and N_2 (dashed lines) through five polymers as a function of temperature.

Table 5.6: Air fractions per soil [99].

Soil	**Air fraction**
Sand	13 - 40 %
Sandy clay, loam, clayish fine sand	12 - 18 %
Clay	7 - 31 %

This can also be seen in Figure 5.7, where two perpendicular cross-sections are given of the subsurface of SatH. Note that there is always an uncertainty in subsurface models.

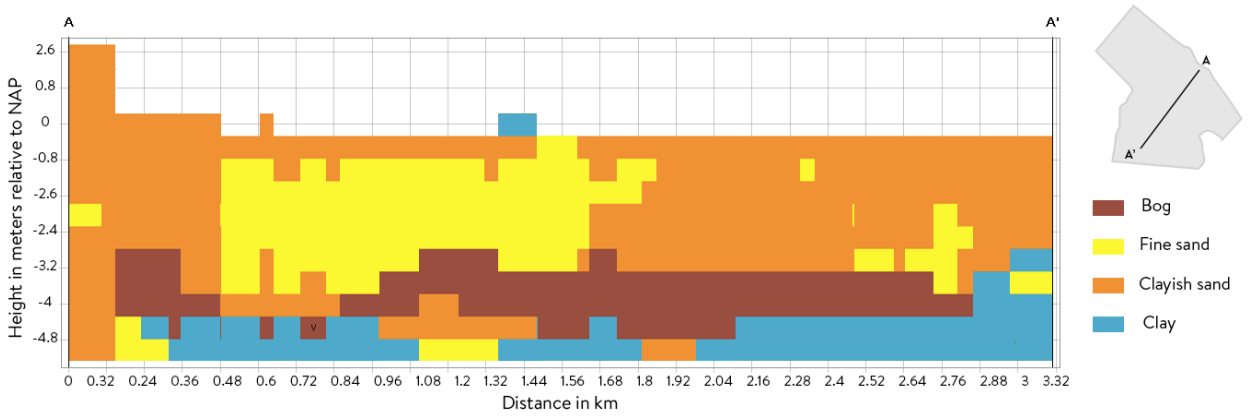

(a)

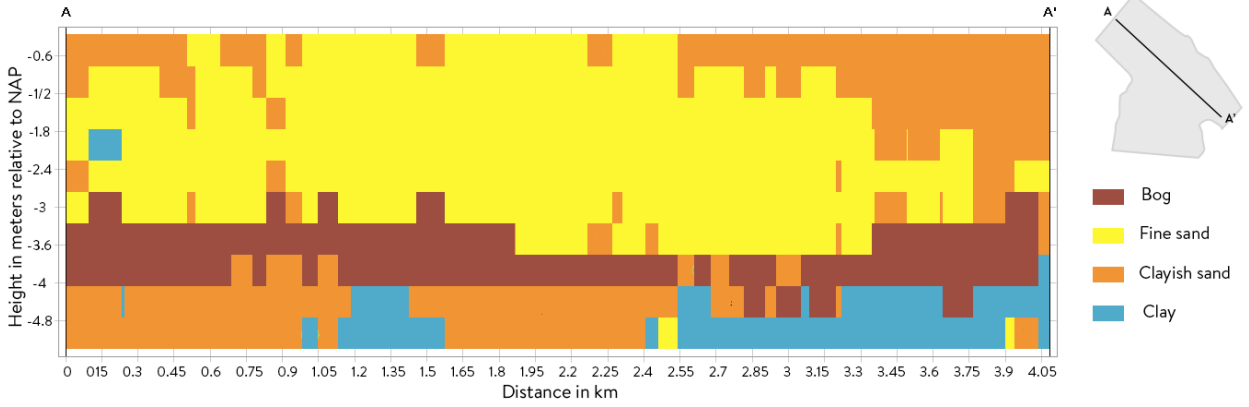

(b)

Figure 5.7: Two cross-sections of the subsurface layers in Stad aan 't Haringvliet. The cross-section starts at A and ends at A', visible from the grey contour in the right upper corner. Data from DINOloket.

6
Discussion

In Chapter 5 the results from the computation model were presented. In this chapter the results from the previous chapter are discussed and interpreted. The goal of the computation model was to find relationships between the seven variables that were tested and the amount of contamination caused by oxygen and nitrogen diffusing into polymer pipelines. In the coming section the results are compared to the limits in the ISO 14687-2 standard, as this is currently the most stringent standard that sets limits to contaminants oxygen and nitrogen in hydrogen fuel. In the first section, the results of all the variables are discussed. Afterwards the results are applied in a case study for Stad aan 't Haringvliet. Finally, in Section 6.4 the limitations of the computation model are explained.

6.1. Parameter dependency

If the results are compared to the ISO 14687-2 norm, where the upper concentration limit of oxygen and nitrogen are 5 ppm and 100 ppm, respectively, one conclusion can easily be drawn. The diffusion of nitrogen through MDPE is always 1.4 times more than oxygen, while the lower limit for nitrogen is 20 times higher than for oxygen. From this perspective, nitrogen poses no threat for short distances. Table 6.1 lists the distance in meters that gas needs to travel to exceed the lower limit of 5 ppm for oxygen.

Table 6.1: The distance in meters that hydrogen needs to travel to exceed the ISO 14687 contamination limit for oxygen at 5 ppm.

Material			**Flow velocity**		
	100 mbarg	2 barg		100 mbarg	2 barg
LDPE	298	812	1 m/s	526	1.44×10^3
MDPE	526	1.44×10^3	3 m/s	1.48×10^3	4.05×10^3
HDPE	5.81×10^3	15.8×10^3	6 m/s	2.87×10^3	7.83×10^3
PVC/CPE	30.0×10^3	81.9×10^3	15 m/s	7.08×10^3	19.3×10^3
PVC	44.1×10^3	12.0×10^3	30 m/s	14.0×10^3	38.3×10^3
Wall thickness			**Inner diameter**		
	100 mbarg	2 barg		100 mbarg	2 barg
3 mm	526	1.44×10^3	26 mm	526	1.44×10^3
6 mm	809	2.21×10^3	32 mm	661	1.80×10^3
8 mm	1.01×10^3	2.77×10^3	50 mm	1.07×10^3	2.93×10^3
10 mm	1.20×10^3	3.27×10^3	90 mm	2.02×10^3	5.50×10^3

The same can be done for nitrogen with the 100 ppm limit by multiplying by 20/1.4, and the smallest distance where it exceeds the limit is 6.6 kilometers through a 100 mbarg MDPE pipeline at 1 m/s. According to Irene PRO data, in the entire area of Goeree-Overvlakkee the average distance through low pressure pipeline per consumer is approximately 95 meters. The distances in Table 6.1 are considerably larger than 95 meters.

For varying flow velocity, wall thickness and inner diameter there is a non-linear correlation. The contamination in ppm per 100 meter travelled for these three variables are plotted in Figures 6.1 to 6.3, for a 100 mbarg and a 2 barg pipeline. A line was fitted to the data points so the data can be inter- and extrapolated and used for pipelines with different proportions. Figures 6.1 to 6.3 show a correlation based on a power function in the form $y = ax^b$. Values a and b were found and they are listed in Table 6.2. When comparing the values for a and b in Table 6.2, it can be seen that the values for b for wall thickness, inner diameter and flow velocity are similar for the two contaminants. Similar results for HDPE can be found in Subsection 6.1.6 and appendix A and for PVC/CPE in Appendix B.

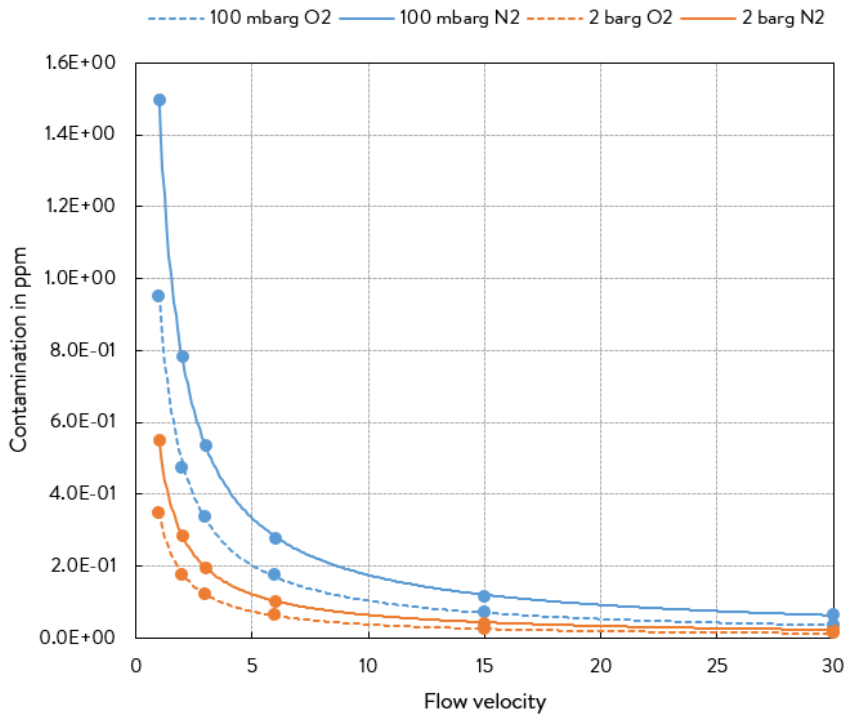

Figure 6.1: Oxygen and nitrogen contamination in ppm per 100 meter in an MDPE pipe for varying flow velocity in m/s.

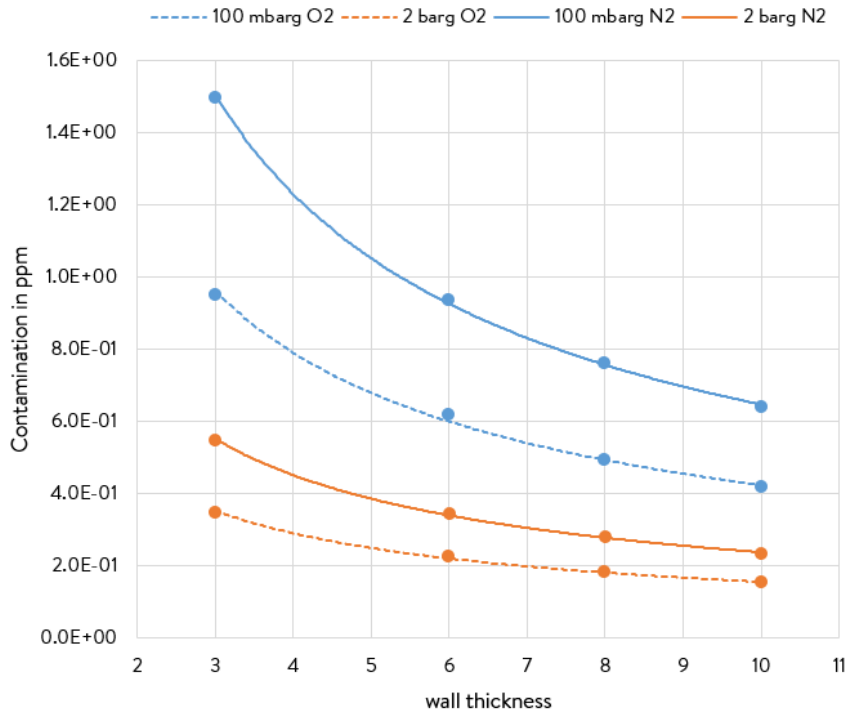

Figure 6.2: Oxygen and nitrogen contamination in ppm per 100 meter in an MDPE pipe for varying wall thickness in mm.

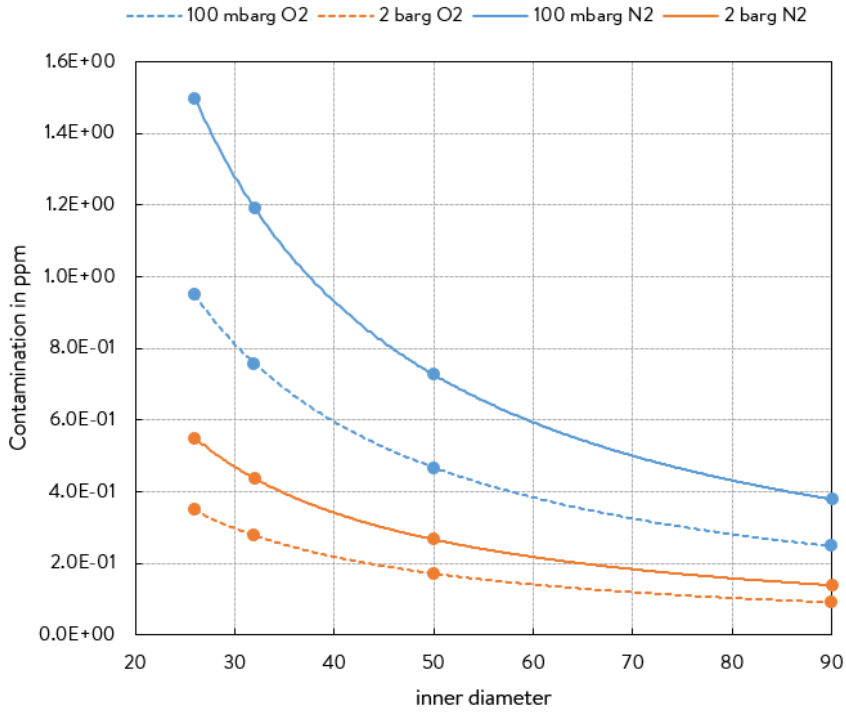

Figure 6.3: Oxygen and nitrogen contamination in ppm per 100 meter in a MDPE pipe for varying inner diameter in mm.

Table 6.2: Power function parameters a and b for fitted lines from Figures 6.1 to 6.3.

O_2						
	Wall thickness		**Inner diameter**		**Flow velocity**	
	100 mbarg	2 barg	100 mbarg	2 barg	100 mbarg	2 barg
a	2.03	0.75	32.1	11.8	0.95	0.35
b	-0.68	-0.68	-1.1	-1.1	-0.96	-0.96
N_2						
	Wall thickness		**Inner diameter**		**Flow velocity**	
	100 mbarg	2 barg	100 mbarg	2 barg	100 mbarg	2 barg
a	3.26	1.19	55.5	20.4	1.48	0.54
b	-0.70	-0.70	-1.1	-1.1	-0.92	-0.92

Looking at the results, a large variety can be noticed in the amount of contamination for different pipelines. The main determinants are material and the flow velocity. Table 6.3 lists the values for flux J through the pipe wall for the six tested flow velocities. As initially expected, a higher flow velocity results in a higher flux.

Table 6.3: The resulting oxygen flux J per flow velocity in mg s^{-1} mm^{-2}.

1 m/s	**2 m/s**	**3 m/s**	**6 m/s**	**15 m/s**	**30 m/s**
7.69×10^{-11}	8.08×10^{-11}	8.31×10^{-11}	8.67×10^{-11}	9.06×10^{-11}	9.18×10^{-11}

6.1.1. Pressure

The inner pressure has no influence on the inwards diffusion, but it does affect the relative contamination. The relative contamination is inversely proportional to the absolute pressure, thus the contamination in a 100 mbarg pipeline is 2.7 times higher than in a 2 barg pipeline. Note that 100 mbarg and 2 barg stand for the maximum pressure in the pipeline. The

minimum pressure is 40 mbarg in a 100 mbarg pipeline and 400 mbarg in a 2 barg pipeline, for example [100]. In addition, in reality the pipeline pressure is never constant.

6.1.2. Zero flow

Next to the laminar and the turbulent flow models there are also results from the zero flow model. Again the nitrogen upper limit of 100 ppm from ISO 14687-2 cannot be reached. But from Figure 5.3a it is visible that the lower limit of 5 ppm is reached within 48 hours. While 30 mbarg pipelines are nearly absent in the grid in Goeree-Overvlakkee, in other parts in the Netherlands it is more common. Running the zero flow computation for a 30 mbarg pipeline results in an excess of the 5 ppm limit after 40 hours. Similar to the pipeline pressure, the actual flow velocity is never constant. Even the route gas takes is dynamic and can only be estimated. There is no data collected of dynamic flows of natural gas, so it is impossible to say whether or how frequently zero flow actually occurs. The flow velocity is dependent on the grid configuration and gas consumption at that certain time. In Figure 6.4 six existing grid configurations in Goeree-Overvlakkee are given as an example. Depending on the lay-out of the streets in that particular area, star- and circle-shaped grids can be distinguished. In Figures 6.4a, 6.4e and 6.4f gas is able to circulate through the loops, with the exception of a number of dead ends. The grids in Figures 6.4b, 6.4c and 6.4e contain more dead ends and thus there is a higher chance that gas reaches a zero flow velocity. Gas standing still for longer than 40 hours will probably occur infrequently, but it is possible. This could occur when consumers located at a dead-end are on holiday or when an industrial consumers halt their activities in the weekend or due to maintenance. The grid location of industrial consumers is often more isolated and thus has the highest probability of receiving contaminated hydrogen as a result of standing gas.

6.1.3. Seasonal fluctuations

Interpretation of the results indicate a seasonal fluctuation of the amount of contamination. Because of the higher temperatures in summer, the permeability is higher than in winter. Table 6.4 gives the multiplication factor to get the permeability at 20°C relative to the permeability at 4°C.

Table 6.4: $P_{O_2}^{20°C}$:$P_{O_2}^{4°C}$, the ratio of permeability between yearly maximum temperature and yearly minimum temperature for the five materials .

LDPE	MDPE	HDPE	PVC/CPE	PVC
2.7	2.7	2.3	1.6	1.5
3.1	3.2	2.6	2.0	1.8

Because of the higher temperatures, there is also a three times lower average gas demand, which could lead to three times lower flow velocity [9].

6.1.4. Safety

Another important aspect of hydrogen and oxygen mixtures is human life safety. The lower flammability limit of hydrogen oxygen mixtures is 4%. Including a safety factor ensuring that a mixture will not reach one tenth of the lower flammability limit, for example, a new reasonable lower limit for oxygen in hydrogen could be 4,000 ppm. A concentration of 4,000 ppm oxygen in hydrogen as a result of diffusion can be achieved after having traveled 800 times the distances in Table 6.1. These distances are in the range of hundreds of kilometers, which is not of realistic proportion.

6.1.5. Soil

In sandy soils the contamination can be expected to be up to 5.7 more than in clay soils, due to the 5.7 times higher air fraction. Because Goeree-Overvlakkee is surrounded by water, the subsurface is more moist than the subsurface in more inland Stedin areas. These areas have a higher vertical datum and the soil in these areas often have a higher air fraction. Because of this, consumers in these areas can expect more contaminated hydrogen fuel. It is important to note that rain leads to decreased air fractions in soils. Furthermore, the fact that Goeree-Overvlakkee largely has a clayish subsurface could lead to more leaks, as clay is subject to subsidence.

Underwater pipelines are not subject to air permeation, but rather water permeation. The rate of water permeation through polyethylene has been found experimentally by van der Laan and Jansma, and is equal to a steady state value of 81 mg mm m^{-2} per day. An underwater pipeline can considered with similar conditions as the standard settings for the calculations

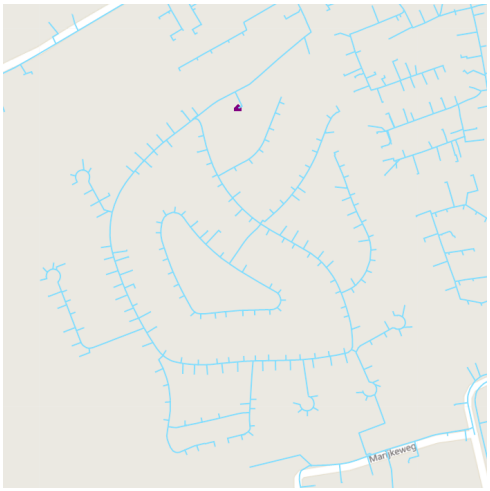

(a)

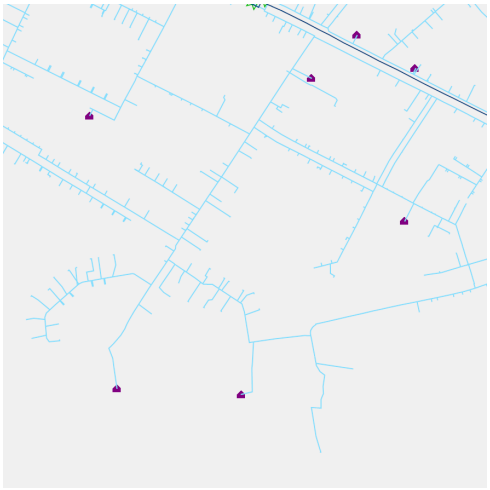

(b)

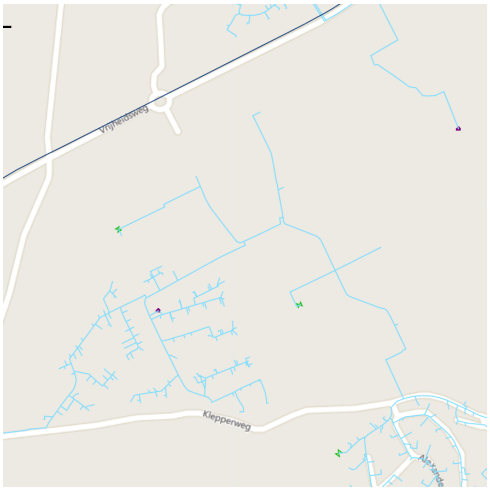

(c)

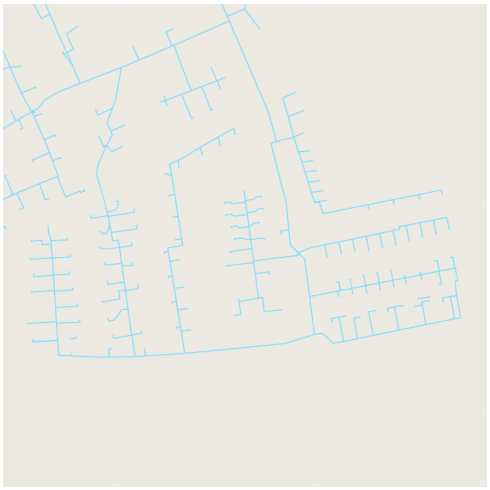

(d)

(e)

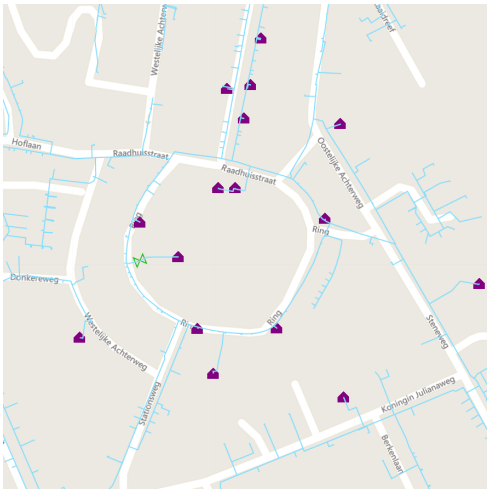

(f)

Figure 6.4: Six 100 mbarg grid configurations in Goeree-Overvlakkee from software Irene PRO. The purple house-shaped icons indicate a large-scale consumer.

in the computation model, as in Table 5.1, meaning d_{in} = 26 mm, w = 3 mm. The resulting relative water content for a zero flow condition can be calculated by the following conversion:

$$\frac{0.081}{18.02}\frac{8\cdot r_m}{w\cdot 0.25\cdot r_{in}^2}\cdot\frac{2.02}{85\cdot p}\times 10^6 = \text{water contamination in } \mu\text{mole/mole } H_2 \text{per day.} \tag{6.1}$$

Equation (6.1) results in a contamination of 5,600 µmole/mole hydrogen per day in a 100 mbarg pipeline, which is almost 4 µmole/mole per minute of zero flow. The limit of water content is only specified in ISO 14687-2 at 5 µmole/mole. For the other two purity grades of hydrogen in Table 3.2 the only requirement is that the water content must always be non-condensing. Literature concerning the water dew point at varying water concentrations in hydrogen was not found. However, it can be said that the ISO 14687-2 limit of 5 µmole/mole can easily be exceeded in underwater pipelines.

6.1.6. Results HDPE

The results in Table 6.1 are conservative, because the majority of the PE pipelines are high density rather than medium density. As oxygen diffusion through HDPE is 11 times less than MDPE, we can draw similar conclusions to MDPE by multiplying the results for MDPE by 0.09. Then the oxygen diffusion through HDPE is 0.09 ppm per 100 meter traveled for 1 m/s flow velocity in the 100 mbarg network, and 0.03 ppm per 100 meter for 1 m/s in the 2 barg network. More results concerning the flow velocity can be found in Table 6.5. Similarly, for wall thickness and inner diameter the results from Table 6.6 can be obtained.

Table 6.5: The distance in kilometers that hydrogen needs to travel to exceed the ISO 14687 contamination limit for oxygen at 5 ppm for HDPE for varying flow velocity.

Flow velocity						
	1 m/s	2 m/s	3 m/s	6 m/s	15 m/s	30 m/s
100 mbarg	5.81	11.6	16.4	31.7	78.2	155
2 barg	15.9	31.7	44.7	86.5	213	423

Table 6.6: The distance in kilometers that hydrogen needs to travel to exceed the ISO 14687 contamination limit for oxygen at 5 ppm for HDPE for varying wall thickness and inner diameter.

Wall thickness				
	3 mm	6 mm	8 mm	10 mm
100 mbarg	5.81	8.93	11.2	13.3
2 barg	15.9	24.4	30.6	36.2
Inner diameter				
	26 mm	32 mm	50 mm	90 mm
100 mbarg	5.81	7.30	11.9	22.3
2 barg	15.9	19.9	32.3	60.7

The distances needed to travel to exceed ISO 14687-2 are now in Table 6.6 in orders of kilometers. Multiplication of the distances in Table 6.6 by 11.7 gives the distance at which the limit for nitrogen at 100 ppm is reached. A complete table of the results for HDPE and for PVC/CPE can be found in Appendices A and B.

6.2. Case: Stad aan 't Haringvliet

The results obtained from the model can be applied to the case study Stad aan 't Haringvliet. A location furthest from a gas entry point with polyethylene pipelines in the grid in SatH was pinpointed to obtain conservative results. There are many possible routes for gas to travel to the consumer, as it is dependent on the consumption of others. The route that was chosen for this case is the most direct route, illustrated in Figure 6.5.

The route starts at the reduction point from the 8 barg to the 2 barg grid, including a short distance through the 2 barg grid, then through a long PVC/CPE pipeline and finally through a polyethylene pipeline that connects the customer at the second black triangle. The grid specifications for this route are listed in Table 6.7. The pipelines are identified with a number under the column *ID* for future reference.

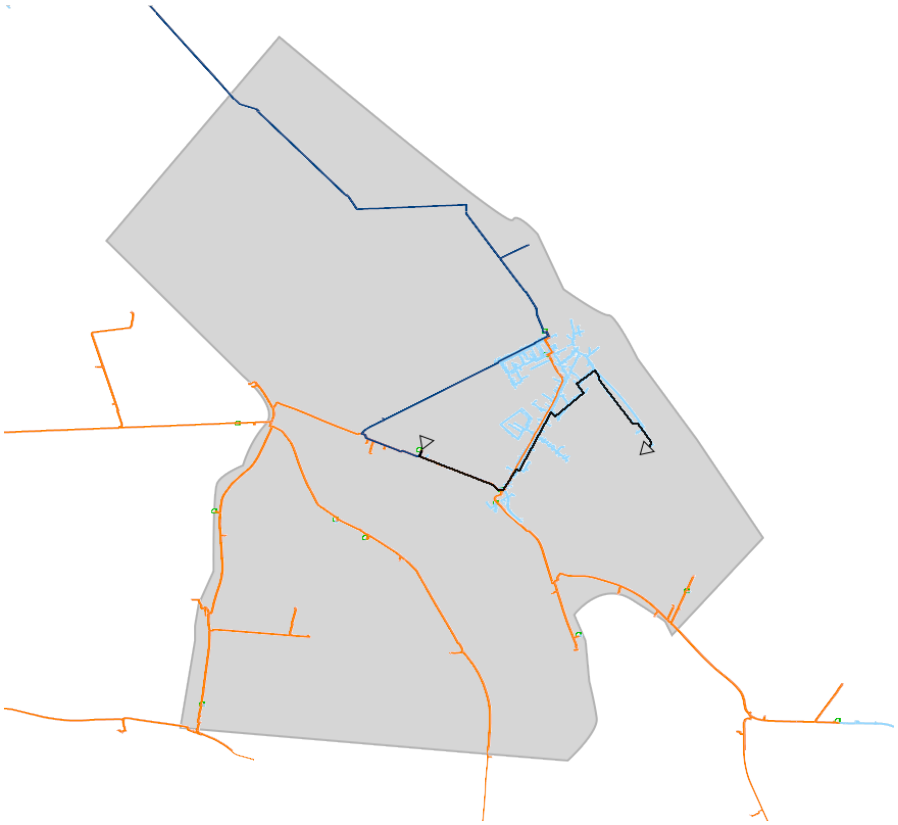

Figure 6.5: Schematic overview of the selected route for the case in Stad aan 't Haringvliet illustrated by the solid black line. The light blue lines represent the 100 mbarg grid, the 2 barg grid is illustrated in orange and the 8 barg grid is illustrated in dark blue. The black triangle connected to the 2 barg grid is the starting point of the route, while the second black triangle connected to the 100 mbarg grid is the exit point at the customer.

The subsurface layers for this route was identified with data from DINOloket, illustrated in Figure 6.6. At 80 centimeters below NAP, part of the subsurface is predominantly clayish sand, and potentially fine sand. Considering the air fractions from Table 5.6, an air fraction of 18% is assumed. With the specifications in Table 6.7 and the relations found in the earlier section, it can be estimated what the contamination will be at the exit point.

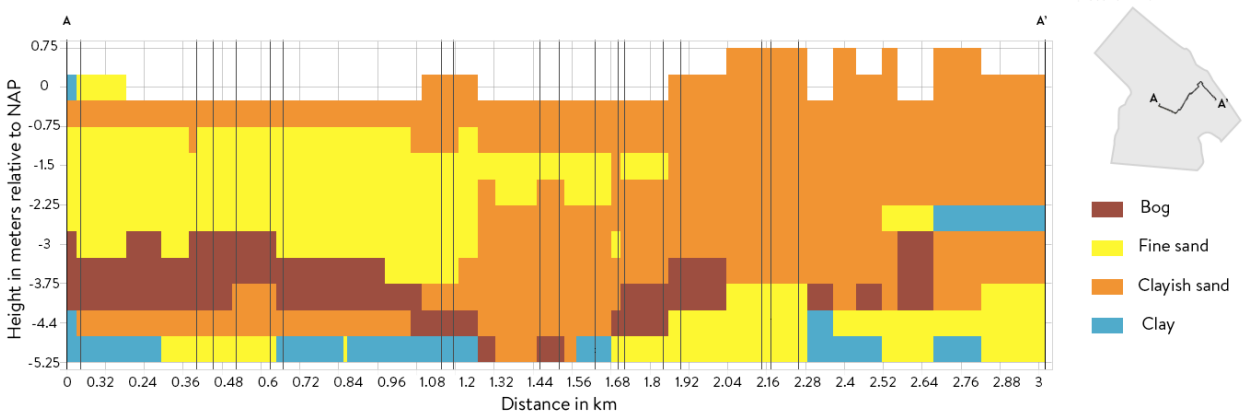

Figure 6.6: The subsurface layers for the specified route from A to A'. The vertical black lines represent direction changes.

The power function parameters a and b were obtained from Tables A.4 and B.4 to find the contamination in the grid. The

Table 6.7: Specifications of the grid for the case in Stad aan 't Haringvliet: materials, lengths, inner diameters and wall thicknesses.

100 mbar				
Material	ID	inner diameter d_{in} (mm)	wall thickness w (mm)	length l (m)
PVC/CPE	1	36	2	3
	2	104.6	2.7	1,134
	3	152.2	3.9	108
PE 80	4	35.4	6.3	43
	5	97.4	6.3	108
2 bar				
Material	ID	d_{in} (mm)	w (mm)	Length (m)
PE 80	6	90	10	580

results are shown in Table 6.8. The expected contamination is 0.057 ppm oxygen and 0.085 ppm nitrogen. This is far below the ISO 14687-2 limit of 5 µmol/mol for oxygen and 100 µmol/mol for nitrogen.

Table 6.8: The expected oxygen and nitrogen contamination for pipeline 1 to 6 in ppm for flow velocity of 1 m/s.

ID	$\mathbf{O_2}$	$\mathbf{N_2}$
1	2.9E-04	4.2E-04
2	2.9E-02	4.3E-02
3	1.3E-03	1.9E-03
4	8.5E-03	1.3E-02
5	7.1E-03	1.1E-02
6	1.1E-02	1.7E-02
Total (ppm)	**0.057**	**0.085**

If the polyethylene pipes in Table 6.7 are considered to be under water, also the water permeation through this pipeline can be calculated, as besides air also water permeates into the pipeline. The value for the water permeation rate through polyethylene was taken from van der Laan and Jansma and is equal to 0.081 g mm m^{-2} per day. Considering the molar mass of water of 18.02 g/mole, it can be calculated how much water permeates in to the polyethylene pipes, approximately from Table 6.7:

$$\text{Water concentration in pipeline 4, 5 and 6} = \sum \frac{0.081}{18.02} \cdot \frac{2 \cdot \pi \cdot r_m \cdot l}{w} \tag{6.2}$$

Equation (6.2) results in a water content of 4.0, 25 and 82 mole per day for pipeline 4, 5 and 6, respectively. If this is converted to the relative contamination in µmole per mole, the result is an average water concentration 2.1, 0.67 and 0.18 µmole/mole per day for zero flow in pipeline 4, 5 and 6.

6.3. Significance of the results

From the interpreted results and from the case study it can be concluded that the amount of contamination that can be expected in the grid is relatively small. The ISO 14687-2 limit can be exceeded, but only after travelling a distance of several kilometers through polyethylene, or several tens of kilometers through PVC/CPE and PVC. The oxygen limit is lower than the nitrogen limit, as oxygen not only dilutes the hydrogen feed but it also has a detrimental effect on metal hydride storage. Despite the fact that ISO 14687-2 was constructed for PEM fuel cells in road vehicles, the storage compartment in the two hydrogen cars currently on the Dutch market does not contain metal hydrides. Also existing hydrogen buses are designed to contain pressured hydrogen tanks as means of storage and thus no problems are expected with a small oxygen concentration in hydrogen fuel.

Furthermore, it is questionable whether it is sensible to connect a hydrogen fueling station to the low pressure grid. As hydrogen vehicles are refueled at either 350 or 700 bar, compression from 1.1 bar, for example, to these high pressures

is energy inefficient, also considering that the outlet pressure of hydrogen production technologies is in the range of tens of bars. Connecting hydrogen refueling stations to the high pressure grid mitigates both the issue of energy loss for compression and possible contamination, as the high pressure grid consists of steel pipelines. The preference of connecting hydrogen refueling stations to the high pressure grid is not seen as a constraint for the future hydrogen grid, as gasoline fuel stations are nevertheless often found alongside highways rather than in residential areas. In the case that despite this a hydrogen refueling station is wished to be installed and pure fuel needs to be guaranteed, a simple solution is placing an electrochemical purification and compression system, as this solves two problems in one.

6.4. Limitations

The most important absence in the computation model is that the grid components were not included. Apart from the pipeline materials there are also many sealing materials, under which rubbers and elastomers [101]. Rubbers and elastomers are more amorphous than polymers and can be 0% crystalline. The study by Michaels and Bixler also considers a rubber with 0% crystallinity besides the three polyethylenes from which data was used in this study. The permeability of rubber is two times higher than that of LDPE [93]. But the diffusion through the small rubber seals could possibly be cancelled out by air that can enter the grid through vents as a result of inadequate sealing. Besides vents in seals there are leaks, which have not been included in this research. But in the case of a leak in a pressurised hydrogen pipeline, escaping hydrogen could possibly be of more priority than the entrance of air into the pipeline. Another simplification in the computation model is that the pipeline is placed directly in the soil without casing. Actually according to asset data from ArcGIS, this is the case for 98% of the pipelines, as 2% of the entire Stedin grid has a casing.

Other inconsistencies between the computed results and experimental results can be exemplified by the assumptions that were needed to build the model. For example, subsurface pipelines limit inward air permeation as a result of limited air surrounding the pipelines. An approach was chosen that assumes that the air fraction in the particular soil equals the contact area of the pipeline with air. As a result, the section of the exterior of the pipeline that is in contact with air has a fixed boundary condition. This boundary condition is necessary to solve the diffusion equations. In reality, the air fraction will cause a limited air supply towards the subsurface pipeline. The composition of air in the subsurface could also deviate from above-ground air composition, as oxygen is absorbed by soil organisms and stems of crops, plants or trees [99].

Other necessary assumptions were the values of the diffusion and solubility constants. Despite the extensive search in literature for reliable references it was not possible to obtain exact values, as the exact values for diffusion and solubility constants are dependent on the manufacturer of the specific material. In addition, in the model a fully developed hydrogen flow is assumed, while because of direction changes, velocity and pressure differences the flow will not be developed at all times.

Despite steel accounting for a large share in the grid materials, as all pipelines in the 8 bar network are made from steel, the focus of this research was on the polymer materials. There has been no motivation to assume that steel has an impact on the hydrogen quality. As air cannot diffuse through steel, until now no potential issues with hydrogen distribution through steel pipelines have been found. The issue of hydrogen embrittlement has previously been raised, but has also been disproved. For temperatures close to room temperature and limited pressure cycling hydrogen embrittlement poses no threat [8, 17, 19].

7
Conclusions and Recommendations

The aim of this thesis was to find and relate the influences that pipeline distribution of hydrogen gas has on the hydrogen quality. This chapter recaps on the main findings that can be conducted from this research. Afterwards, recommendations for further research are given.

7.1. Conclusions

The main research question was as follows:

What influence does distribution through the existing gas grid have on the quality of hydrogen?

Upon arrival at the end-user, hydrogen can be contaminated caused by five sources:

1. **Odorant**, either present in hydrogen as a result of remainders of natural gas that effuse with the hydrogen feed, or a new odorant that will be added to hydrogen as safety measure. The current natural gas odorant, THT, is expected to evaporate from the pipe wall into the hydrogen feed during a time period in the range of months after natural gas has been phased-out. No information about the interaction between THT and the pipeline materials was found to be able to estimate the time scale more accurately. The sulphur compound in THT is an irreversible contaminant that is able to poison electrodes or catalysts of PEM, SO, MC and PA fuel cells. Odorisation is the conventional method for gas leak detection, but other detection methods could be preferable considering the questionable functionality of odorant in hydrogen and quality aspects. To avoid absorbed odorant causing fuel cell poisoning, fuel cells should be connected to the grid when it is believed that the odorant has completely desorbed from the pipeline. Alternatively, hydrogen can be purified before entering the fuel cell.
2. **Particles** in the grid caused by entering soil at the moment of installation of the pipeline or particles in the form of corroded steel. Hydrogen is not expected to cause corroded steel particles, as well as an other metal corrosion because of the low pressures and temperatures of the grid. But current contamination by particles is expected to continue to circulate in the gas grid. Few data was found about the quantity and size of particles currently circulating the grid. In addition, the maximum allowable quantity and particle size in hydrogen appliances are not clearly specified. Filters offer a solution to this contaminant, which is similar to proceedings in the gas grid. Existing filter are possibly needed to upgraded to fit the requirements for hydrogen. For example, hydrogen filter need to withstand a three times higher flow velocity.
3. **Leaks**, mostly as a consequence of subsidence and excavation damage. As DNOs are responsible for safe energy at all times, the management of leaks is of top priority, especially with hydrogen. DNOs should consider the possibility of an increase of contaminants during and after a gas leak. Possible contaminants are soil, air or moisture.
4. **Byproducts** from production technologies. Especially carbon monoxide, a byproduct from SMR and ATR poses a threat to PEM fuel cells. In addition, alkaline fuel cells have a low tolerance towards the contaminant carbon dioxide, another byproduct from SMR and STR. In addition, hydrogen that has been stored in depleted gas reserves can be expected to contain traced of natural gas. However, storage in depleted gas reserves is a solution for the long term due to its large scale and the fact that the Dutch gas reserves are not yet depleted. Hydrogen stored in salt caverns also might contain traces of contaminants present in the subsurface.
5. Inward **permeation** of surrounding air or water, caused by a concentration difference between the exterior and the interior of the pipeline.

This study focuses on the last aspect, the inward permeation of air. The permeation of oxygen and nitrogen through low pressure polymer pipelines was computed according to Fick's laws for diffusion. Permeation was tested based on eight changing variables: pipeline material, flow velocity, wall thickness, inner diameter, soil temperature, soil type, distance and pressure. The impact on the hydrogen contamination was found for each variable and related to each other. General conclusions that can be drawn from the computation model are:

- After traveling 100 meters through an MDPE pipeline with 26 mm inner diameter and wall thickness of 3 mm at a flow velocity of 1 m/s, 1.4 mg oxygen and 1.9 mg of nitrogen per m^3 hydrogen will have diffused into the pipeline.

- Permeation of oxygen through PVC is 80 times more than through MDPE and 57 times more through PVC/CPE. For nitrogen these numbers are 220 and 180, respectively.
- There is a non-linear correlation between flow velocity, wall thickness and inner diameter and the amount of contamination based on a power function.
- The amount of permeated oxygen and nitrogen through polymer pipeline materials increases linearly with increasing distance.
- A sandy subsurface can be expected to have 5.7 times more permeation than a clay soil as a result of a higher air fraction.
- A wider pipe wall results in less permeation.
- A smaller diameter results in more permeation.
- The absolute pipeline pressure is inversely proportional to the relative contamination; a two times higher pressure results in two times less relative contamination. The pipeline pressure does not affect the amount of permeation.
- In summer hydrogen can be expected to be more contaminated as a result of three times lower average flow velocities and 1.5 to 3.2 higher permeability of oxygen and nitrogen through polymers, depending on the material.
- Stagnant hydrogen gas in a 26 mm inner diameter pipeline with a wall thickness of 3 mm under 100 mbarg pressure will be contaminated with 5 ppm oxygen and over 10 ppm nitrogen after 48 hours.

The presence of oxygen or nitrogen in hydrogen feed has three threats:

- Dilution, causing a decrease in the fuel efficiency of hydrogen appliances
- Risk of explosion
- Damage to metal hydride storage

There were no restrictions found for connecting hydrogen boilers to the existing grid. In fact, diluted hydrogen fuel lowers the risk of NO_x emissions of the boiler. As hydrogen boilers are currently in development, it is believed that there will be no purity requirement coming from boiler manufacturers. Rather, the agreement of a national hydrogen purity will be formed first which will be needed to be taken into consideration for the design of hydrogen boilers. More specifically, the grade of hydrogen dilution affects the calorific value which is relevant for the design of the burner. Oxygen and hydrogen mixtures can explode starting from the lower flammability limit of 4%, or 40,000 ppm. A tenth of the lower flammability limit was reached by oxygen permeation after hundreds of kilometers. Hydrogen is not expected to travel a distance of hundreds of kilometers through a low pressure polymer grid. Inward permeation of air is thus not expected to cause danger for explosion. Furthermore, steel is not expected to have an influence of the hydrogen quality, as gases will not diffuse through steel and embrittlement will not occur at pipeline pressures and temperatures. The presence of nitrogen in hydrogen feed can deteriorate the impact of carbon monoxide poisoning in PEM fuel cells, but only at high concentrations of several tens of percents. This high concentration cannot be achieved under the conditions that have been modeled in this research.

A case study was done for a consumer 1.4 km from the starting point of the low pressure grid. This was the longest possible direct route for gas in Stad aan 't Haringvliet. The resulting contamination was found to be 0.057 ppm oxygen and 0.085 ppm nitrogen assuming 1 m/s flow velocity.

The contamination found through computation was compared to ISO 14687-2, as that is the most stringent norm for hydrogen quality, based on the requirements of PEM fuel cells for road vehicles. Conclusions that can be drawn from the model relative to exceeding the ISO 14687-2 limit are:

- When there is no flow in the grid, the limit is exceeded after 40 hours in a 30 mbarg grid and in 48 hours in a 100 mbarg grid.
- The nitrogen limit is not expected to be exceeded, as the travel distance to exceed the limit is in the range of tens of kilometers.
- In a 100 mbarg MDPE pipeline in a sandy soil with a wall thickness of 3 mm, inner diameter of 26 mm and flow velocity of 1 m/s the limit can be exceeded after having traveled 529 meters. For an HDPE pipeline this distance is 5.8 km.

The oxygen concentration in hydrogen fuel is limited by ISO 14687-2 because of the fuel requirements for metal hydride storage. As the existing hydrogen road vehicles on the Dutch market do not contain a metal hydride storage compartment, exceeding the ISO 14687-2 limit is not seen as a constraint for the development of a hydrogen grid. In addition, connecting a hydrogen refueling station to the high pressure grid is more preferable due to the high pressure refueling conditions. A potential concern for the distribution of hydrogen through polymer pipelines is the inward permeation of water. With the permeation rate found in literature the limit for H_2O in ISO 14687-2 can be exceeded within minutes. This problem can simply be

solved by placing gas dryers where necessary. For other hydrogen appliances there is no specific limit for the water content in hydrogen fuel. More research is needed to specify the limits for water and particle content in hydrogen fuel.

7.2. Recommendations

In this research a theoretical approach was chosen for the computation of the amount of diffusant impurities. The theoretical results can not be compared to experimental data on the actual permeation, because the data does not exist yet. The computation model in this research was based on a robust theoretical framework found in diverse literature. However, because diffusion is a complex phenomenon deviations of the theoretical results might occur. It is because of this, that field tests would be valuable to obtain experimental data. Furthermore, literature review and conversations with stakeholders pointed out that there are knowledge gaps around the scale of contamination caused by current pipeline distribution of natural gas. This section specifies topics that need more attention and suggests possibilities for experimental research.

7.2.1. Discovered knowledge gaps

Upon doing literature review during this project, knowledge gaps were found concerning current-day gas distribution. Despite the gas grid existing for several decades, very few is known about the the current-day contamination in the distribution grid. For a future-proof grid that is capable of distributing hydrogen, current-day conditions of the grid are very relevant. Little is known about particles in the grid and the effect of leaks on the gas quality. A simple suggestion would to let mechanics take samples of the particles when the filters are cleaned. More information about current-day gas quality could be gathered by connecting a valve at the end of a distribution pipeline and inspect a sample taken from that valve on moisture and particles. As the permeation of water is one of the concerns of distributing hydrogen through the grid, more information is needed about the interaction between water and hydrogen, including the influence of the water dew point. The behaviour of a leak in a hydrogen pipeline is one of the subjects of upcoming research in connection with the DNO association *Hydrogen grid research group*. During this research it would be possible to also consider the effects on the gas quality. Furthermore, more information about THT absorption could be gathered by inspecting out of service pipelines.

In this research no distinction was made between the age of the pipelines. It could be interesting to investigate a relationship between the hydrogen quality and the age of the pipeline, as old pipelines could be more contaminated, or could contain more cracks. Finally, odourisation of hydrogen also deserves attention, as it is very relevant to the hydrogen quality.

7.2.2. Establishment of a hydrogen purity standard

The production, transportation, storage and applications of hydrogen is currently of interest to many researchers. During this research there was much literature to substantiate the significance of pure hydrogen, especially for PEM fuel cells. Within the found studies the focus had primarily been on carbon monoxide and hydrogen sulphide poisoning on PEM fuel cell catalysts. These two contaminants are especially relevant for hydrogen producers. For DNOs the effect of dilution and particles are more relevant contaminants, while these two contaminants have hardly been found in literature. The norm ISO 14687 does not accurately specify the particle diameter, for example, and neither does it explain the rationale behind the limits for dilution and particulate matter. Insight on the effect of dilution and particles on hydrogen appliances, such as boilers and fuel cells, can be provided by experimental research, for which the planned pilot projects (Green Village or Entrance) will serve as a suitable experimental environment.

In a broader context, for the establishment of a hydrogen fuel purity standard it is recommended to do a cost comparison analysis, taking into consideration the costs for hydrogen fuel of different purity grades and the costs for contamination caused damage in fuel cells for the end-user. For example, as a result of contaminants hydrogen appliances might be subject to more maintenance. An agreement on a standard hydrogen purity is required for a flourishing hydrogen economy in the Netherlands and in the rest of the world. A balance must be found between cost-effectiveness of a hydrogen grid and the performance and durability of fuel cells.

7.2.3. Green Village

One of Stedin's ongoing pilot projects is situated at the Green Village. In the Green Village lies an old distribution pipeline connected to a replicated home, which will be heated by a hydrogen boiler. The goal of the pilot project is to gain knowledge and practical experience with hydrogen through a gas grid. This pilot project gives an opportunity to perform measurements on the ingoing and outgoing hydrogen quality. The grid exists of steel, PVC/CPE and PE materials under 8 barg or 100 mbarg pressure. The full lay-out of the grid can be found in Appendix C. The only customer connected to the grid is an average household consumer, in the drawing in Appendix C indicated by *1x G4*. *G4* indicates an average household consumer. The average household has a peak consumption of 6 m^3 natural gas per hour. With the same pressure drop this is translated into

a peak hydrogen consumption of 18 m^3/hour. As G4 is connected with a 26 mm inner diameter PE pipeline and assuming wall thickness of 3 mm, the maximum flow velocity in that pipeline is 2.4 m/s.

Before hydrogen is fed into the grid, it will be rinsed with an inert gas, air or nitrogen, similar to current proceedings. Normally when a pipeline is cleansed, there is an exit point where the gas mixture is either vented or combusted, until the remainder has been fully removed from the pipeline. These points are located at points indicated by numbers 001 and 036. In this case nitrogen will be preferred for rinsing and rather than air and the mixture will be vented due to the wide flammability range of hydrogen. A completed rinsing process is necessary before any measurements on the hydrogen purity can initiate.

A gas composition can be measured by gas chromatography. It is important that the gas chromatograph with mass spectrometry has a sufficient accuracy to read small concentrations in the range of µmol/mol. Pre-concentration devices, which can increase the concentration by a certain prior known amount to overcome the detection threshold, can be used for more accurate measurements otherwise [75]. Other gas chromatography methods for oxygen and nitrogen detection are thermal conductivity detection (TCD) and pulsed discharge helium ionisation detection (PDHID) [102]. TCD has a higher detection limit, and is thus less suitable. Furthermore, when taking a hydrogen sample, assurance that the sample is taken accurately is key. Further instructions on accurate procedures for taking samples can be referred to in ISO 16664 [103]. Samples taken from this experiment could also be tested on the presence of THT. Even though the pipeline in the Green Village has already had the time to evaporate, there is a possibility that there is still a presence of THT in the pipe wall. It could be monitored after what time THT has completely desorbed of the pipeline.

Practical sampling points are located at 001 and 1x G4. The point at 001 is situated at the end of an islanded pipeline, which could simulate a zero flow condition to validate the computation model from this research. Also varying flow velocities could be tested. To validate the computations in this research, it is also recommended to experiment with different soils. A way to achieve this is taking section of a pipeline and cover it in different soils. In a lab it could be tested what the differences are between the inward permeation of air between those soils. This experiment can also be executed with another gas than hydrogen, as hydrogen in the pipeline is not estimated to have an influence on the inward permeation.

In addition, it would be interesting to test the long time exposure of hydrogen appliances to contaminated or diluted hydrogen, as this is a new concept.

Bibliography

[1] CBS Statline, "Energiebalans; aanbod, omzetting en verbruik," CBS Statline, Tech. Rep., 2019. [Online]. Available: https://opendata.cbs.nl/statline/#/CBS/nl/dataset/83140NED/table?ts=1553261691744

[2] Ministerie van Economische Zaken, "Klimaatakkoord," p. 239, 2019.

[3] A. van Wijk, "The Green Hydrogen Economy in the Northern Netherlands," *Noordelijke Innovation Board*, p. 92, 2017.

[4] A. Van Wijk, G. Van Rhee, J. Reijerkerk, C. Hellinga, and H. Lucas, "Naar een groene waterstofeconomie in Zuid-Holland," Provincie Zuid-Holland, Tech. Rep., 2019.

[5] J. Gigler and W. Marcel, "Outlines of a Hydrogen Roadmap," TKI Nieuw Gas, Tech. Rep., 2018.

[6] Hydrogen Council, "A sustainable pathway for the global energy transition," *Hydrogen Council*, no. November, 2018.

[7] W. Terlouw, D. Peters, and K. van der Leun, "Gas for Climate: The optimal role for gas in a net zero emissions energy system," Navigant, Tech. Rep., 2019.

[8] R. Hermkens, S. Jansma, M. van der Laan, H. de Laat, B. Pilzer, and K. Pulles, "Toekomstbestendige gasdistributienetten," Kiwa, Tech. Rep., 2018. [Online]. Available: www.kiwatechnology.nl

[9] EBN, "Energie in Nederland," 2018. [Online]. Available: www.ebn.nl/wp-content/uploads/2018/01/EBN-Infographic-2018-pdf.pdf

[10] CBS, "Energieverbruik van particuliere huishoudens," 2018. [Online]. Available: www.cbs.nl

[11] ——, "In- en uitvoerwaarde van aardgas," 2019.

[12] Stedin, "Kwaliteits- en capaciteitsdocument gas 2018 - 2020," Tech. Rep., 2018.

[13] KNMI, "Freqentietabellen temperatuur." [Online]. Available: http://projects.knmi.nl/klimatologie/frequentietabellen/maand.cgi

[14] "Basisgegevens Aardgassen.pdf," NV Nederlandse Gasunie, Tech. Rep., 1980.

[15] U.S. Department of Energy, "Safety, Codes, and Standards," *Fuel cell Technologies Program*, 2011. [Online]. Available: https://www1.eere.energy.gov/hydrogenandfuelcells/pdfs/doe_h2_safety.pdf

[16] L. Oprinsen, "The Transition of Natural Gas to 100% Hydrogen in an Existing Distribution Network," 2018.

[17] M. W. Melaina, O. Antonia, and M. Penev, "Blending Hydrogen into Natural Gas Pipeline Networks: A Review of Key Issues," *U.S. Department of Energy*, vol. 65, no. 1, pp. 56–61, 2013.

[18] F. Kippers and H. Ophoff, "Waterstof in aardgas op Ameland," no. april, 2012.

[19] Northern Gas Networks, "H21 North of England," Tech. Rep. 101, 2018.

[20] Cadent, "HyNet North West," 2018.

[21] D. R. Hoogma, "Overzicht van Nederlandse waterstofinitiatieven, -plannen en -toepassingen," TKI Gas Topsector Energie, Tech. Rep., 2017. [Online]. Available: www.dwarsverband.nl

[22] "CO 2-vrije waterstof uit gas," TNO, Berenschot, Tech. Rep., 2017.

[23] IEA, "The Future of Hydrogen: Seizing today's opportunities," no. June, p. 203, 2019. [Online]. Available: https://webstore.iea.org/the-future-of-hydrogen

[24] J. Holstein, R. v. Gerwen, J. Douma, Y. v. Delft, and M. Saric, "Technologiebeoordeling van groene waterstofproductie," no. november, p. 29, 2018.

[25] Hygear, "Hy.GEN on-site hydrogen generation system."

[26] T. Bacquart, A. Murugan, M. Carré, B. Gozlan, F. Auprêtre, F. Haloua, and T. A. Aarhaug, "Probability of occurrence of ISO 14687-2 contaminants in hydrogen: Principles and examples from steam methane reforming and electrolysis (water and chlor-alkali) production processes model," *International Journal of Hydrogen Energy*, vol. 43, no. 26, pp. 11 872–11 883, 2018.

[27] J. Z. Zhang, J. Li, Y. Li, and Y. Zhao, *Hydrogen Generation, Storage, and Utilization*, 2014. [Online]. Available: https://app.knovel.com/web/toc.v/cid:kpHGSU000V/viewerType:toc//root_slug:hydrogen-generation-storage?kpromoter=marc

[28] I. Dincer and C. Acar, "Review and evaluation of hydrogen production methods for better sustainability," *International Journal of Hydrogen Energy*, vol. 40, no. 34, pp. 11 094–11 111, 2014. [Online]. Available: http://dx.doi.org/10.1016/j.ijhydene.2014.12.035

[29] M. Sankir and N. D. Sankir, *Hydrogen Production Technologies*. John Wiley and Sons, 2017.

[30] J. Larminie and A. Dicks, *Fuel Cell Systems Explained (2nd Edition)*. John Wiley and Sons, Ltd, 2003.

[31] The Department of Energy, "Fuel Cells Fact Sheet," 2015.

[32] A. L. Dicks and D. A. J. Rand, *Fuel Cell Systems Explained (3rd Edition)*. John Wiley and Sons, 2018. [Online]. Available: https://app.knovel.com/web/view/khtml/show.v/rcid:kpFCSEE01P/cid:kt011UCA51/viewerType:khtml//root_slug:1-introducing-fuel-cells/url_slug:introducing-fuel-cells?kpromoter=marc&b-toc-cid=kpFCSEE01P&b-toc-root-slug=&b-toc-url-slug=introducing-fuel-cells&b-t

[33] I. Staffell, D. Scamman, A. Velazquez Abad, P. Balcombe, P. E. Dodds, P. Ekins, N. Shah, and K. R. Ward, "The role of hydrogen and fuel cells in the global energy system," *Energy and Environmental Science*, vol. 12, no. 2, pp. 463–491, 2019.

[34] A. Mehmeti, F. Santoni, M. Della Pietra, and S. J. McPhail, "Life cycle assessment of molten carbonate fuel cells: State of the art and strategies for the future," pp. 97–108, 3 2016.

[35] M. F. Hordeski, *Hydrogen and Fuel Cells - Advances in Transportation and Power*. Fairmont Press, Inc, 2009.

[36] K. Brooks, A. Makhmalbaf, D. Anderson, J. Amaya, S. Pilli, V. Srivastava, and J. Upton, "Business Case for a Micro-Combined Heat and Power Fuel-Cell System in Commercial Applications," *Pacific Northwest National Laboratory*, vol. PNNL-22831, no. October, p. 85, 2013.

[37] H. R. Ellamla, I. Staffell, P. Bujlo, B. G. Pollet, and S. Pasupathi, "Current status of fuel cell based combined heat and power systems for residential sector," *Journal of Power Sources*, vol. 293, pp. 312–328, 2015. [Online]. Available: http://dx.doi.org/10.1016/j.jpowsour.2015.05.050

[38] P. E. Dodds, I. Staffell, A. D. Hawkes, F. Li, P. Grünewald, W. McDowall, and P. Ekins, "Hydrogen and fuel cell technologies for heating: A review," *International Journal of Hydrogen Energy*, vol. 40, no. 5, pp. 2065–2083, 2015.

[39] D. Hart, J. Howes, B. Madden, and E. Boyd, "Hydrogen and Fuel Cells: Opportunities for Growth," *E4Tech*, no. November, 2016.

[40] "Viessmann residential CHP fuel cell system launches in Europe," *Fuel Cells Bulletin*, vol. 2014, no. 4, p. 5, 2014.

[41] M. Gandiglio, A. Lanzini, M. Santarelli, and P. Leone, "Design and optimization of a proton exchange membrane fuel cell CHP system for residential use," *Energy and Buildings*, vol. 69, pp. 381–393, 2014. [Online]. Available: http://dx.doi.org/10.1016/j.enbuild.2013.11.022

[42] Toyota, "2017 Mirai Product Information." [Online]. Available: www.toyota.com

[43] Hyundai USA, "Hyundai Nexo Fuel Cell SUV." [Online]. Available: www.hyundaiusa.com/nexo/

[44] A. Mayyas and M. Mann, "Manufacturing competitiveness analysis for hydrogen refueling stations," *International Journal of Hydrogen Energy*, 2019.

[45] P. Bouwman, "Electrochemical Hydrogen Compression (EHC) solutions for hydrogen infrastructure," *Fuel Cells Bulletin*, vol. 2014, no. 5, pp. 12–16, 2014. [Online]. Available: http://dx.doi.org/10.1016/S1464-2859(14)70149-X

[46] Frazer-Nash Consultancy, "Appraisal of Domestic Hydrogen Appliances," no. 1, 2018.

[47] J. Sampson, "No Title," 2018. [Online]. Available: https://www.gasworld.com/toyota-develops-worlds-first-hydrogen-burner/2015852.article

[48] M. Gambini, T. Stilo, and M. Vellini, "Hydrogen storage systems for fuel cells: Comparison between high and low-temperature metal hydrides," *International Journal of Hydrogen Energy*, 2019.

[49] K. Jaspers, "Mitsubishi Hitachi Power Systems stapt in Magnum-waterstofcentrale," 2017. [Online]. Available: www.fluxenergie.nl

[50] K. Liu, C. Song, and V. Subramani, *Hydrogen and Syngas Production and Purification Technologies*. American Institute of Chemical Engineers, 2009.

[51] Ministerie van Economische Zaken, "Regeling Gaskwaliteit," 2018.

[52] M. Vos, "HyQuality : Hydrogen Quality Compatibility," pp. 1–23.

[53] A. Amid, D. Mignard, and M. Wilkinson, "Seasonal storage of hydrogen in a depleted natural gas reservoir," *International Journal of Hydrogen Energy*, vol. 41, no. 12, pp. 5549–5558, 2016. [Online]. Available: http://dx.doi.org/10.1016/j.ijhydene.2016.02.036

[54] "Werken met Odorant," N.V. Nederlandse Gasunie, Tech. Rep., 2016.

[55] R. N. Haneng, "Eindrapport Zwavelvrij Odorant," 2014.

[56] A. Mcintosh, "SGN Energy Futures," no. December, 2018.

[57] J. P. Kopasz, "Fuel cells and odorants for hydrogen," *International Journal of Hydrogen Energy*, vol. 32, no. 13, pp. 2527–2531, 2007.

[58] P. S. Chauhan and S. Bhattacharya, "Hydrogen gas sensing methods, materials, and approach to achieve parts per billion level detection: A review," *International Journal of Hydrogen Energy*, 2019.

[59] B. Fuster, D. Houssin-Agbomson, S. Jallais, E. Vyazmina, G. Dang-Nhu, G. Bernard-Michel, M. Kuznetsov, V. Molkov, B. Chernyavskiy, V. Shentsov, D. Makarov, R. Dey, P. Hooker, D. Baraldi, E. Weidner, D. Melideo, V. Palmisano, A. Venetsanos, and J. Der Kinderen, "Guidelines and recommendations for indoor use of fuel cells and hydrogen systems," *International Journal of Hydrogen Energy*, vol. 42, no. 11, pp. 7600–7607, 2017.

[60] P. Wichers Schreur, "Schade door stof in het gasdistributienet," GASTEC, Tech. Rep., 1997.

[61] J. M. Ohi, N. Vanderborgh, G. V. Consultants, S. Ahmed, R. Kumar, D. Papadius, A. N. Laboratory, T. Rockward, and L. Alamos, "Hydrogen Fuel Quality Specifications for Polymer Electrolyte Fuel Cells in Road Vehicles," Tech. Rep., 2016. [Online]. Available: https://www.energy.gov/sites/prod/files/2016/11/f34/fcto_h2_fuel_quality_specs_pem_fc_road_vehicles.pdf

[62] M. van der Laan and S. Jansma, "Invloed van waterpermeatie bij PE leidingen op het water- dauwpunt van aardgas," Kiwa Technology, Tech. Rep. september, 2019.

[63] Publicatiereeks Gevaarlijke Stoffen, "Aardgas - afleverinstallaties voor motorvoertuigen," Tech. Rep., 2011.

[64] "ISO 14687 Hydrogen Fuel - Product Specification," vol. 2008, pp. 40–42, 2012.

[65] M. Voldsund, K. Jordal, and R. Anantharaman, "Hydrogen production with CO2 capture," *International Journal of Hydrogen Energy*, vol. 41, no. 9, pp. 4969–4992, 2016. [Online]. Available: http://dx.doi.org/10.1016/j.ijhydene.2016.01.009

[66] M. Schulze and E. Gülzow, "Overview Performance and Operational Conditions," *Encyclopedia of Electrochemical Power Sources*, no. V, pp. 901–911, 2009. [Online]. Available: http://www.sciencedirect.com/science/article/pii/B9780444527455002331

[67] Y. Matsuda, T. Shimizu, and S. Mitsushima, "Adsorption behavior of low concentration carbon monoxide on polymer electrolyte fuel cell anodes for automotive applications," *Journal of Power Sources*, vol. 318, pp. 1–8, 2016. [Online]. Available: http://dx.doi.org/10.1016/j.jpowsour.2016.03.104

[68] B. Shabani, M. Hafttananian, S. Khamani, A. Ramiar, and A. Ranjbar, "Poisoning of proton exchange membrane fuel cells by contaminants and impurities: Review of mechanisms, effects, and mitigation strategies," *Journal of Power Sources*, vol. 427, no. March, pp. 21–48, 2019. [Online]. Available: https://linkinghub.elsevier.com/retrieve/pii/S0378775319303520

[69] S. K. Das, A. Reis, and K. J. Berry, "Experimental evaluation of CO poisoning on the performance of a high temperature proton exchange membrane fuel cell," *Journal of Power Sources*, 2009.

[70] H. F. Oetjen, V. M. Schmidt, U. Stimming, and F. Trila, "Performance data of a proton exchange membrane fuel cell using H2/CO as fuel gas," *Journal of the Electrochemical Society*, vol. 143, no. 12, pp. 3838–3842, 1996.

[71] M. S. Naughton, F. R. Brushett, and P. J. A. Kenis, "Carbonate resilience of flowing electrolyte-based alkaline fuel cells," *Journal of Power Sources*, 2011.

[72] M. Inaba, M. Sugishita, J. Wada, K. Matsuzawa, H. Yamada, and A. Tasaka, "Impacts of air bleeding on membrane degradation in polymer electrolyte fuel cells," *Journal of Power Sources*, 2008.

[73] K. K. Bhatia and C. Y. Wang, "Transient carbon monoxide poisoning of a polymer electrolyte fuel cell operating on diluted hydrogen feed," *Electrochimica Acta*, vol. 49, no. 14, pp. 2333–2341, 2004.

[74] "ISO 14687-2 Hydrogen fuel — Product fuel cell applications for road vehicles," 2012.

[75] A. Murugan and A. S. Brown, "Review of purity analysis methods for performing quality assurance of fuel cell hydrogen," *International Journal of Hydrogen Energy*, vol. 40, no. 11, pp. 4219–4233, 2015.

[76] F. H. Garzon, T. Rockward, R. Mukundan, B. Kienitz, J. Chlistunoff, E. L. Brosha, J.-M. Sansiñena, and N. Garland, "Effects of Fuel and Air Impurities on PEM Fuel Cell Performance, DOE Hydrogen Program FY 2010 Annual Progress Report," pp. 722–726, 2007. [Online]. Available: https://www.hydrogen.energy.gov/pdfs/progress10/v_c_1_garzon.pdf

[77] F. A. Uribe, E. Brosha, F. Garzon, and M. Mikkola, "VII. I. 4 Effect of Fuel and Air Impurities on PEM Fuel Cell Performance," *Hydrogen.Energy.Gov*, pp. 1046–1051, 2005. [Online]. Available: http://hydrogen.energy.gov/pdfs/progress05/vii_i_4_uribe.pdf

[78] G. Bernardo, T. Araújo, T. da Silva Lopes, J. Sousa, and A. Mendes, "Recent advances in membrane technologies for hydrogen purification," *International Journal of Hydrogen Energy*, 7 2019. [Online]. Available: https://linkinghub.elsevier.com/retrieve/pii/S0360319919324620

[79] L. Schorer, S. Schmitz, and A. Weber, "Membrane based purification of hydrogen system (MEMPHYS)," *International Journal of Hydrogen Energy*, 2019.

[80] Holtec gas systems, "PSA vs membrane application." [Online]. Available: http://www.holtecllc.com/our-products/technology-comparison.html

[81] Air Liquide, "Cryogenic Hydrogen Purifier – ULTRAL H2." [Online]. Available: https://advancedtech.airliquide.com/cryogenic-hydrogen-purifier-ultral-h2

[82] A. Basile, F. Dalena, J. Tong, and T. N. Veziroğlu, *Hydrogen production, separation and purification for energy*. Institution of Engineering and Technology, 2017.

[83] HyET, "HyET Hydrogen efficient purification and compression."

[84] R. M. Barrer, R. Mallinder, and P. S. Wong, "Solution and diffusion of gases in poly(vinylchloride)," *Polymer*, vol. 8, no. C, pp. 321–336, 1967.

[85] H. Huldy, "Gasdoorlatendheid van kunststoffen en rubbers," *Centraal Laboratorium TNO*, 1967.

[86] R. Scheichl, M. H. Klopffer, Z. Benjelloun-Dabaghi, and B. Flaconnèche, "Permeation of gases in polymers: Parameter identification and nonlinear regression analysis," *Journal of Membrane Science*, 2005.

[87] L. W. McKeen, *Permeability Properties of Plastics and Elastomers*, 2nd ed. William Andres Pub., 2017.

[88] M.-H. Klopffer, P. Berne, and E. Espuche, "Development of Innovating Materials for Distributing Mixtures of Hydrogen and Natural Gas. Study of the Barrier Properties and Durability of Polymer Pipes," *Oil & Gas Science and Technology – Revue d'IFP Energies nouvelles*, vol. 70, no. 2, pp. 305–315, 2014.

[89] R. Barrer, *Diffusion In and Through Solids*. Cambridge University Press, 1941.

[90] J. Crank, "the Mathematics of Diffusion," pp. 1–421, 2005.

[91] Y. J. Shur and B. Ranby, "Gas Permeation of Polymer Blends. III. Poly(vinyl Chloride) (PVC)/Chlorinated Polyethylene (CPE)," *Journal of Applied Polymer Science*, vol. 20, pp. 3105–3119, 1976.

[92] R. Roberts, "Molecular Diffusion of Gases," *American Institute of Physics Handbook*, 1957.

[93] A. S. Michaels and H. J. Bixler, "Flow of gases through polyethylene," *Journal of Polymer Science*, vol. 50, no. 154, pp. 413–439, 1961.

[94] ——, "Solubility of Gases in Polyethylene," *Journal of Polymer Science*, vol. L, pp. 393–412, 1961.

[95] KNMI, "Grondtemperatuur station Wilhelminadorp," 2019. [Online]. Available: www.knmi.nl

[96] P. Kjeldsen, "Evaluation of gas diffusion through plastic materials used in experimental and sampling equipment," *Water Research*, vol. 27, no. 1, pp. 121–131, 1993.

[97] R. Bird, W. E. Stewart, and E. N. Lightfoot, *Transport phenomena, second edition*, 2012, vol. 1, no. 2. [Online]. Available: http://eu.wiley.com/WileyCDA/WileyTitle/productCd-0470115394.html

[98] R. J. Adrian, R. Friedrich, and F. T. Nieuwstadt, "Fully developed turbulent pipe flow: A comparison between direct numerical simulation and experiment," *Journal of Fluid Mechanics*, vol. 268, pp. 175–210, 1994.

[99] J. Bakker, F. Boone, and P. Boekel, "Diffusie van gassen in grond en zuurstofdiffusiecoëfficiënten in Nederlandse akkerbouwgronden," Instituut voor Cultuurtechniek en Waterhuishouding, Tech. Rep., 1987.

[100] E. Huijzer, "Handboek gasstoffilters," Gastec, Tech. Rep., 1997.

[101] R. Valk, "Bestandheid van gasdistributiematerialen tegen zwavelvrij odorant," Kiwa, Tech. Rep. april, 2017.

[102] P. E. V. de Miranda, *Science and Engineering of Hydrogen-Based Energy Technologies*, 2018.

[103] "ISO-16664 Gas analysis — Handling of calibration gases and gas mixtures — Guidelines," 2017.

A
Results HDPE

Table A.1: The amount of oxygen and nitrogen contamination in ppm per 100 meter for an HDPE pipeline for varying flow velocity.

O_2						
	1 m/s	2 m/s	3 m/s	6 m/s	15 m/s	30 m/s
100 mbarg	8.6E-02	4.3E-02	3.1E-02	1.6E-02	6.4E-03	3.2E-03
2 barg	3.2E-02	1.6E-02	1.1E-02	5.8E-03	2.3E-03	1.2E-03
N_2						
100 mbarg	1.5E-01	7.7E-02	5.3E-02	2.7E-02	1.1E-02	6.5E-03
2 barg	5.4E-02	2.8E-02	1.9E-02	1.0E-02	4.2E-03	2.4E-03

Table A.2: The amount of oxygen and nitrogen contamination in ppm per 100 meter for an HDPE pipeline for varying wall thickness.

O_2				
	3 mm	6 mm	8 mm	10 mm
100 mbarg	8.6E-02	5.6E-02	4.5E-02	3.8E-02
2 barg	3.2E-02	2.1E-02	1.6E-02	1.4E-02
N_2				
	3 mm	6 mm	8 mm	10 mm
100 mbarg	1.5E-01	9.2E-02	7.5E-02	6.3E-02
2 barg	5.4E-02	3.4E-02	2.7E-02	2.3E-02

Table A.3: The amount of oxygen and nitrogen contamination in ppm per 100 meter for an HDPE pipeline for varying inner diameter.

O_2				
	26 mm	32 mm	50 mm	90 mm
100 mbarg	8.6E-02	6.8E-02	4.2E-02	2.2E-02
2 barg	3.2E-02	2.5E-02	1.5E-02	8.2E-03
N_2				
100 mbarg	1.5E-01	1.2E-01	7.1E-02	3.7E-02
2 barg	5.4E-02	4.3E-02	2.6E-02	1.4E-02

Table A.4: Power function parameters a and b for fitted lines from of power function for wall thickness, inner diameter and flow velocity.

O_2						
	Wall thickness		**Inner diameter**		**Flow velocity**	
	100 mbarg	2 barg	100 mbarg	2 barg	100 mbarg	2 barg
a	0.18	0.07	2.9	1.1	0.09	0.03
b	-0.68	-0.68	-1.1	-1.1	-0.96	-0.96
N_2						
	Wall thickness		**Inner diameter**		**Flow velocity**	
	100 mbarg	2 barg	100 mbarg	2 barg	100 mbarg	2 barg
a	0.32	0.12	5.5	2.0	0.15	0.05
b	-0.70	-0.70	-1.1	-1.1	-0.92	-0.92

B

Results PVC/CPE

Table B.1: The amount of oxygen and nitrogen contamination in ppm per 100 meter for an HDPE pipeline for varying flow velocity.

O_2						
	1 m/s	2 m/s	3 m/s	6 m/s	15 m/s	30 m/s
100 mbarg	1.7E-02	8.3E-03	5.9E-03	3.1E-03	1.2E-03	6.2E-04
2 barg	6.1E-03	3.1E-03	2.2E-03	1.1E-03	4.5E-04	2.3E-04
N_2						
100 mbarg	8.2E-03	4.3E-03	2.9E-03	1.5E-03	6.3E-04	3.6E-04
2 barg	53.0E-03	1.6E-03	1.1E-03	5.6E-04	2.3E-04	1.3E-04

Table B.2: The amount of oxygen and nitrogen contamination in ppm per 100 meter for a PVC/CPE pipeline for varying wall thickness.

O_2				
	3 mm	6 mm	8 mm	10 mm
100 mbarg	1.7E-02	1.1E-02	8.6E-03	7.3E-03
2 barg	6.1E-03	4.0E-03	3.2E-03	2.7E-03
N_2				
	3 mm	6 mm	8 mm	10 mm
100 mbarg	8.2E-03	5.1E-03	4.2E-03	3.5E-03
2 barg	3.0E-03	1.9E-03	1.5E-03	1.3E-03

Table B.3: The amount of oxygen and nitrogen contamination in ppm per 100 meter for a PVC/CPE pipeline for varying inner diameter.

O_2				
	26 mm	32 mm	50 mm	90 mm
100 mbarg	1.7E-02	1.3E-02	8.2E-03	4.4E-03
2 barg	6.1E-03	4.9E-03	3.0E-03	1.6E-03
N_2				
100 mbarg	8.2E-03	6.5E-03	4.0E-03	2.1E-03
2 barg	3.0E-03	2.4E-03	1.5E-03	7.6E-04

Table B.4: Power function parameters a and b for fitted lines of the power function of wall thickness, inner diameter and flow velocity.

O_2						
	Wall thickness		**Inner diameter**		**Flow velocity**	
	100 mbarg	2 barg	100 mbarg	2 barg	100 mbarg	2 barg
a	0.036	0.013	0.56	0.21	0.017	0.0061
b	-0.68	-0.68	-1.1	-1.1	-0.96	-0.96
N_2						
	Wall thickness		**Inner diameter**		**Flow velocity**	
	100 mbarg	2 barg	100 mbarg	2 barg	100 mbarg	2 barg
a	0.018	0.0065	0.30	0.11	0.0081	0.0030
b	-0.70	-0.70	-1.1	-1.1	-0.92	-0.92

C

Green Village

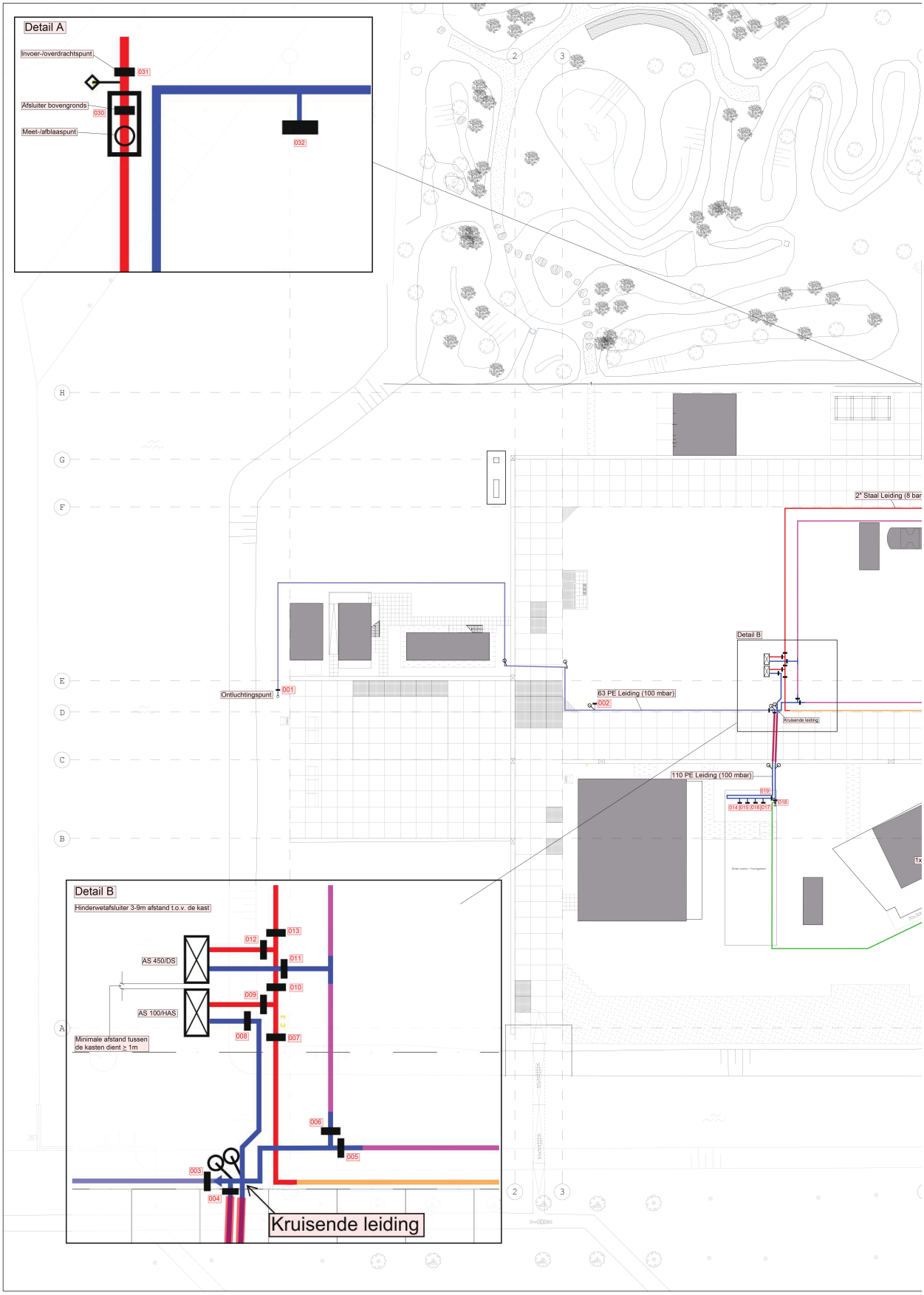
Detail A
Invoer-/overdrachtspunt
031
Afsluiter bovengronds
030
Meet-/afblaaspunt
032
2" Staal Leiding (8 bar
Detail B
Ontluchtingspunt
001
63 PE Leiding (100 mbar)
002
Kruisende leiding
110 PE Leiding (100 mbar)
Detail B
Hinderwetafsluiter 3-9m afstand t.o.v. de kast
AS 450/DS
AS 100/HAS
Minimale afstand tussen de kasten dient ≥ 1m
012
013
011
010
009
008
007
006
005
003
004
Kruisende leiding

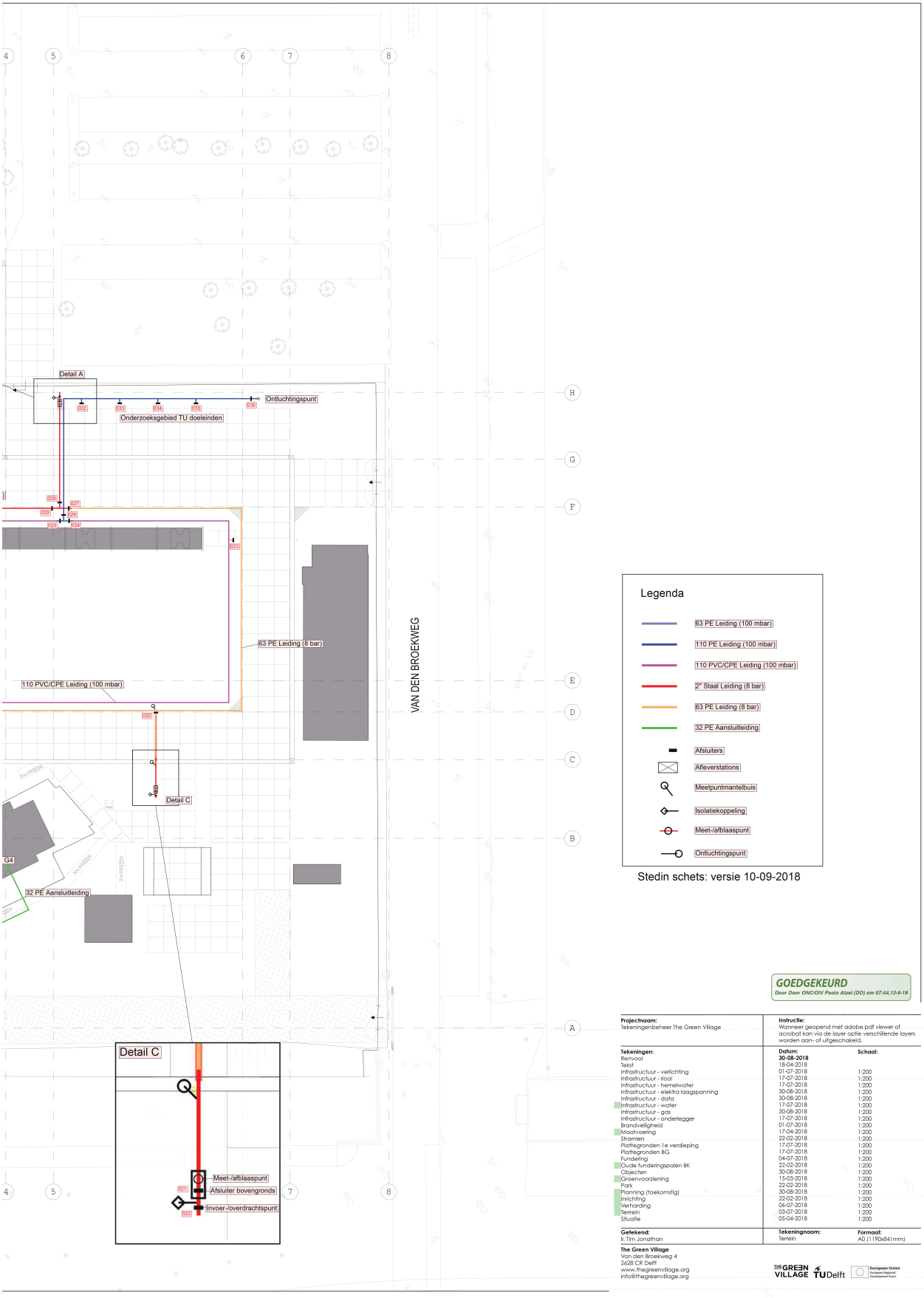
Detail A
Ontluchtingspunt
Onderzoeksgebied TU doeleinden
VAN DEN BROEKWEG
63 PE Leiding (8 bar)
110 PVC/CPE Leiding (100 mbar)
Detail C
32 PE Aansluitleiding
Detail C
Meet-/afblaaspunt
Afsluiter bovengronds
Invoer-/overdrachtspunt
Legenda
63 PE Leiding (100 mbar)
110 PE Leiding (100 mbar)
110 PVC/CPE Leiding (100 mbar)
2" Staal Leiding (8 bar)
63 PE Leiding (8 bar)
32 PE Aansluitleiding
Afsluiters
Afleverstations
Meetpuntmantelbuis
Isolatiekoppeling
Meet-/afblaaspunt
Ontluchtingspunt
Stedin schets: versie 10-09-2018
GOEDGEKEURD
Door Door ONO/OIV Paolo Atzei (DO) om 07:44,13-9-18
Projectnaam:
Tekeningenbeheer The Green Village
Instructie:
Wanneer geopend met adobe pdf viewer of acrobat kan via de layer optie verschillende layers worden aan- of uitgeschakeld.
Tekeningen:
Datum:
Schaal:
Rentvool 30-08-2018
Tekst 18-04-2018
Infrastructuur - verlichting 01-07-2018 1:200
Infrastructuur - fiool 17-07-2018 1:200
Infrastructuur - hemelwater 17-07-2018 1:200
Infrastructuur - elektra laagspanning 30-08-2018 1:200
Infrastructuur - data 30-08-2018 1:200
Infrastructuur - water 17-07-2018 1:200
Infrastructuur - gas 30-08-2018 1:200
Infrastructuur - onderlegger 17-07-2018 1:200
Brandveiligheid 01-07-2018 1:200
Maatvoering 17-04-2018 1:200
Stramien 22-02-2018 1:200
Plattegronden 1e verdieping 17-07-2018 1:200
Plattegronden BG 17-07-2018 1:200
Fundering 04-07-2018 1:200
Oude funderingspalen BK 22-02-2018 1:200
Objecten 30-08-2018 1:200
Groenvoorziening 15-03-2018 1:200
Park 22-02-2018 1:200
Planning (toekomstig) 30-08-2018 1:200
Inrichting 22-02-2018 1:200
Verharding 04-07-2018 1:200
Terrein 03-07-2018 1:200
Situatie 05-04-2018 1:200
Getekend:
ir. Tim Jonathan
Tekeningnaam:
Terrein
Formaat:
A0 (1190x841mm)
The Green Village
Van den Broekweg 4
2628 CR Delft
www.thegreenvillage.org
info@thegreenvillage.org
THE GREEN VILLAGE TU Delft
European Union